Solution Plasma Synthesis and Characteristic for Mesoporous Silica and Metal Nanoparticles System

Panuphong Pootawang

Solution Plasma Synthesis and Characteristic for Mesoporous Silica and Metal Nanoparticles System

A Doctoral Dissertation by

Panuphong Pootawang

March, 2011

Graduate School of Engineering,

Department of Materials, Physics and Energy Engineering,

Nagoya University,

In partial fulfillment of the requirements for the degree of

DOCTOR OF ENGINEERING

Contents

Chapter 1. Introduction

Outline of study

Chapter 1 describes the fundamental of solution plasma process, its advantages, and its applications. Additionally, the fundamental of the interested nanoparticles, e.g. Ag nanoparticles and the mesoporous silica are introduced.

Chapter 2 describes and discusses the investigation of solution plasma for organic template removal inside mesoporous silica which is prepared by sol-gel method in various acid concentrations. Moreover, the effect of synthesized acid concentration is reported in the term of mesopores morphology, mesoporous silica particle morphology, and the surface area.

Chapter 3 describes the influences of pHs of discharge solution and discharge time on the capability of solution plasma for organic template removal. The investigations of the structural morphology, structural parameters, and density of active species during discharge are presented.

Chapter 4 describes and discusses the determination of the feasibility of solution plasma process as a single-step process for Ag nanoparticles incorporation on mesoporous silica and organic template removal inside mesoporous silica. The structural morphologies of both Ag nanoparticles and mesoporous silica are investigated and the mechanisms of the expected reactions are also described.

Chapter 5 describes and discusses the ability of Ag nanoparticles incorporated mesoporous silica for the unsaturated oleic acid hydrogenation converting to the saturated stearic acid under controlled conditions.

Chapter 6 is the summary of all chapters.

1.1. Solution plasma process

The low temperature plasma in aqueous solution, as called solution plasma process (SPP) has been increasing attention owing to their applicability to various fields of industrial processing. For the duration of discharge, SPP generates the variety of active species with low thermal loading and accumulation originating from a character of low temperature plasma process [1,2]. Various applications for instance nanoparticles synthesis, organic compound decomposition, and microorganism inhibition are obtained by the efficient solution plasma process. Comparing with the conventional processes for the mention applications, SPP provides the superior benefits as non-equilibrium materials fabrication, short consumption time, low contamination, ease of handling, and low cost whilst considering in the large scale use.

1.1.1. Solution plasma configuration

Concerning the lab-scale design, solution plasma is physically generated by discharge in aqueous under the controlled conditions. Fig. 1.1 displays one of conventional experimental setups for solution plasma which consists of several parts and power supply generation. The detail of main parts is described as follow.

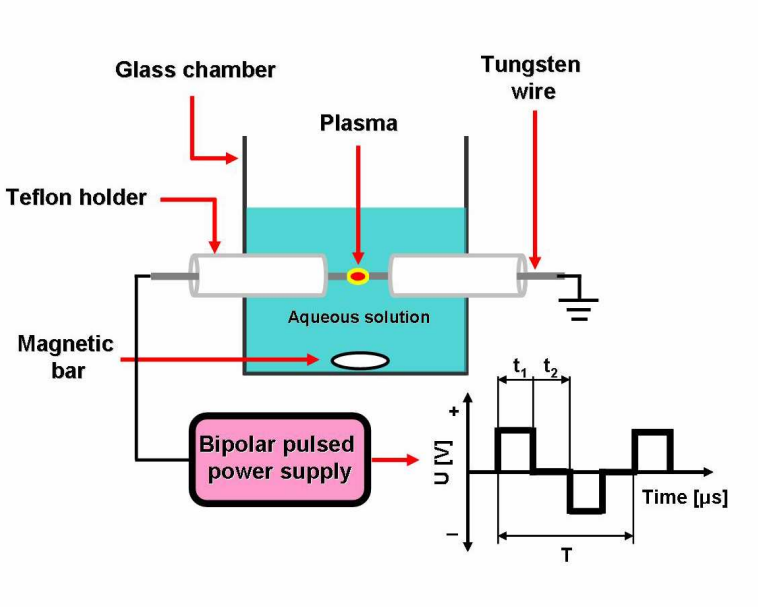

Fig. 1.1. Schematic image of solution plasma setup.

Reactor chamber/vessel

A chamber to contain the solution is required. Various types of materials are used for containing solution that is the glass chamber, Pyrex beaker and plastic vessel. The properties such as high chemical resistivity, thermal resistivity, and strength are adjusting to the solution. For an example, the poly(methyl methacrylate) (PMMA) vessel is the simplest option to make solution plasma reactor. However, such a reactor is not suitable for organic solvents such as acrylic acid and high concentration of organic-type acid.

Electrode

Various types of electrode can be utilized to generate plasma in solution, for example, tungsten (W), tantalum (Ta), copper (Cu), silver (Ag), and gold (Au). The selection of electrode depends on the purpose of discharge. Normally, tungsten (W) is applied to be electrode owing to its superior characteristics for instance high electron

current, high stability, high chemical resistivity, and continuous plasma generation [2,3]. In our system, the gap between electrodes can be easily adjusted with the assistant of Teflon holder to fix at given positions, which is one of crucial parameters.

Teflon holder

Teflon (polytetrafluoroethylene, PTFE) holder has a role to hold the electrodes in the proper position for plasma generation. This material is the high chemical and thermal resistant and high stable, hence, it is available in various solutions under plasma conditions without the melting and impurities generation.

Power supply

In order to generate solution plasma, the bipolar pulsed power supply has been used. Such a power supply lets us to operate low temperature plasma stably. Likewise, it is possible to immediately clean up both of electrodes from any impurity which might cover in the tip of electrode [4]. The considered parameters for plasma generation, applied voltage, pulse width, and frequency, are strictly controlled and only slight adjustment can be changed the plasma condition during discharge. To generate plasma in solution, more than breakdown voltage is needed. Fig. 1.2 shows the relations of voltage and current against time. At the beginning step, the plasma cannot be generated since the energy is not enough to accelerate the excitation of electrons in the electrode. Until the continuously increased external energy to reach the breakdown voltage, the plasma can be formed and stabilized which obviously observed in the first maximum peak on the voltage-time relation.

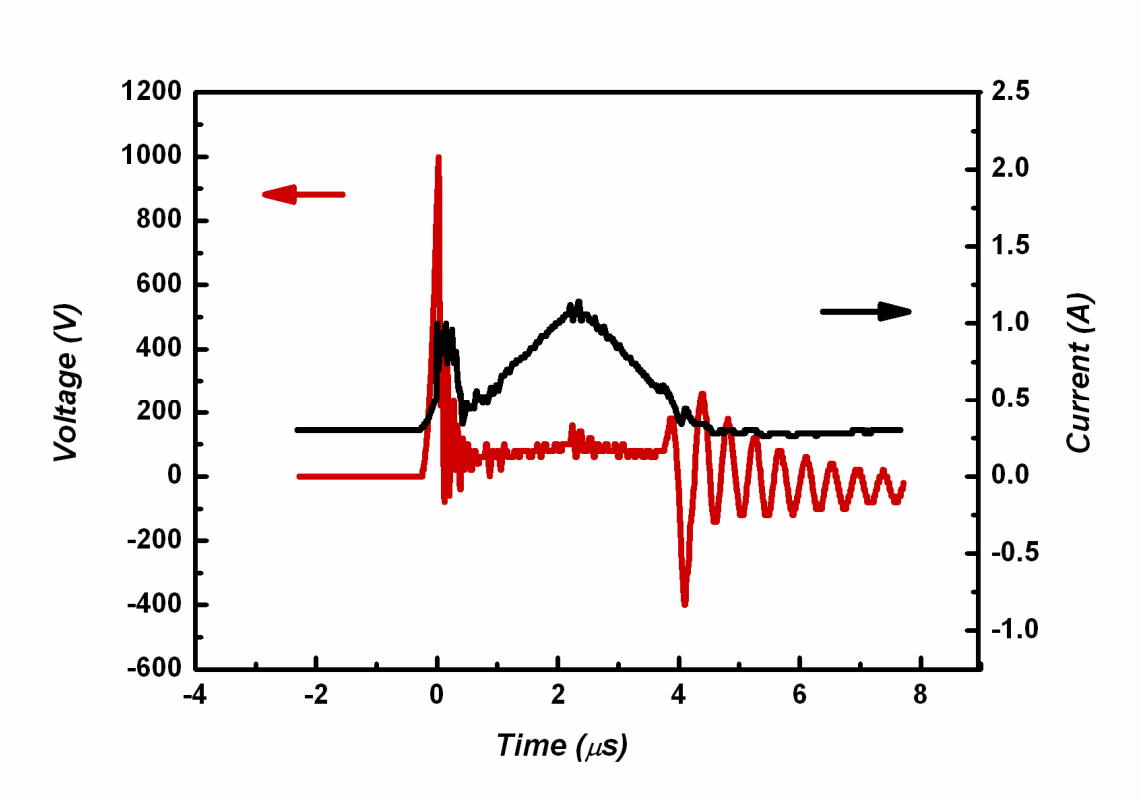

Fig. 1.2. Voltage and current characteristics against time in an aqueous solution.

For the formation of continuous discharge, excluding the gap between electrodes, applied voltage, pulse width, and frequency, solution conductivity also play an important role for plasma generation. The stable and non-fluctuate plasma can be formed in solution with the adequate conductivity. The adequate conductivity helps the transition of liquid to gas phases. Therefore, SPP provides a drawback that it is limited to generate plasma in the nonpolar solvent with the low conductivity and low pressure [1].

1.1.2. Reactivity of solution plasma process

During discharge, the plasma is continuously formed and it generates various kinds of active species. Fig. 1.3 shows the schematic illustration of solution plasma process during discharge and the expected chemical species.

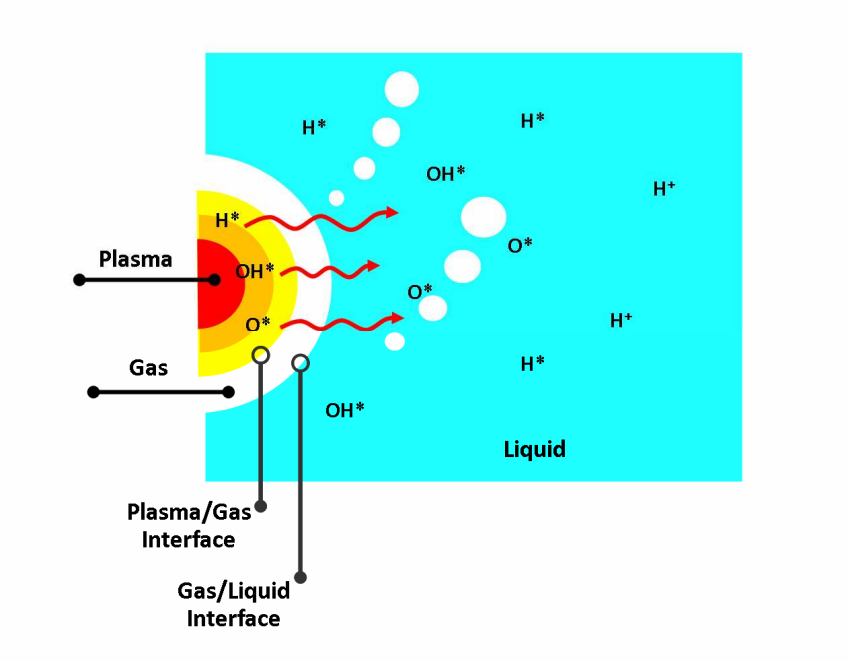

Fig. 1.3. Schematic illustration of solution plasma and their chemical species.

In the discharge system, there are two types of current originating from ions in the solution and plasma. Before reaching of the breakdown voltage, the small bubble is formed by the collisions of ions in the solution between electrodes. For the duration of discharge, both of ionic current and discharge current between electrodes are physically occurred. The formation of the small bubbles in system is affected by the water electrolysis which mostly dependable to the ionic current. The active species are generated by the discharge current of plasma discharge.

In the plasma zone, the water molecules (H_2O) are dissociated by hitting of high energy electron generated during discharge to produce the hydrogen ($H^{\cdot}$) and hydroxyl ($OH^{\cdot}$) radicals and continuously generated the high energy electrons. Their species

extensively attack the surrounding water molecules and stepwise excite to generate the numerous active species. The outcomes of discharge are incessantly formed in dependence of the energy distribution of electrons and they diffuse and transfer into the liquid phase by passing the two boundaries between plasma/gas interface and gas/liquid interface. The competitive reactions can take place in this system to form the molecules of H_2, H_2O_2 and the reform water molecules [4-7]. Moreover, the radiation of UV-ray is observed during discharge in proportional to the solution conductivity and applied voltage [8]. The occurred reaction can be explained by following reactions.

$$H_2O + e^- \longrightarrow OH^\bullet + H^\bullet + e^- \quad (1.1)$$

$$H_2O + e^- \longrightarrow H_2O^+ + 2e^- \quad (1.2)$$

$$H^\bullet + H^\bullet \longrightarrow H_2 \quad (1.3)$$

$$OH^\bullet + OH^\bullet \longrightarrow H_2O_2 \quad (1.4)$$

$$H^\bullet + OH^\bullet \longrightarrow H_2O \quad (1.5)$$

In the liquid phase, consequently, the excitation by the high energy active species is propagated with the solute in the liquid phase and the high number of active species is generated. Such obtained species can be acted as the initiator for various reactions in liquid phase dependent on the desired reaction and the component of chemical solute.

Owing to the continuous generation of active species, SPP is a high efficient process for various applications e.g. nanoparticles synthesis, organic compound decomposition, and water purification [9].

1.1.3. Solution plasma application

Nanoparticles synthesis

The example of the advantages of SPP is Au nanoparticles synthesis. The formation of Au nanoparticles can be observed after discharge in the mixture solution of hydrogen tetrachloroaurate ($HAuCl_4$, $AuCl_4^-$), and sodium dodecyl sulfonate as the stabilizing agent. The reaction of Au nanoparticles formation can be expressed by following reaction.

$$M^+ + H^\bullet \longrightarrow M^0 + H^+ \qquad (1.6)$$

$$Au^{3+} + 3H^\bullet \longrightarrow Au + 3H^+ \qquad (1.7)$$

The general reaction of the metallic particle formation and the occurrence of Au nanoparticles during discharge are explained by the reduction of $H^\cdot$, Equations 1.6 and 1.7, respectively. The reduction rate directly depends on the applied voltage and the $AuCl_4^-$ concentration. The pH of discharge solution turns down in proportional to an increase in discharge time since the H^+ species are increasingly generated. Furthermore, in solution plasma process, the control of Au nanoparticles size and morphology can be adjusted by the discharge time and the concentration of $AuCl_4^-$ and stabilizing agent [10,11].

Organic compound decomposition

It is well known that the oxidative species such as $OH^{\cdot}$ are extensive applicable to the advanced oxidation process for breaking the expected chemical bonding via oxidation [12-14]. Solution plasma process is purposed to be very promising process for organic decomposition in aqueous solution by the dominated active species as $OH^{\cdot}$. The organic dyes, fluorescein-4-isothiocyanate ($C_{21}H_{11}NO_5S$) can be fully decomposed in 300 s using solution plasma incorporated with small amount of potassium chloride (KCl) for simulating the solution conductivity as the real wastewater [4]. The Azo dyes, acid dyes, Direct red B, Reactive brilliant red X-3B, and Cationic red X-GRL can be degraded under the discharge in liquid phase using pulsed high voltage. The presences of O_2 and O_3 play an important role to accelerate the degradation rate of these dyes [15].

Sterilization

SPP is applicable to kill the microorganism in solution instead of the chemical use, ozone, and UV treatment. Due to the clean process of this method comparing to the chemical pathway and UV irradiation, solution plasma process pays regarding to be high performance and non-toxic process for sterilization in water. The efficiency of this method has been realized by the killing and inhibition of two kinds of bacteria, *E. coli* and *S. aureus* which represent gram-negative and gram-positive bacteria, respectively. Only few second of discharge, all bacterial dispersed in water are killed [1]. The bactericidal effect of *E. coli* type gram-negative bacteria is also presented in the generation of plasma by a capillary discharge in water [3]. A role of UV radiation which is one of the high efficient products from solution plasma plays a response for contribution to kill the *E. coli* gram-negative bacterial in water [8].

The next finding of the distinct applications of solution plasma is under developing. Owning to their characteristic and performance, SPP can be further applied into the variety of materials science and chemical engineering to accomplish the desired purposes for instance to decompose the high organic compounds as the polymer structures, to modify the chemical functionality of materials, as well as to generate the novel hybrid materials.

1.2. Mesoporous silica

1.2.1. History of mesoporous silica

Mesoporous silica is defined as the nanoporous material of polysilicate framework with diameter between 2–50 nm. Mesoporous silica was firstly discovered and patented in 1971 by Chiola et al. but it was not unrecognized and unnoticed as much during this time [16]. Until 1990, mesoporous silica was reproduced and studied by Yanagisawa et al. in Waseda University, Japan [17] and it was further developed to notice as the popular nanoporous materials in 1992 by Mobil Corporation laboratories. The first assigned mesoporous silica was named MCM-41 which is abbreviated from Mobil Corporation Materials corresponding to the first notice of this organization and this type mesoporous silica was purposed to be used for molecular sieve. In 2003, the researchers in the University of California, Santa Barbara reported the new type of the mesoporous silica with the hexagonal mesoporous arrangement and larger mesopore size than ever. This type of mesoporous silica has been called Santa Barbara Amorphous type material, SBA-15. Since 1997, the novel exploratory research in the field of mesoporous silica was started and various types of mesoporous silica with

containing the different mesopore size, mesopore morphologies, and mesopore arrangement have been increasingly discovered. Fig. 1.4 shows the mesopore morphology of MCM-41 and SBA-15 type mesoporous silica [18,19]. Until now, there are many types of mesoporous silica which have been investigated around the world. Other examples of the mesoporous silica types are SMS, MSU, and FDU with mesopore arrangement of sponge type, wormlike hole, and cubic, respectively as shown in Fig. 1.5 [20-22].

1.2.2. Mesoporous silica synthesis

Mesoporous silica particles are generally formed in the micron size with being as solid and colorless powder, see Fig. 1.6. It can be easily synthesized via sol-gel method in acid or base condition containing the silica precursor and the surfactant micelles as the template. The schematic illustration of mesoporous silica synthesis is displayed in Fig.1.7. In particular, the formation of the hybrid compound with a periodic structure in which surfactant micelles is firstly surrounded by polycondensed silica species. Chemically, the silica precursor is an important reagent to prepare mesoporous silica. One of the most popular of silica precursors is tetraethoxysilane (TEOS). The surfactant micelle is also necessary to provide the mesopores inside silica matrix. The surfactant type, the surfactants combination, and the concentration of surfactant system are strongly affected to the mesopore morphology and size.

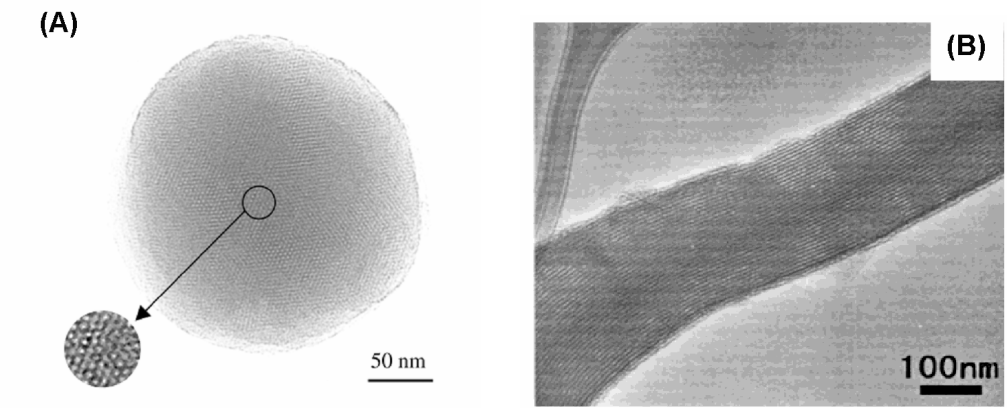

Fig. 1.4. Mesoporous silica particles at beginning discoveries, (A) MCM-41 and (B) SBA-15 types [18,19].

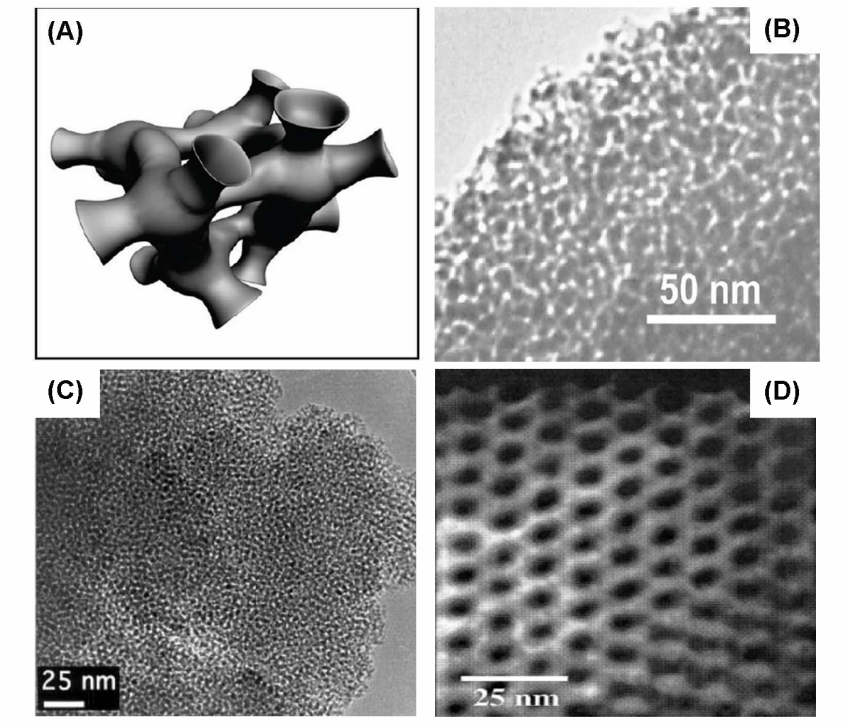

Fig. 1.5. Mesoporous silica particles next generation, (A), (B) SMS type, (C) MSU-J type, and (FDU-1) type [20-22].

The type of surfactant that widely used to prepare mesoporous silica can be classified into 3 categories: cationic surfactant for instance cetyltrimethylammonium

bromide (CTAB), stearyltrimethylammonium bromide (STAB) [23], cetyltrimethylammonium chloride (CTAC) [24], anionic surfactant for instance sodium octylsulfate (SOS) and sodium laurate (SL) [23], and nonionic surfactant for instance triblock copolymer Pluronic type P123 ($EO_{20}PO_{70}EO_{20}$), F127 ($EO_{106}PO_{70}EO_{106}$), F108 ($EO_{133}PO_{50}EO_{133}$), and P104 ($EO_{27}PO_{61}EO_{27}$) [25-29], and amine-type surfactant (n-octylamine) [30]. Moreover, the combination of different types of surfactant has high potential to use as the extraordinary option for mesoporous synthesis.

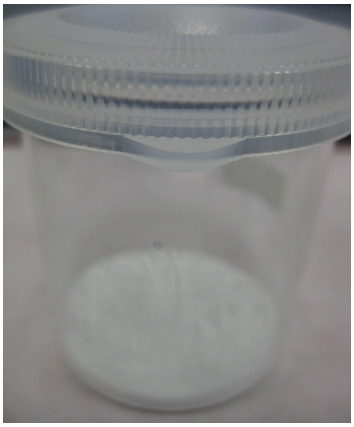

Fig. 1.6. Mesoporous silica appearance.

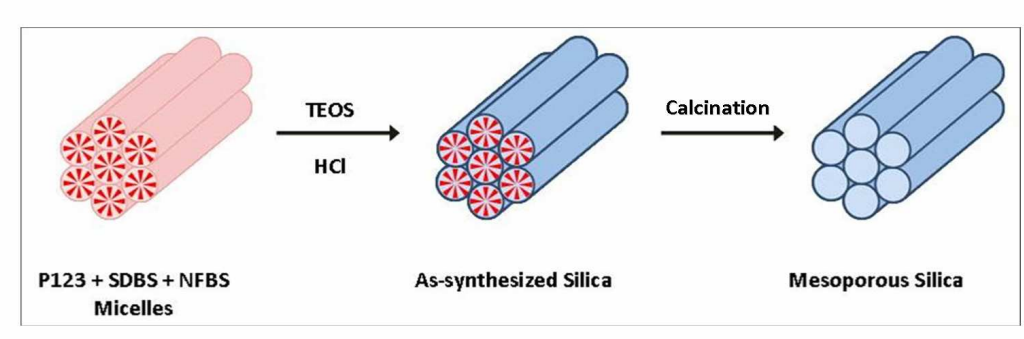

Fig. 1.7. Schematic illustration of the mesoporous silica synthesis.

The sol-gel process combines with the two main reactions: hydrolysis of the organosilane to organosilanol and silanol and condensation of organosilanol and

silanol to polysilicate framework. The use of TEOS as silica precursor in acid condition can be explained by following reactions.

Hydrolysis

$$Si(OR)_4 + H_2O \longrightarrow HO\text{-}Si(OR)_3 + ROH \quad (1.8)$$

$$Si(OR)_4 + H_2O \longrightarrow Si(OH)_4 + 4ROH \quad (1.9)$$

Condensation

$$(OR)_3\text{-}Si\text{-}OH + HO\text{-}Si\text{-}(OR)_3 \longrightarrow (OR)_3\text{-}Si\text{-}O\text{-}Si\text{-}(OR)_3 + H\text{-}OH \quad (1.10)$$

$$(OR)_3\text{-}Si\text{-}OR + HO\text{-}Si\text{-}(OR)_3 \longrightarrow (OR)_3\text{-}Si\text{-}O\text{-}Si\text{-}(OR)_3 + R\text{-}OH \quad (1.11)$$

$$(OH)_3\text{-}Si\text{-}OH + HO\text{-}Si\text{-}(OH)_3 \longrightarrow (OH)_3\text{-}Si\text{-}O\text{-}Si\text{-}(OH)_3 + H\text{-}OH \quad (1.12)$$

Typically, TEOS is hydrolyzed by H_2O in acid solution which acts as the hydrolysis catalyst to form the silanol end-chain molecules. Consequently, the condensation reaction is automatically occurred by the surrounding silanol molecules and the water molecules and the small alcohol are released as the byproduct.

As chemical aspect, the mechanism of the mesopore formation can be explained by the 3 steps:

1. The aggregation of surfactant and silica species is cooperative assembly in the mixture with a beginning step of hydrolysis of silica precursor. The important interactions of the aggregation mechanism are the Van der Waal and hydrogen bonding of the silanol groups and the surrounding surfactant micelles.

2. The liquid crystal-like phase is occurred in these aggregates with the micron size. The hydrolysis of silica precursor is still continuously undergone.

3. The phase separation of such liquid crystal-like phase from solution is occurred and the growth of solid precipitates is stepwise driven by the condensation reaction of the hydrolyzed silicate species. In this step, the morphologies of mesoporous silica are developed dependent on the competition between the mesopore structure self-assembly surface free energy and their overall surface free energy. This means that the mesopore structure self-assembly surface free energy is dominant as the high rate of the mesopore structure formation. The mesoporous silica morphology, particle size, and size distribution are determined by the regularity and the occupying degree of surfactant micelles by the silica species, the rate of condensation depending on acidity and temperature, and the Brownian movement during the precipitation step mainly effecting from temperature [28].

In each type of mesopore morphology, the mechanism of the mesopore formation can be explained by the effect of the interaction of inorganic species, surfactant species and ionic species during the synthesis. The common arrangements of mesopores inside mesoporous silica are presented in the array of hexagonal, worm-like, and cubic.

Hexagonal arrangement

The well-know mesoporous types consisting the hexagonal array of mesopores are MCM-41 and SBA-15. Typically, the crucial role of the different synthesis conditions is chemically described. The MCM-41 type mesoporous silica is generally synthesized in acid solution containing the cationic surfactant micelles (i.e. cetyltrimethylammonium bromide, CTAB) as template. The obtained mesopore size

in this case is generally observed to be about 1.5 nm and it can be expanded up to 10 nm due to the influence of the use of organic cosolvent such as 1,3,5-trimethylbenzene (TMB) for increasing the swelling ability of cationic surfactant micelles [24,31].

The SBA-15 type mesoporous silica provides the superior properties which exhibit the enhanced thermal stability because of their thicker silica walls and high polycondensed silica framework comparing to MCM-41 type. There are three categories of the SBA-15 pores which are primary main mesopore, complementary intrawall mesopore, and intrawall micropore. In such case, the nonionic surfactants for instance the triblock copolymer of poly(ethylene oxide)-poly(propylene oxide)-poly(ethylene oxide) are widely employed as template to synthesize the SBA-15 type mesoporous silica with the ordered 2D hexagonal arrangement [32,33]. Owing to their mesostructural ordering properties, high commercial availability, wide-length accessibility, and ease of removal, this type of surfactant is as a good candidate. The hexagonal mesopore arrangement can be formed by the many types of interactions of surfactant species (S), halide ions (X^-), and inorganic species (I). The synthetic pathways of this type mesopore formation can be explained on the basis of the interaction of (S^+I^-), ($S^+X^-I^+$), (S^-I^+), (S^0I^0), (S^0H^+)(X^-I^+), and ($S^0F^-I^+$), where F^- represents fluoride ion. Other effects e.g. the synthesis pH, temperature, the acid concentration, and the inorganic salt play an important role to the micelle formation. The suitable H-bonding resulting from the properly enough acid concentration and the chemical strength of inorganic salt can be stabilized the arrangement of the surfactant micelles in the form of the ordered 2D rod-like structure [33].

Disordered wormlike structure

The formation of a mesopore structure in the form of the disordered wormlike structure for instance FDU-1 type mesoporous silica has been investigated and the mechanism is still indistinct. The formation mechanism this mesoporous silica type might be constructed via the combination matters of surfactant self-assembly, and surfactant and silicate species self-assembly complexes. Additionally, it might be formed by the influence of the other effects that chemically controlling the mesophases transformation during polycondensation step [29,33].

Cubic symmetry

One of the cubic mesopore structure or cage-like structure is the SBA-1 type mesoporous silica. The cubic (*Pm3n*) type can be formed through the suitable interactions of the surfactant, halide, and inorganic species as described by the $S^+X^-I^+$ pathway, where S^+ represents cationic surfactant species, X^- is halide ion, and I^+ corresponds to positive charge of silica species, in the strong acid concentration. By effectuation of the strong acid concentration affecting to the formation of the cage-like template, the specific surfactant with a large headgroups for instance cetyltriethylammonium bromide, namely CTEABr is highly required. Comparing with the hexagonal arrangement, the special requirements involving acid concentration, type of surfactant especially the large headgroups, and low synthesized temperature, for synthesis this type of mesoporous silica are much more sensitive [28,34].

Moreover, the cage-like mesoporous silica containing the cavities connected to neighbors of 8 and 12, namely SBA-16 (*Im3m*) and FDU-12 (face centered cubic mesopores, *Fm3m*) can be chemically prepared in acid solution using the triblock

copolymer of Pluronic F127 or F108 and F127 with different conditions, respectively [28].

The last process for mesoporous silica preparation is to remove the template inside mesopores, denoted as calcination process which is an important process to obtain the numerous mesopores. The thermal calcination and chemical leaching are the well-know processes which are conventionally employed for organic template removal. Thermal calcination is processed by the high temperature over 500 °C about 5-6 h in air atmosphere. In this process, the organic template is completely removed by the oxidation of organic compounds with oxygen in the system to be small carbonaceous species or volatile carbon species, carbon dioxide (CO_2), and water vapor (H_2O). The decomposition mechanism of template by thermal calcination in air atmosphere can be described. The small fragments of the volatile carbons are located in the main framework at temperature below 200 °C. Consequently, the autooxidation is completed the remained organic species releasing CO_2 and H_2O as the product of the combustion of organic compound in the air atmosphere [35,36]. Mesoporous silica after thermal calcination provides a high thermal and chemical stability because the silica framework is fixed and the small polysilicate molecules which interpenetrate into polysilicate framework providing the flexibility of silica framework are totally removed. On contrary, this calcination process promotes a well-know and acceptable drawback to mesopore size which is extremely reduced as comparing with the as-synthesized silica before calcination. The shrinkage of the silica lattice naturally occurs affecting from the high temperature treatment [35,37].

As another way to remove the organic template inside mesopores, the chemical leaching is accepted to be used. The consideration of the solubility between organic template and subtracted solvent is a crucial point to select the suitable chemical

reagent to totally extract the undesired template. Although this method offers the advantage better to thermal calcination with no influence on the silica lattice shrinkage yielding the retained mesopore size, it strictly requires a high amount of the extracting solvent and occupies a lot time to complete a removal [38]. Following sentences are the commercial solutions or mixtures for chemical extraction to eliminate the organic template in mesoporous silica synthesis. The combinations of HCl/ethanol and HCl/diethyl ether are commercially applied for removing CTAB and CTAC [24,34]. Low acid concentrations such as HCl, H_2SO_4, and HNO_3 are effectively dissolved nonionic surfactant system. Furthermore, the hot ethanol is for extracting the amine-type surfactant [30].

Likewise, the oxidative ozone treatment [39], microwave digestion [40], and CO_2 supercritical fluid extraction [38] as the new pathways for eliminating the organic template are recently investigated to be the additional process which can be appreciatory chosen.

1.2.3. Mesoporous silica application

In the term of application, mesoporous silica is planned to be used as molecular sieves in the beginning discovery. Nowadays, mesoporous silica is highly promising to be employed in many applications for instance the supporting materials for catalyst, water purification, biomedical, and biosensor owing to its properties as high chemical and thermal resistant, inert, as well as non-toxic. Moreover, the modification of mesoporous silica with nanometallic particles and the organic function not only by immersion in the desired solution but also by chemical grafting during synthesis has been increasingly studied for catalyst and biomedical engineering uses.

Catalyst

Based on the host-guest chemistry that is the strategy for promising the simple and economical methods, the nanometallic particles as guest specie incorporated the host mesoporous silica are particularly indispensable for many catalytic capabilities owing to a highly dispersed state of catalytic components in mesopores and a good diffusion of the absorbed molecules during catalysis occasion. Mesoporous silica incorporating with various nanoparticles such as Ag and Au nanoparticles provide a unique opportunity to tune the materials for specific use in the fields of hydrogenation and oxidation. The Ag nanoparticles on mesoporous silica have been chemically proved as the hydrogenation catalyst in the presence of H_2. The nanocatalyst of Pt incorporated mesoporous silica in the form of core-shell nanoparticles is synthesized to be a high performance for oxidation of carbon monoxide (CO) and ethylene hydrogenation owing to the natural catalytic activity of Pt. The catalytic activity of this material is comparable to bare Pt metal but it can provide higher activity and selectivity as well as higher temperature resistant [41].

The functionalized mesoporous silica with the heteroatoms for instance Ti and Al by the chemical reaction for bonding such heteroatoms in the silica framework during synthesis is potentially exhibited the catalytic activity which is promisingly undertake the olefin epoxidation [38].

Water and gas purification

Some efforts have been incorporate the organic moieties into the polysilicate framework in the synthesis pathway for water pollution treatment. The huge amounts of the absorptions of heavy metals for instance chromium (Cr), nickel (Ni), iron (Fe), manganese (Mn), and palladium (Pd) are chemically absorbed on the modified

mesoporous silica with aminopropyl and mercatopropyl groups [42]. Moreover, the SBA-15 type mesoporous silica with the functional groups of ethylenediaminetriacetic acid (EDATAS) on its surfaces can be bonded with the copper ions (Cu^{2+}) and this effect may provide useful as complementary binding groups in molecular imprinting benefits [31]. The absorption of the large molecule pesticides as DDT (1,1,1-trichloro-2,2-bis(p-chlorophenyl)ethane) is shown the good performance in the variety of mesoporous silica types including HMS, MCM-41, SBA-15, and MCM-48. The absorption efficiency of all types reaches over 89% of the initial concentration of DDT solution [43]. To consider the handling of gas pollution, the triamine-grafted MCM-41 type mesoporous silica with the pore expansion is applied to entrap the undesired toxic gases such as carbon dioxide (CO_2) and it also has a small capability for oxygen (O_2), nitrogen (N_2), methane (CH_4), and hydrogen (H_2) uptake [44].

Biomedical application

Mesoporous silica is most promising for immobilization of bioactive molecules for instance β-galactosidase from Kluyleromyces lactis, heparin, and lipase and for drug delivery systems of toremifene citrate and Ibuprofen owing to its characteristics [45-49]. In the field of bio medical application, this material offers the ease of handling, biocompatible with human organism, high pH and thermal resistant, and continuously flow rate providing.

The mesoporous silica support exhibits the high efficiency of immobilization process regarding high surface area and the pores size is nearly the same or slightly higher than the natural biomolecule size. The enzyme activity can be improved by the entrapment of their mesopores owing to the preservation of its native protein structural integrity whereas the free enzyme is still being in the form of prone array

[50]. The rate of drug delivery and the transportation of the enzymes from the support by the controlled diffusion process are affected by the parameters of size, connectivity, and mesopores geometry [49,51]. In the case of enzymes, the properly loaded bioactive in mesoporous supports is strictly concerned because the transportation of those enzymes must be obstructed and the ability of transportation is also related to the adsorption and electrostatic interactions between the mesopores and the immobilized enzymes. Several improvements to stabilize the interaction between enzyme and mesoporous silica include the covalent attachment, partially closed mesopore inlets after enzyme adsorption, encapsulation of the enzyme by loading using by polyelectrolyte or organic polymer metrics, and chemically crosslink of the adsorbed enzyme by crosslinking agents [47,52].

Owing to the presence of silanol groups in the mesoporous silica surface, it makes a favor for the biomolecules adsorption [53]. The functionalization by various methods can be improved the biomolecules absorption. The chemically functional groups presented on the silica surface, the covering degree and homogeneity of surface can evaluate the immobilization capability and the transportation rate of the biomolecules. The functionalization process affects the mesostructure to provide the narrow pore entrances allowing the enzyme impregnation to the channels and the rapid loss of immobilized enzyme activity by leakage. To reduce particle sizes, the increase in external surface area can allow a rapid and high biomolecule loading [54-56].

As the mentioned content, mesoporous silica has been highly developed to be used in many fields of application. Using mesoporous silica as the supporting materials for incorporation of the preferred molecules or particles, it has been studied in the wide ranges of the molecules and particles types, the mechanism of incorporation process,

and their distinct properties. Ag nanoparticles are the most interested nanoparticles which are incorporated into the variety of supporting materials, including mesoporous silica. The hybrid nanocomposite has highly attention applicable to many fields of application for instance catalyst, water purification, as well as biomedical use.

1.3. Silver nanoparticles

Silver (Ag) is the noble metal containing in the IB group of transition element with the atomic number 47 and the atomic mass 109. Ag is naturally found in the form of pure metal and alloy with gold (Au) and other metals such as copper (Cu), lead (Pb), and zinc (Zn), therefore, the pure Ag can be produced as the byproduct of the metal refining process of their alloy. The characteristics of Ag are ductile, soft, and luster. Moreover, Ag provides the high physical properties for instance the highest electrical conductivity and the highest thermal conductivity of all metals. Ag can be used in many fields of application which are the currency coin, jewelry, decorative mirrors, silverware, dentistry, cable line, and optic. Not only the bulk silver can obtain many advantages but also the small Ag particles, namely Ag nanoparticles also provide a wide range of applications.

Ag nanoparticles are the metallic silver in the form of colloid with the diameter less than 100 nm. Considering the difference of the bulk Ag and Ag nanoparticles, it can be observed that the physical properties of nanoparticles are still similar to the bulk whereas the portion of the number of atoms with the particles size is much higher. It results in a change of the physical properties. The position of Ag nanoparticles acts as the bridging in the gap between bulk and atomic forms. Hence, the researches in this field have been developed to produce the possible smallest Ag nanoparticles

without the aggregation effect to improve the physical properties when such particles are applied to the electrical and optical applications [57-59]. Ag nanoparticles have been studied not only in the electrical and optical fields but also in the medical field, especially the microbial inhibition and catalyst. Ag nanoparticles are currently being utilized in several technological fields and are gaining popularity as a form of counter measure against several illnesses that cannot be treated through conventional means.

Ag nanoparticles have several characteristics that make it currently among the most widely used nanoparticles in science. One highly useful characteristic is its antimicrobial property. Ag is transformed into nanoparticle, this anti-microbial property is intensified, making it useful in effectively eliminating fungus, bacteria, and virus.

1.3.1. Silver nanoparticles synthesis

Chemical reaction (wet chemistry)

There are many researches have been reported the chemical path way to synthesize Ag nanoparticles. The solution containing the silver salts that can chemically generate the silver ions and the reducing agent is typically used for creating Ag nanoparticles. The chemical reaction of Ag nanoparticles synthesis is written in below.

$$Ag^{+} + e^{-} \longrightarrow Ag^{0} \qquad (1.13)$$

The most common Ag ions precursor is silver nitrate ($AgNO_3$) and the reducing agent is added to transfer the electrons for Ag ions reduction to be Ag nanoparticles. While it is rarely to find the other sources of silver for instance silver tetradecanoate, silver chlorate, and silver benzoate [60-62]. One of the most common reducing agent

is sodium borohydride ($NaBH_4$) which provides a strong reducing activity to generate the free electrons for reduction [59,63-65]. Not only $NaBH_4$ but also other reducing agents were chemically chosen to reduce the Ag ions to Ag particles. Sodium ascorbate, amino acids serine, aspartic acid, histidine, tyrosine, tannic acid, glycerine, sodium linoleate/linoleic acid, sodium oleate, and hydrazine hydrate are also employed as the reducing agent in the Ag ions system [66-71].

In addition, in order to control the particle size and morphology, the stabilizing agents as various types of the water-soluble polymers for instance polyvinyl alcohol (PVA), poly(vinyl acetate) (PVAc), poly(vinylpyrrolidone) (PVP), sodium dodecyl sulfate (SDS), and hyperbranched poly(amido-amine) are generally used [59,68,71-73].

In various bio-polymer systems for instance peptides, gelatin, and methylhydroxy ethyl cellulose, the formation of Ag nanoparticles with the stable small average particles size was occurred using $AgNO_3$ as the Ag source [66,67].

Chemical deposition

In general, the chemical vapour deposition (CVD) has been widely employed to fabricate the metallic nanofilms because of the low temperature need and the variety of metallic precursors. The CVD setup is schemed as shown in Fig. 1.8. The Chemical vapour deposition technique is applicable to the preparation of Ag nanofilms with various available precursors. The silver halide (e.g. AgF and AgI), Silver organohalide ($[C_4F_7Ag]_n$) and silver complex molecules (e.g. $Ag(O_2CCF_3)(PEt_3)$, $Ag(O_2CC_2F_5)(PEt_3)$, $Ag(OC_6H_4Me\text{-}2(PPh_3)_3$, $[Ag(OC_6H_4Me\text{-}2(PPh_3)_3]\cdot PhOH$ and $[Ag(3,5\text{-}(CF_3)_2C_3HN_2)]_3$) are the examples of the distinct Ag precursors [74-77]. The enhancement of the chemical vapour deposition has been developed to broadly use for

Ag nanofilms deposition on the desired substrate. One of the examples is the direct liquid injection metal-organic CVD by using silver pivalate (AgPiv) as Ag precursor which provide the large scale deposition and low consuming time [78].

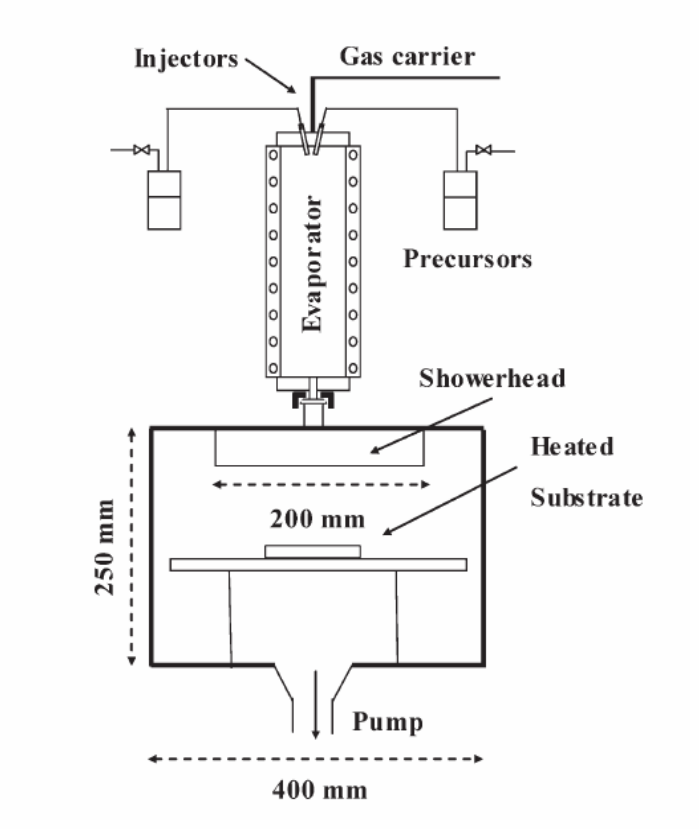

Fig. 1.8. Direct liquid injection metal-organic chemical vapour deposition (DLI-MOCVD) setup [78].

Laser ablation

Laser ablation (LA) technique is a versatile process studying on a focused high power laser beam hitting onto the surface of a solid target, which is submerged under a liquid, see Fig. 1.9. The interaction of the laser attacking to the target causes the vaporization of target in the form of an ablation cloud containing species such as atoms, ions, and clusters with high kinetic energy. The species in the cloud can collide and react with the surrounding molecules in liquid, forming new compounds which

consist of the components from both the target and the liquid. Compared to the conventional methods for instance chemical vapour deposition, pulsed laser ablation in vacuum, and chemical synthesis, this technique provides many distinct advantages which include a chemically simple and clean synthesis without any byproduct, economically experimental setup, and ease of control. Owing to their advantages, it can allow to extensively design the combination of the selected solid targets and liquid to fabricate the desired compound nanostructures [79]. The formation of Ag nanoparticles is one of the products which can be produced by laser ablation in liquid. By using the liquid ammonium as the ablation medium, the laser beam is focused to Ag target and the Ag nanoparticles are formed and stabilized by this medium as the nanosuspension [80]. Ag nanosize colloids are produced by the fragmentation of Ag hydrosol which is prepared by the chemical synthesis. The laser wavelength uses pay regarding to the particles morphology, size, and size distribution varied in the wide range scale [81,82].

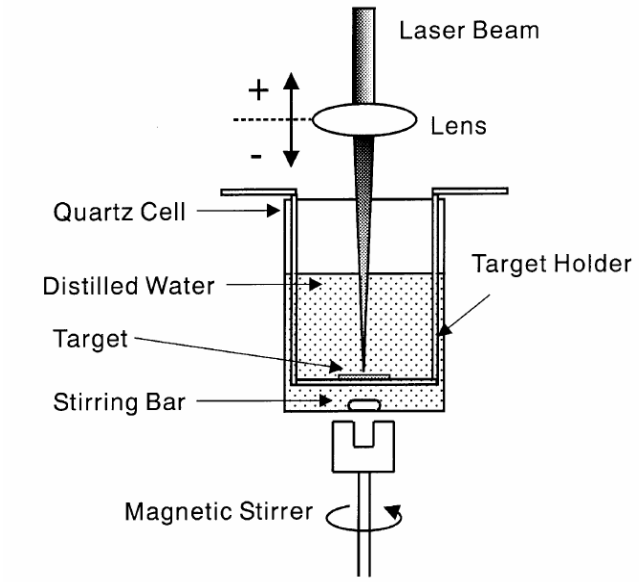

Fig. 1.9. Schematic image of laser ablation setup [82].

1.3.2. Silver nanoparticles application

Antimicrobial agent

It is well know that Ag nanoparticles pay attention a lot to be incredibly promising to the antimicrobial agent. The killing and inhibition mechanism of Ag nanoparticles affecting to the survival of the microorganism can be described.

Bactericidal effects using of Ag nanoparticles which provide the high number of particles per unit area result high reactivity and their maximized anti-bacterial effects due to the nanosize particles. Ag nanoparticles which have an extremely large relative surface area and a extremely small size increases the contact to microorganism such as bacteria, virus, and fungi resulting to vastly improve their effectiveness and the capability for antibacterial residual killing. Ag nanoparticles have very high reactivity with protein molecules. After contacting to bacteria and fungus, they harmfully affect cellular metabolism and inhibit cell growth. The basal respiration of cell with the propagation of the metabolism of the electron transfer system and the substrate transportation into the microbial cell membrane is suddenly suppressed. Furthermore, their inhibition activity has the influence on the proliferation, multiplication, and growth of those microorganism cells which cause infection, odor, itchiness, and sores [83-87].

Ag nanoparticles incorporated into various kinds of materials as the support have been prepared to retain and improve the life time of the bactericidal effects by reducing the rate of diffusion and protect of the chemical change. Hence, such hybrid materials are widely applied to use in order to prohibit the growth of bacteria. In addition, they can be applied to other healthcare products such as wound dressings, anti-bacterial hand gel, and household surfactant [62].

Catalyst

It is considered that part of the gases in the atmosphere is turned into active gas species by means of catalysis on the metallic Ag nanoparticles, thereby exploring the catalytic activity and selectivity for various reactions for instance hydrogenation and oxidation by the absorption of H_2 and O_2, respectively.

Ag nanoparticles play an important role for hydrogenation catalysis for high activity and selectivity. The bear Ag nanopaticles as well as the incorporation of Ag nanoparticles in the support materials can provide the mentioned benefits to produce the desired compounds in the different conditions. The hydrogenation of acrolein can be performed to convert into the allyl alcohol and propanol by the bare Ag nanopaticles and the Ag nanoparticles on the SiO_2 and Al_2O_3 support materials. The hydrogenation efficiency depends on the amount of applied H_2, the pressure, and the properties of support material which reported that the high acidity of supporting surface decreased the hydrogenation efficiency [88,89]. The hybrid nanocomposites of Ag nanoparticles and SiO_2 are applicable to the chloronitrobenzenes hydrogenation in the presence of H_2. The hydrogenation efficiency is strongly depended on the size of Ag nanoparticles and the interaction between Ag nanoparticles and silica framework also play a crucial role in the catalytic system [90]. The hydrogenation mechanism of ethylene can be described by the homoexchange of H_2 in the Ag surface to generate hydrogen species and their species further react to the ethylene molecules converting to ethane molecules [91]. In addition, the incorporation of Ag nanoparticles on SBA-15 mesoporous silica has high potential to be used as the oxidation catalyst. The high percent conversion of carbon monoxide (CO) to carbon dioxide (CO_2) is occurred in the surface of Ag nanoparticles with the small nanosize [92].

1.4. Objective

The objectives of this study are written as following sentences:

1. I studied and evaluated the feasibility of solution plasma process for the organic template removal inside mesoporous silica which was prepared in various acid solutions. The solution plasma ability for template removal and the mesoporous silica characteristics were confirmed by the characterizations of X-ray diffraction (XRD), transmission electron microscope (TEM), scanning electron microscope (SEM), thermogravimetric analysis (TGA), Fourier transform infrared spectroscopy (FTIR), N_2 adsorption-desorption measurement, and optical emission spectroscopy (OES).

2. The pH and discharge time characteristics influencing to the feasibility of solution plasma process for organic template removal were scientifically determined in the comparisons of the XRD, TEM, OES, and BET surface area results.

3. The solution plasma process was proposed to employ as a single-step process for Ag nanoparticles incorporation on mesoporous silica and organic template removal inside mesoporous silica. The outcomes after solution plasma process were characterized using X-ray diffraction (XRD), transmission electron microscope (TEM), scanning electron microscope (SEM), Fourier transform infrared spectroscopy (FTIR), UV-VIS spectroscopy, electron-dispersive X-ray spectroscopy (EDX), N_2 adsorption-desorption measurement, and optical emission spectroscopy (OES).

4. The obtained outcome, Ag nanoparticles incorporated mesoporous silica was preliminarily evaluated as the hydrogenation catalyst for the unsaturated oleic acid conversion to the saturated stearic acid in ethanol and butanol system. The hydrogenation outcome was determined by the remained permanganate ions after oxidation using the measurement of UV-VIS spectroscopy.

References

[1] O. Takai, *Pure Appl. Chem.*, 2008, **80**, 2003.

[2] S. Potocky, N. Saito, and O. Takai, *Thin Solid Films*, 2009, **518**, 918.

[3] Y. C. Hong, H. J. Park, B. J. Lee, W. S. Kang, and H. S. *Uhm, Phys. Plasma*, 2010, **17**, 053502.

[4] P. Baroch, V. Anita, N. Saito, and O. Takai, *J. Electrostat.*, 2008, **66**, 294.

[5] J. W. T. Spinks and R. J. Woods, "An Introduction to Radiation Chemistry", 3rd edn., Wiley, New York, 1976.

[6] C. J. Hochanadel, *J. Phys. Chem.*, 1952, **56**, 587.

[7] X. Lu, Y. Pan, K. Liu, and M. Liu, *J. Appl. Phys.*, 2002, **91**, 24.

[8] P. Lukes, M. Clupek, V. Babicky, and P. Sunka, *Plasma Sources Sci. Technol.*, 2008, **17**, 024012.

[9] P. Baroch, N. Saito, and O. Takai, *J. Phys. D: Appl. Phys.*, 2008, **41**, 085207.

[10] J. Hieda, N. Saito, and O. Takai, *Mater. Res. Soc. Symp. Proc.*, 2008, **1056**, HH 03-39.

[11] J. Hieda, N. Saito, and O. Takai, *J. Vac. Sci. Technol. A*, 2008, **26**, 854.

[12] M. Sun, Y. Wu, J. Li, N. H. Wang, J. Wu, K. F. Shang, and J. L. Zhang, *Plasma Chem. Plasma Process.*, 2005, **25**, 31-40.

[13] H. Wang, J. Lei, X. Quan, and Y. Wu, *Appl. Catal. B: Environ.*, 2008, **83**, 72.

[14] A. T. Sugiarto, T. Ohshima, and M. Sato, *Thin Solid Films*, 2002, **407**, 174.

[15] B. Yang, M. Zhou, and L. Lei, *Chemosphere*, 2005, **60**, 405-411.

[16] V. Chiola, J. E. Ritsko, and C. D. Vanderpool, Application No. US 3556725D A filed on 26-Feb-1969; Publication No. US 3556725 A published on 19-Jan-1971.

[17] T. Yanagisawa, T. Shimizu, K. Kuroda, and C. Kato, *Bull. Chem. Soc. Jpn.*, 1990, **63**, 988.

[18] M. Etienne, B. Lebeau, and A. Walcarius, *New J. Chem.*, 2002, **26**, 384.

[19] D. Zhao, J. Sun, Q. Li, and G. D. Stucky, *Chem. Mater.*, 2000, **12**, 275.

[20] A. Galarneau, F. Sartori, M. Cangiotti, T. Mineva, F. D. Renzo, and M. F. Ottaviani, *J. Phys. Chem. B*, 2010, **114**, 2140.

[21] E. Prouzet, F. Cot, C. Boissiere, P. J. Kooyman, and A. Larbot, *J. Mater. Chem.*, 2002, **12**, 1553.

[22] C. Yu, Y. Yu, and D. Zhao, *Chem. Commun.*, 2000, 575.

[23] T. Ohkubo, T. Ogura, H. Sakai, and M. Abe, *Micropor. Mesopor. Mater.*, 2007, **312**, 42.

[24] C. Y. Chen, H. X. Li, and M. E. Davis, *Micropor. Mater.*, 1993, **2**, 17.

[25] X. Meng, D. Lu, and T. Tatsumi, *Micropor. Mesopor. Mater.*, 2007, **105**,15.

[26] D. Li, H. Zhou, and I. Honma, *Nat. Mater.*, 2004, **3**, 65.

[27] C. W. Wu, T. Ohsuna, T. Edura, and K. Kuroda, *Angew. Chem.*, 2007, **119**, 5460.

[28] M. Mesa, L. Sierra, and J. L. Guth, *Micropor. Mesopor. Mater.*, 2008, **112**, 338.

[29] Z. Jin, X. Wang, and X. Cui, *J. Non-Cryst. Solids.*, 2007, **353**, 2507.

[30] A. G. S. Prado and C. Airoldi, *J. Mater. Chem.*, 2002, **12**, 3823.

[31] M. A. Markowitz, J. Klaehn, R. A. Hendel, S. B. Qadriq, S. L. Golledge, D. G. Castner, and B. P. Gaber, *J. Phys. Chem. B*, 2000, **104**, 10820.

[32] D. Zhao, J. Feng, Q. Huo, N, Melosh, G. H. Fredrickson, B. F. Chmelka, and G. D. Stucky, *Science*, 1998, **279**, 548.

[33] Z. Jin, X. Wang, and X. Cui, *Colloids Surfaces A: Physicochem. Eng. Aspects.*, 2008, **316**, 27.

[34] H. M. Kao, T. Y. Shen, J. D. Wu, and L. P. Lee, *Micropor. Mesopor. Mater.*, 2008, **110**, 461.

[35] F. Bérubé and S. Kaliaguine, *Micropor. Mesopor. Mater.*, 2008, **115**, 469.

[36] C.-M. Yang, B. Zibrowius, W. Schmidt, and F. Schuth, *Chem. Mater.*, 2004, **16**, 2918.

[37] F. Kleitz, W. Schmidt, and F. Schüth, *Micropor. Mesopor. Mater.*, 2003, **65**, 1.

[38] R. Van Grieken, G. Calleja, G. D. Stucky, J. A. Melero, R. A. García, and J. Iglesias, *Langmuir*, 2003, **19**, 3966.

[39] M. T. J. Keene, R. Denoyel, and P. L. Llewellyn, *Chem. Commun*., 1998, 2203.

[40] B. Tian, X. Liu, C. Yu, F. Gao, Q. Luo, S. Xie, B. Tu, and D. Zhao, *Chem. Commun.*, 2002, 1186.

[41] S. H. Joo, J. Y. Park, C. K. Tsung, Y. Yamada, P. Yang, and G. A. Somorjai, *Nat. Mater.*, 2009, **8**, 126.

[42] A. M. Burke, J. P. Hanrahan, D. A. Healy, J. R. Sodeau, J. D. Holmes, and M. A. Morris, *J. Hazard. Mater.*, 2009, **164**, 229.

[43] H. Tian, J. Li, L. Zou, Z. Mu, and Z. Hao, *J. Chem. Technol. Biotechnol.* 2009, **84**, 490.

[44] Y. Belmabkhout, R. Serna-Guerrero, and A. Sayari, *Ind. Eng. Chem. Res.*, 2010, **49**, 359.

[45] C. Giacomini, A. Villarino, L. Franco-Fraguas, and F. Batista-Viera, *J. Mol. Catal. B: Enzym.*, 1998, **4**, 313.

[46] M. S. Ahola, E. S. Sailynoja, M. H. Raitavuo, M. M. Vaahtio, J. I. Salonen, and A. U. O. Yli-Urpo, *Biomater.*, 2001, **22**, 2163.

[47] J. He, Y. Xu, H. Ma, Q. Zhang, D. G. Evans, and X. Duan, *J. Colloid Interface Sci.*, 2006, **298**, 780.

[48] P. Kortesuo, M. Ahola, S. Karlsson, I. Kangasniemi, A. Yli-Urpo, and J. Kiesvaara, *Biomater.*, 2000, **21**, 193.

[49] J. Andersson, J. Rosenholm, S. Areva, and M. Linden, *Chem. Mater.*, 2004, **16**, 4160.

[50] A. K. Dunker and A. Fernandez, *Trends Biotechnol.*, 2007, **25**, 189.

[51] P. Horcajada, A. Ramila, J. Perez-Pariente, and M. Vallet-Regi, *Micropor. Mesopor. Mater.*, 2004, **68**, 105.

[52] A. S. M. Chong and X. S. Zhao, *Catal. Today*, 2004, **93–95**, 293.

[53] A. Salis, D. Meloni, S. Ligas, M. F. Casula, M. Monduzzi, V. Solinas, and E. Dumitriu, *Langmuir*, 2005, **21**, 5511.

[54] I. Izquierdo-Barba, A. Martinez, A. L. Doadrio, J. Perez-Pariente, and M. Vallet-Regı, *Eur. J. Pharm. Sci.*, 2005, **26**, 365.

[55] W. Zeng, X. F. Qian, Y. B. Zhang, J. Yin, and Z. K. Zhu, *Mater. Res. Bull.*, 2005, **40**, 766.

[56] L. F. Giraldo, B. L. Lopez, L. Perez, S. Urrego, L. Sierra, and M. Mesa, *Macromol. Symp.*, 2007, **258**, 129.

[57] Y. Ohko, T. Tatsuma, T. Fujii, K. Naoi, C. Niwa, Y. Kubota, and A. Fujishima, *Nat. Mater.*, 2003, **2**, 29.

[58] S. K. Medda, M. Mitra, and G. De, *J. Chem. Sci.*, 2008, **120**, 565.

[59] J. Nelayah, M. Kociak, O. Stephan, F. J. Garcia de Abajo, M. Tence, L. Henrard, D. Taverna, I. Pastoriza-Santos, L. M. Liz-Marzan, and C. Colliex, *Nat. Phys.*, 2007, **3**, 348.

[60] M. Yamamoto, Y. Kashiwagi, and M. Nakamoto, *Langmuir*, 2006, **22**, 8581.

[61] T. H. Tsai, S. Thiagarajan, and S. M. Chen, *J. Appl. Electrochem.*, 2010, **40**, 493.

[62] A. Kumar, P. K. Vemula, P. M. Ajayan, and G. John, *Nat. Mater.*, 2008, **7**, 236.

[63] F. Douglas, R. Yanez, J. Ros, S. Marin, A. de la Escosura-Muniz, S. Alegret, and A. Merkoci, *J. Nanopart. Res.*, 2008, **10**, 97.

[64] A. Y. Olenin, Y. A. Krutyakov, A. A. Kudrinskii, and G. V. Lisichkin, *Colloid J.*, 2008, **70**, 71.

[65] M. S. Leite, V. Rodrigues, and D. Zanchet, *Progr. Colloid Polym. Sci.*, 2004, **128**, 131.

[66] K. Belser, T. V. Slenters, C. Pfumbidzai, G. Upert, L. Mirolo, K. M. Fromm, and H. Wennemers, *Angew. Chem.*, 2009, **121**, 3715.

[67] N. V. Serebryakova, O. Y. Uryupina, and V. I. Roldughin, *Colloid J.*, 2005, **67**, 79.

[68] J. L. Elechiguerra, J. L. Burt, J. R. Morones, A. Camacho-Bragado, X. Gao, H. H. Lara, and M. J. Yacaman, *J. Nanotech.*, 2005, **3**, 1.

[69] R. Das, S. S. Nath, D. Chakder, G. Gope, and R. Bhattacharjee, *J. Nanotech. Online*, 2009, **5**, 1.

[70] Y. H. Kim, D. K. Lee, and Y. S. Kang, *Colloids Surfaces A: Physicochem. Eng. Aspects*, 2005, **257-258**, 273.

[71] W. Zhang, X. Qiao, and J. Chen, *Mater. Chem. Phys.*, 2008, **109**, 411.

[72] N. A. M. Barakat, K.-D Woo, M. A. Kanjwal, K. E. Choi, M. S. Khil, and H. Y. Kim, *Langmuir*, 2008, **24**, 11982.

[73] C. J. Huang and F. S. Shieu, *Colloid Polym. Sci.*, 2005, **284**, 192.

[74] R. Szczesny, I. Szymanska, P. Piszczek, L. Dobrzanska, and E. Szlyk, *Mater. Sci. Poland*, 2005, **23**, 671.

[75] L. Gao, P. Harter, Ch. Linsmeier, A. Wiltner, R. Emling, and D. Schmitt-Landsiedel, *Microelectro. Eng.*, 2005, **82**, 296.

[76] D. A. Edwards, M. F. Mahon, K. C. Molloy, and V. Ogrodnik, *Inorg. Chim. Acta*, 2003, **349**, 37.

[77] Y. Chi, E. Lay, T. Y. Chou, Y. H. Song, and A. J. Carty, *Chem. Vap. Deposition*, 2005, **11**, 206.

[78] J. Mungkalasiri, L. Bedel, F. Emieux, J. Dore, F. N. R. Renaud, C. Sarantopoulos, and F. Maury, *Chem. Vap. Deposition*, 2010, **16**, 35.

[79] D. Jang and D. Kim, *Appl. Phys. A*, 2004, **79**, 1985.

[80] P. Smejkal, J. Pfleger, and B. Vlckova, *Appl. Phys. A*, 2010, **101**, 37.

[81] P. Smejkal, J. Pfleger, K. Siskova, B. Vlckova, O. Dammer, and M. Slouf, *Appl. Phys. A*, 2004, **79**, 1307.

[82] T. Tsuji, K. Iryo, Y. Nishimura, and M. Tsuji, *J. Photochem. Photobiology A: Chem.*, 2001, **145**, 201.

[83] M. Rai, A. Yadav, and A. Gade, *Biotech. Adv.*, 2009, **27**, 76.

[84] D. M. Eby, N, M, Schaeublin, K. E. Farrington, S. M. Hussain, and G. R. Johnson, *ACS Nano*, 2009, **3**, 984.

[85] O. Choi, K. K. Deng, N. J. Kim, L. Ross Jr., R. Y. Surampalli, and Z. Hu, *Water Res.*, 2008, **42**, 3066.

[86] J. S. Kim, E. Kuk, K. N. Yu, J. H. Kim, S. J. Park, H. J. Lee, S. H. Kim, Y. K. Park, Y. H. Park, C. Y. Hwang, Y. K. Kim, Y. S. Lee, D. H. Jeong, and M. H. Cho, *Nanomed-Nanotechnol., Biol. Med.*, 2007, **3**, 95.

[87] V. K. Sharma, R. A. Yngard, and Y. Lin, *Adv. Colloid Interface Sci.*, 2009, **145**, 83.

[88] K. Brandt, M. E. Chiu, D. J. Watson, M. S. Tikhov, and R. M. Lambert, *J. Am. Chem. Soc.*, 2009, **131**, 17286.

[89] C. E. Volckmar, M. Bron, U. Bentrup, A. Martin, and P. Claus, *J. Catal.*, 2009, **261**, 1.

[90] Y. Chen, C. Wang, H. Liu, J. Qiu, and X. Bao, *Chem. Comm.*, 2005, 5298.

[91] H. Ehwald, A. A. Shestov, and V. S. Muzykantov, *Catal. Lett.*, 1994, **25**, 149.

[92] D. Tian, G. Yong, Y. Dai, X. Yan, and S. Liu, *Catal. Lett.*, 2009, **130**, 211.

Chapter 2. Solution Plasma Process for Template Removal in Mesoporous Silica Synthesis

The plasma discharge in aqueous solution was scientifically studied and applied to template removal in mesoporous silica synthesis. Highly dispersed spherical mesoporous silica particles were synthesized by the ternary surfactant system containing the Pluronic P123 copolymer ($EO_{20}PO_{69}EO_{20}$), sodium dodecylbenzene sulfonate, and 1,1,2,2,3,3,4,4,4-nonafluoro-1-butane sulfonate, via the sol-gel method in acid solutions. The solution plasma process (SPP), instead of conventional thermal calcinations, was used to remove the template. The mechanism of the removal of the organic template occurred via oxidation by the hydroxyl radicals generated during discharge. The transformation of a mesopore structure from a disordered wormlike structure to a hexagonally arranged structure was observed by X-ray diffraction analysis and was confirmed by transmission electron microscopy. The results of the thermal analysis and functional group identification of mesoporous silica after SPP showed evidence of organic template removal. The surface area calculated using the Brunauer-Emmett-Teller (BET) theory and the mean pore diameter results could be used to evaluate the plasma efficiency, demonstrating that this method does not affect the pore size in the case of discharge in a solution of pH 3 compared with the results of thermal calcination. Hence, SPP was proved to be highly efficient for organic template removal, exhibiting short consumption time and less contamination.

2.1. Introduction

The solution plasma process (SPP) has been increasingly investigated owing to its many benefits such as nanoparticle synthesis, sterilization, and water treatment. Even though SPP is quite a new process, it has already shown versatility owing to its advantages. During a discharge process, active species such as O, H, and OH radicals, UV radiation, and high energy electrons are extensively produced [1-5]. The numbers of various active species are directly dependent on various SPP parameters including the pH of the discharge solution, the distance between electrodes, the solution conductivity, and the usage of power voltage. Gold nanoparticles were successfully synthesized using glow discharge in an aqueous solution via reduction by H radicals, which were abundantly generated during the discharge process [6]. Organic compounds could also be decomposed by the discharge in liquid. In one study, it was reported that the DC nonpulsed diaphragm discharge in various solutions has high potential for use in the decomposition of the nonelectrolyte Saturn red L4B and Malachite green dyes via oxidation by OH radicals [7]. Moreover, in the sterilization application, gram-negative bacteria are killed under the action of pulsed spark discharge in water and the action of sterilization was similar to the action of the energy consumption for other plasma sources, including corona, arc, and DC discharges [8].

The discovery of mesoporous silica was first reported by the Mobil group researchers in 1992. Until now, the study of mesoporous silica materials and their modifications has been extensively performed owning to their many applications such as in catalyst support, water filtration membranes, and selective membranes, as well as in biomedical fields [9-12]. One of the highly studied parameters of mesoporous

silica is mesopore texture. There are many structures of mesopores of mesoporous silica containing lamellar arrangement, hexagonal arrangement, cubic symmetry, and disordered wormlike mesostructures [13,14]. All these mesostructures directly depend on the pH of the synthesized solution, the type of surfactant used as the template, and the temperature of the isothermal process during synthesis [15]. Pluronic-type surfactant is one of the most popular surfactants to be employed as the template; examples of this type of surfactant are the Pluronic copolymers P123 ($EO_{20}PO_{69}EO_{20}$), F127 ($EO_{106}PO_{70}EO_{106}$), F108 ($EO_{133}PO_{50}EO_{133}$), and P104 ($EO_{27}PO_{61}EO_{27}$),[9,14,16,17] which can be used to prepare different types of mesopore inside mesoporous silica containing hexagonal arrangement (SBA-15) and cubic symmetry (SBA-16) mesopore structures [16,17]. Additionally, to prepare highly dispersed single-crystal mesoporous silica, it is necessary to use a fluorinated surfactant or a low-surface-tension surfactant to reduce surface tension in the system. For instance, a single-crystal rhombododecahedron mesoporous morphology was successfully synthesized using various fluorinated surfactants such as FC-4911 ($CF_3(CF_2)_3SO_2NH(CH_2)_3N(CH_3)_3I$) and FC-480 ($CF_3(CF_2)_3SO_3K$).[18] All of the synthesized mesoporous silica particles exhibited a mesoporous morphology in the form of the cubic symmetry [18].

In this present study, SPP plays an important role in template removal after the synthesis of the mesoporous silica particles. The ternary surfactant system containing Pluronic P123 copolymer ($EO_{20}PO_{69}EO_{20}$), sodium dodecylbenzene sulfonate (SDBS), and 1,1,2,2,3,3,4,4,4-nonafluoro-1-butane sulfonate (NFBS) was successfully used to prepare spherical mesoporous silica particles via a simple sol-gel method under various acid concentrations using 1, 2, and 3 M hydrochloric acid (HCl) solutions, hereafter denoted PFS1M, PFS2M, and PFS3M (PFS*a*M), respectively, where PFS is

the mesoporous silica synthesized using the surfactant system of the **P**123 copolymer, **F**luorinated surfactant (NFBS), and **S**odium dodecylbenzene sulfonate (SDBS), and *a*M is the acid concentration of the synthesized solution. For instance 1 M means that 1 M HCl solution was used. Subsequently, SPP, instead of conventional processes, was employed under controlled plasma conditions to remove the surfactant template. The pH of the SPP solutions in the range of 3-11 was evaluated as a function of the acid concentration of the solutions during synthesis. The overall reaction of mesoporous silica in this present study is shown in Fig. 2.1.

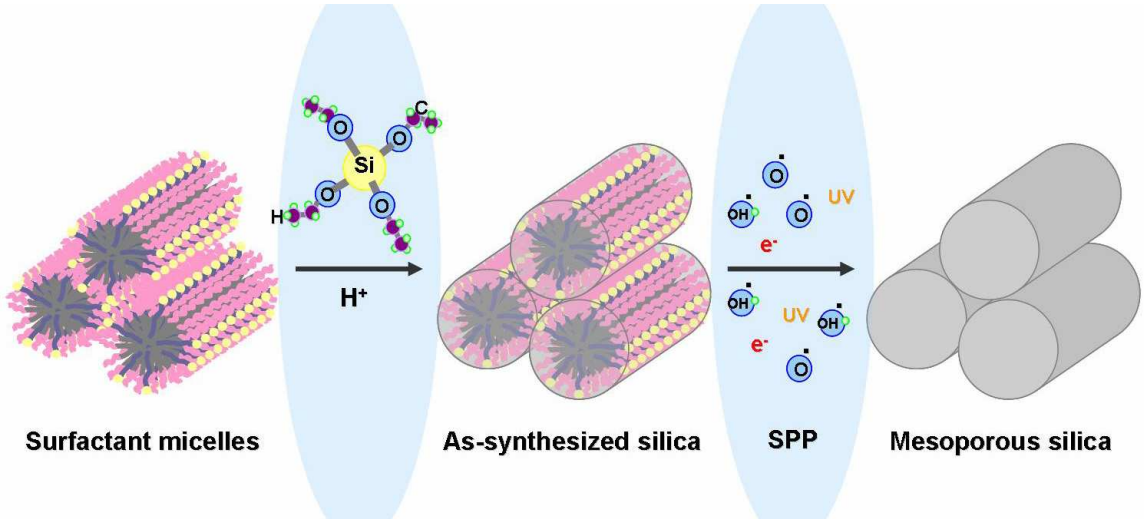

Fig. 2.1. Schematic representation of overall reaction in mesoporous silica synthesis using ternary surfactant system as template, TEOS as silica precursor, and calcination by solution plasma process (SPP).

2.2. Experimental Procedures

In the synthesis, the surfactant system was first prepared by dissolving 0.5 g of the P123 copolymer ($EO_{20}PO_{69}EO_{20}$), 0.1 g of 1,1,2,2,3,3,4,4,4-nonafluoro-1-butane

sulfonate (NFBS), and 0.084 g of sodium dodecylbenzene sulfonate (SDBS) in 38 ml of 1-3 M HCl solutions. The mixture was continuously stirred until a solution was formed. Consequently, 2.15 g of tetraethoxysilane (TEOS) was added to the solution, and then the solution was further kept under static condition at room temperature for 24 h to generate a white precipitate. The precipitate was collected by filtration, thoroughly washed with distilled water, and dried by air drying. To remove the surfactant template, SPP was carried out in an aqueous solution by adjusting the pH of the media to 3, 7, and 11. The typical solution plasma conditions, namely, voltage, pulse frequency, pulse width, and electrode distance were 2.4 kV, 15 kHz, 2 μs, and 0.3 mm, respectively. The SPP setup scheme image is displayed in Fig. 2.2. Moreover, the discharge time for SPP was fixed at 15 min.

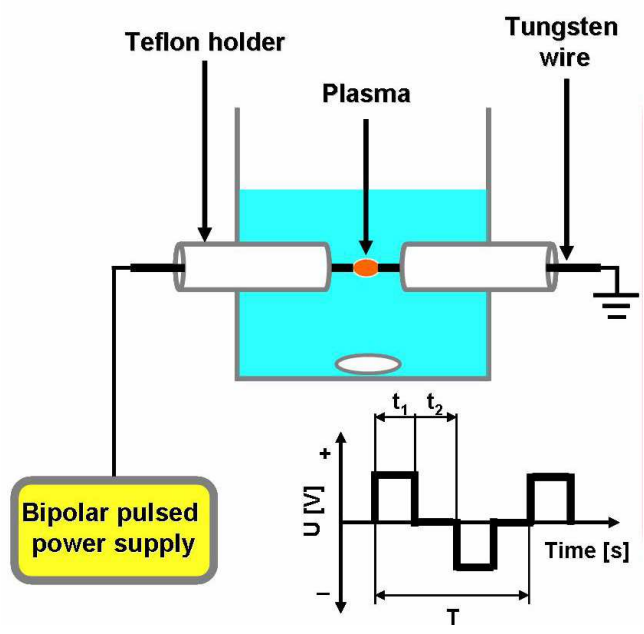

Fig. 2.2. Schematic image of the experimental setup of solution plasma.

For the characterization of all the samples, X-ray diffraction (XRD) patterns were measured using XRD Rigaku Smartlab with Cu Kα radiation (λ = 0.154 nm). The

diffraction patterns were collected in the range of 2θ = 0.1-5.0° using a scanning rate of 0.5°/min. Transmission electron microscopy (TEM) observations were performed on JEM-2500SE at an acceleration voltage of 200 kV. Scanning electron microscopy (SEM) images were obtained on JSM-6330F (JEOL) at an acceleration voltage of 15 kV and the magnification in the range of 1500-3500. Thermograms were investigated by thermogravimatric analysis (TGA-TA instrument) while controlling the heating rate at 10 °C/min in the temperature range of 50-500 °C. The purge gas was He with a 10 ml/min flow rate. Fourier transform infrared (FTIR) spectra were measured on a Digilab FTS-7000 series. All the samples were mixed with dehydrated potassium bromide (KBr) and then made into pellets using a hydraulic press. The collected spectra were measured with 128 scans in the range of 4000-400 cm^{-1}. The resolution of collection was 2 cm^{-1}. The BET surface area, total pore volume, and pore diameter of the mesoporous silica particles were calculated from N_2 adsorption-desorption isotherms, which were determined on Belsorp-mini II. All the samples were degassed at 150 °C for 24 h prior to the measurement. The BET surface areas were calculated using the Brunauer-Emmett-Teller method. The optical emission spectra (OES) were collected using an AvaSpec-3648 Fiber optic spectrometer with 300 lines/mm of grating and a 50 μm slit size. The OES profiles were detected with an optical fiber through the quartz window in the direction perpendicular to the axis of the two electrodes.

2.3. Results and Discussion

Fig. 2.3 displays the XRD patterns of the mesoporous silica after thermal calcination and SPP under various SPP solutions. In the cases of PFS3M and PFS2M,

the XRD patterns of mesoporous silica after SPP are observed at diffraction peak positions (2θ) at 0.76 and 0.71°, respectively [Figs. 2.3A(a) and 2.3A(b)].

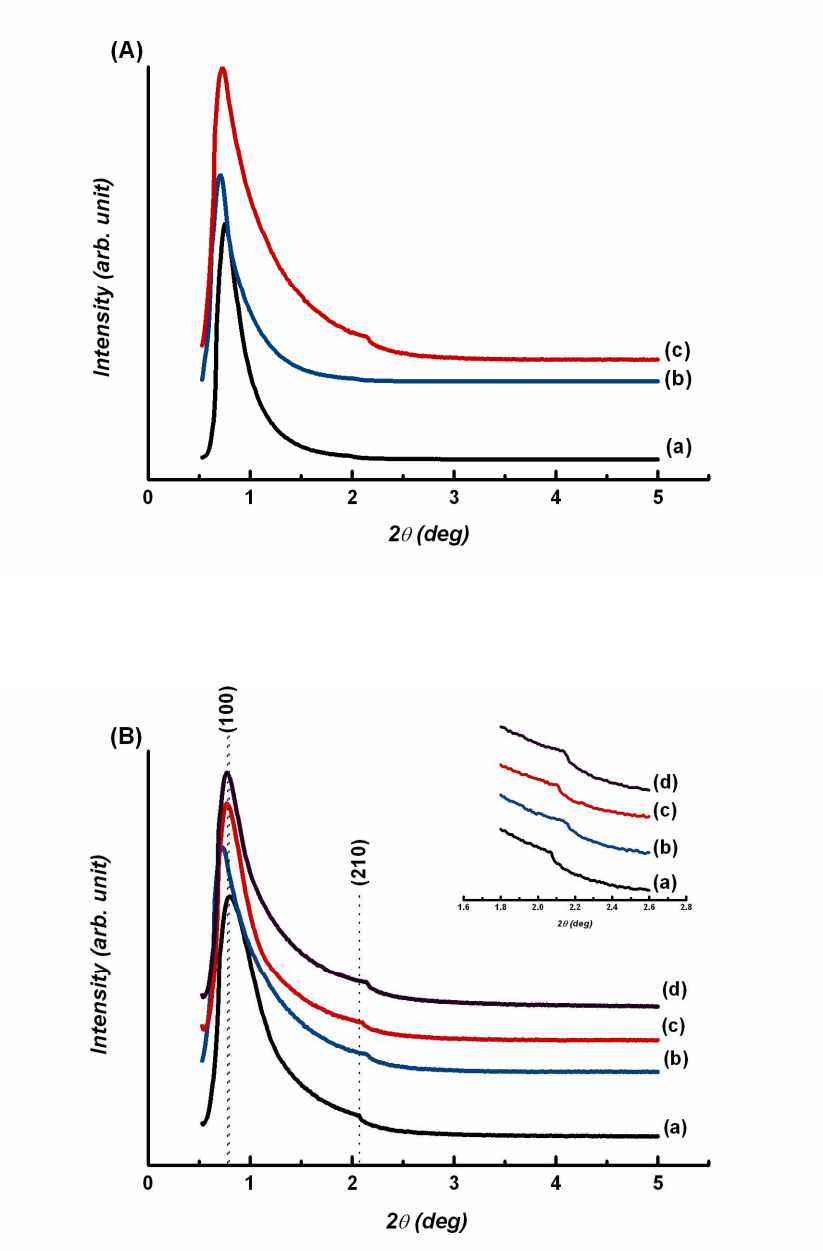

Fig. 2.3. XRD patterns of mesoporous silica: (A) mesoporous silica in synthesized acid solutions of different pHs: (a) 3 M HCl (PFS3M), (b) 2 M HCl (PFS2M) and (c) 1 M HCl (PFS1M) after SPP for 15 min in pH 3 solution.

(B) Comparison of thermal calcination and SPP in PFS1M solutions of various pHs: (a) thermal calcination, and SPP in (b) pH 3, (c) pH 7, and (d) pH 11 solutions.

At these diffraction peak positions, we calculated the pore sizes of PFS3M and PFS2M to be 11.61 and 12.43 nm, respectively. Other diffraction peaks cannot be observed in these cases. From these results, the disordered wormlike mesoporous structure was represented [17,19]. In the case of PFS1M [Fig. 2.3A(c)] the two positions of the diffraction peaks are observed at 0.77 and 2.1°. These diffraction peaks respectively correspond to the plane reflections of (100) and (210), which are characteristic of the 2D hexagonal structure. The main pore size of PFS1M was estimated to be 11.46 nm. By decreasing the acidity of the synthesized solution, the mesotexture of mesoporous silica was transformed from a disordered wormlike structure to an ordered 2D hexagonal structure. The possibility of this occurrence might be explained by the fact that, among various factors affecting mesoporous silica formation, in the case of PFS1M, the acid condition is appropriate for the formation of a strong hydrogen bonding between surfactant species in the surfactant system. The formation mechanism of mesoporous silica particles in such a case was $(S^0H^+)(X^-I^+)$, where S is an organic micelle, H is hydrogen, X is a halide ion, and I is an inorganic species, to assemble the ordered 2D hexagonal arrangement [17,20,21]. The formation of a mesoporous structure in the form of the disordered wormlike structure, however, seems to be unclear. The PFS3M and PFS2M formation mechanisms might be constructed via a complex of surfactant self-assembly, and surfactant and silicate species self-assembly, and the other effects that influence the transformation of mesophases during polycondensation [17,21]. To consider the effect of pH during SPP, Figs. 2.3B(b)-2.3B(d) show comparable results of PFS1M in discharge solutions of various pHs. The first diffraction peak of PFS1M after SPP in solution of pH 3 is slightly shifted to the lower diffraction peak position compared with the first diffraction peaks of PFS1M after SPP in pH 7 and pH 11 solutions, which showed no

significant difference. This suggests that the acid solution used as SPP solution for template removal in mesoporous silica does not reduce the size of mesopores inside mesoporous silica, whereas the neutral and base solutions used slightly reduce the size of the mesopores, similar to the result of thermal calcination, a commercial process; it is well-known that the size of mesopores can be reduced after processing [Fig. 2.3B(a)]. This result might be explained by the fact that, in the acid solution, end-chain hydroxyl groups of silanols inside mesopores could be protonated by hydrogen ions and exhibit a high density of positive charges. Thus, the size of mesopores increased owing to the repulsion between such positive charges. On the other hand, the second peak of PFS1M after SPP in pH3 solution is slightly shifted to the higher diffraction peak position, indicating that the lattice position of the second plane is contracted. This result might be explained by the fact that, during SPP, the removal of the surfactant template and the shrinkage of the polysilicate network and the mesopores in all dimensions simultaneously occurred, as observed after treatment by thermal calcination [22,23]. Considering the same bulk of PFS1M after discharge at pH 3, the polysilicate network physically contracted when the surfactant template was gradually removed, whereas the mesopores tried to expand as a result of the influence of the mentioned repulsion induced by the high density of positive charges. Therefore, the second plane position was narrower, thereby affecting the shift in the diffraction angle at a higher position in a reverse tendency in other cases.

TEM images of PFS3M, PFS2M, and PFS1M are revealed in Fig. 2.4, which directly provide evidence of the mesopore structure; the images are in good agreement with the XRD results. Disordered wormlike mesopore structures are observed in the cases of PFS3M and PFS2M [Figs. 2.4(a) and 2.4(b)] and ordered 2D hexagonal structures [Fig. 2.4(c)] are observed in PFS1M. It is therefore valid to conclude that

the characteristics of mesopore structures are dependent on the acidity of the synthesized solution, which is strongly affected by structural micelle formation.

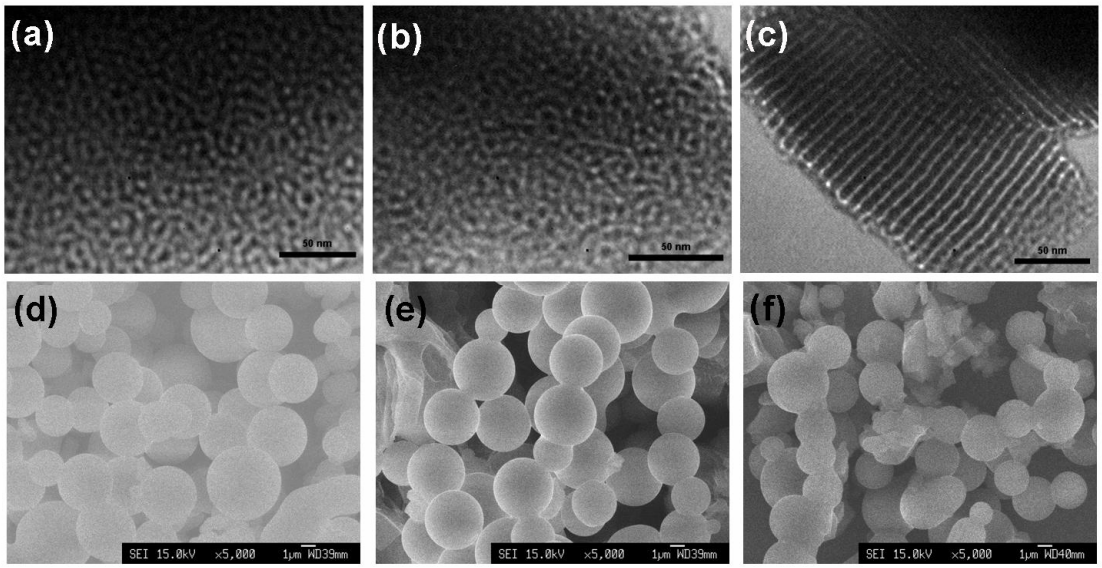

Fig. 2.4. TEM images of mesoporous silica after SPP for 15 min in pH 3 solution: (a) PFS3M, (b) PFS2M, and (c) PFS1M, and SEM images of mesoporous silica after SPP for 15 min in pH 3 solutions: (d) PFS3M, (e) PFS2M, and (f) PFS1M.

The mesoporous silica morphology is studied from SEM and the SEM images of PFS3M, PFS2M, and PFS1M are displayed in Figs. 2.4(d)-2.4(f), respectively. The sample morphology was controlled by adjusting the acidity of the synthesized solutions by varying the acid concentration from 1 to 3 M. Spherical particles are observed under all conditions, suggesting that the spherical shape has the lowest surface energy and is the most suitable shape for silica particles prepared at ambient temperature [18]. The SEM images of PFS3M, PFS2M, and PFS1M show evidence of a good dispersive sphere, an irregular sphere, and an aggregated sphere, respectively.

The good dispersion and stability of spherical particles straightforwardly depended on the rates of hydrolysis and condensation reactions during the sol-gel process, with increasing synthesized acid concentration. The mean size diameters of PFS3M, PFS2M, and PFS1M were recorded to be 3.08, 3.59, and 3.71 μm, respectively. The particle size distribution tended to increase with a decrease in the synthesized acid concentration. From the results of the particle size and particle size distribution, the high rates of hydrolysis and condensation during the sol-gel process were observed in 3 M HCl, resulting in particles smaller than those observed at lower acid concentrations.

The FTIR spectra of the as-synthesized mesoporous PFS3M and PFS1M and the mesoporous silica samples after thermal calcination and SPP for 15 min are displayed in Fig. 2.5. In the cases of the as-synthesized silica PFS3M and PFS1M [Figs. 2.5A(a) and 2.5B(a)], the major band of O-H stretching, which corresponds to the physisorption of water molecules and the OH association of the silanol group, is found to be the broad band in the range of 3000-3700 cm^{-1}; an O-H bending band is also observed at approximately 1730 cm^{-1} [24,25]. The high-intensity bands in the range of 2800-3000 cm^{-1} are assigned to the C-H stretching of methyl groups and C-H stretching of aromatic groups of P123 and SDBS, respectively. The FTIR bands at 1630 and 1482, and 1382 cm^{-1} correspond to the characteristic ring C=C stretching and SO_3 stretching vibrations, respectively. The peaks from 1000 to 1250 cm^{-1} and the peak at 800 cm^{-1} are from mesoporous silica, corresponding to the asymmetric stretching of Si-O groups and Si-O bending vibration, respectively [19,24-26]. The unclear bands from 1150 to 1250 cm^{-1} represent the C-F_x stretching vibration of the fluorinated surfactant [27,28]. In the FTIR spectra of the mesoporous silica specimens PFS3M and PFS1M after discharge for 15 min [Figs. 2.5A(c) and 2.5B(c)], most of

the bands clearly observed at 2800-3000, 1630, 1482, and 1382 cm^{-1} before discharge disappeared, as a result of the template removal by SPP. In contrast, the bands at 1000-1250 and 800 cm^{-1} corresponding to the important functional groups of mesoporous silica still remained at high intensities. Moreover, the peaks at 1730 and 1650 cm^{-1}, which are characteristic of a strong O-H bending resulting from the hydrogen bonding interaction of free water molecules and the surface of mesoporous silica containing silanol groups, are observed. To confirm the ability of SPP for template removal, the FTIR spectra of mesoporous silica after SPP were compared with the FTIR spectra of mesoporous silica after thermal calcination [Figs. 2.5A(b) and 2.5B(b)]. Insignificant spectra were observed in both cases of PFS3M and PFS1M. Thus, we suggest that SPP is comparable to conventional processes and is a high-potential process for template removal in mesoporous silica.

The thermal decomposition of as-synthesized mesoporous silica can provide information on the amount of surfactants and the effect of a surfactant system on the formation of mesopore structures, as well as confirm the ability of SPP in such an application field. The thermograms of the as-synthesized silica specimens PFS3M, PFS2M, and PFS1M are shown in Fig. 2.6A. Two steps in the surfactant decomposition were observed in the decomposition profiles: the first step in the range of 125-169 °C, which indicates that this region corresponds to the decomposition of both the P123 copolymer and SDBS; the second step at approximately 210-250 °C, which is attributed to the fluorinated surfactant (NFBS) decomposition [18]. The percentage weight loss of the P123 copolymer and SDBS in mesoporous materials was calculated to be 16.71, 16.37, and 16.65% for PFS3M, PFS2M, and PFS1M, respectively. The percentage fluorinated surfactant (NFBS) weight losses in

mesoporous materials are 9.66, 8.30, and 6.91% for PFS3M, PFS2M, and PFS1M, respectively.

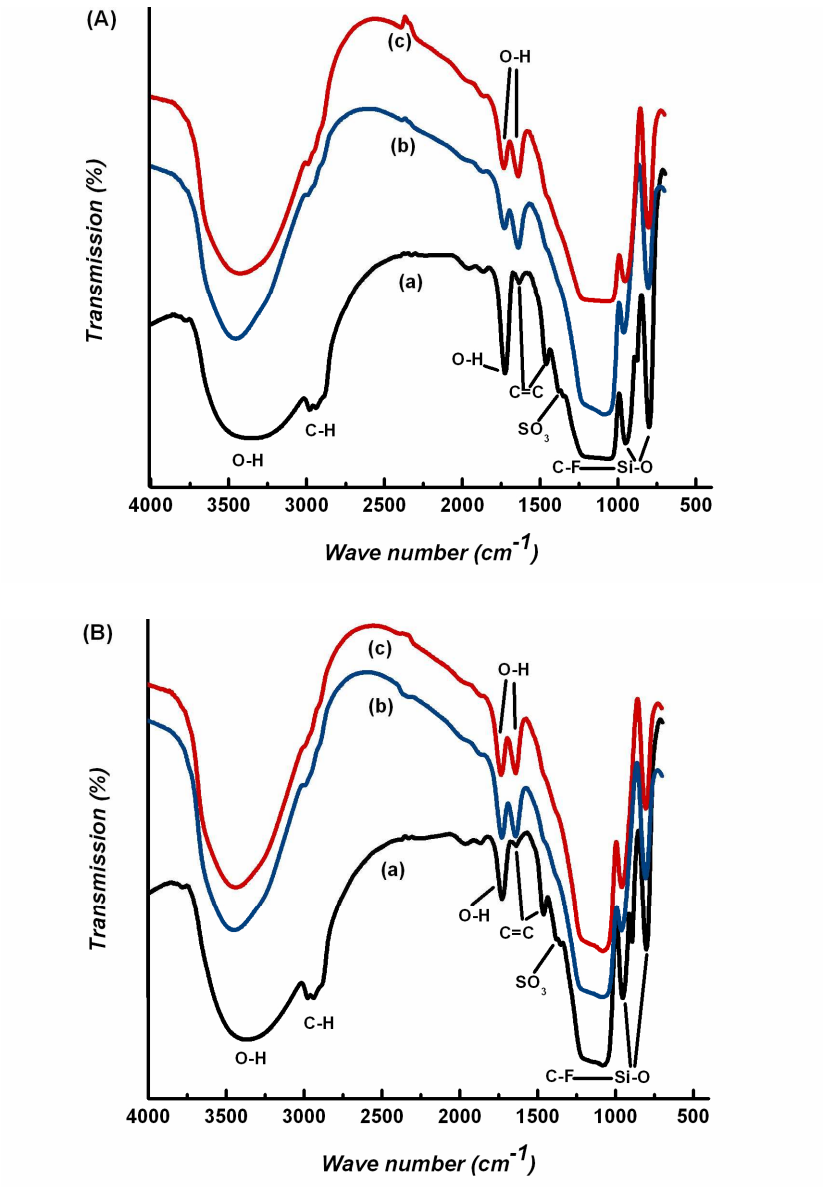

Fig. 2.5. FTIR spectra of mesoporous silica: (A) PFS3M and (B) PFS1M: (a) as-synthesized silica, and after SPP for 15 min in (b) pH 3 and (c) pH 11 solutions.

Additionally, a gradual decrease in weight was observed up to 500 °C, resulting from the loss the surface silanol groups [29]. In the case of PFS3M, the high amount of NFBS in the system could stabilize the formation of mesoporous silica resulting in highly dispersive particles; this result is in good agreement with the SEM observation.

The result of the evaluation of the thermal decomposition of mesoporous silica under various conditions revealed by the thermogram of PFS1M after thermal calcination and SPP in solutions of various pHs for 15 min is displayed in Fig. 2.6B. Different thermograms are shown to reveal the difference in calcination conditions. For thermal calcination [Fig. 2.6B(a)], a small amount of free moisture was decomposed at approximately 50-100 °C. In the cases of PFS1M after SPP in pH 3 and pH 11 solutions [Figs. 2.6B(b) and 2.6B(d)], the weight loss can be observed as two transitions. The decrease in weight after a rise in temperature from 50 °C up to approximately 200 °C was found to be about 5.51% due to the decomposition of both free moisture and bound water molecules, which interacted with hydroxyl groups of silanols by hydrogen bonding [29]. The water molecules require a high temperature for complete decomposition owing to the effects of the small mesopore size and the high density of hydrogen bonds between water molecules and silanol groups. Subsequently, the temperature was continuously increased up to 500 °C, and the weight gradually decreased continuously. The percentage weight losses were found to be 8.43 and 11.94% for PFS1M after SPP in pH 3 and pH 11 solutions, respectively. This decrease can be considered as the loss of silanol groups, which is clearly observed at a temperature of over 200 °C [29,30]. Nevertheless, the decrease is significant in the case of PFS1M after SPP in pH 7 solution [Fig. 2.6B(c)]. The water molecules were removed before the temperature reached 200 °C, and the apparent transition of the decomposed profile in the range of 280-400 °C was observed. This

transition was considered to be the decomposition of the remaining surfactant inside the mesopores; however, the decomposition temperature shifted to higher values compared with that observed for the as-synthesized silica. Note that, after SPP, the organic surfactant became highly rigid owing to the crosslink reaction of the highly active species generated during discharge. Such results confirm that the removal of the surfactant template can be completed by SPP in pH 3 and pH 11 solutions.

Fig. 2.7 shows the N_2 adsorption-desorption patterns of PFS3M, PFS2M, and PFS1M, and the surface areas calculated using the Brunauer-Emmett-Teller theory (BET surface area), total pore volumes, and mean pore diameters are summarized in Table 2.1. The type IV isotherm patterns were classified using plots showing the cylindrical pore structure characteristic [15,19]. N_2 adsorption-desorption isotherms exhibited sloping curves of the hysteresis loop within the range of relative pressures (p/p_0) from 0.4 to 0.6. The isotherm patterns of PFS3M and PFS2M are relatively broad compared with that of PFS1M, indicating the low capillary condensation due to the disordered mesoporous structure characteristic. To summarize the structural parameters of mesoporous silica particles, the BET surface area, total pore volume, and mean pore diameter ranges are 330-882 m^2/g, 0.13-0.33 cm^3/g, and 2.6-3.3 nm, respectively. In the case of PFS3M after SPP in pH 7 solution, the BET surface area was estimated to be 330 m^2/g; the BET surface area increased to 710 and 760 m^2/g when the pH of the SPP solution was changed to 3 and 11. Not only in the case of PFS3M but also in the cases of PFS2M and PFS1M were higher BET surface areas observed when discharge occurred in pH 3 and pH 11 solutions. Therefore, we can state that the discharge process is less efficient in neutral solutions than in acid and base solutions owing to the influence of the quantity of active species generated during SPP.

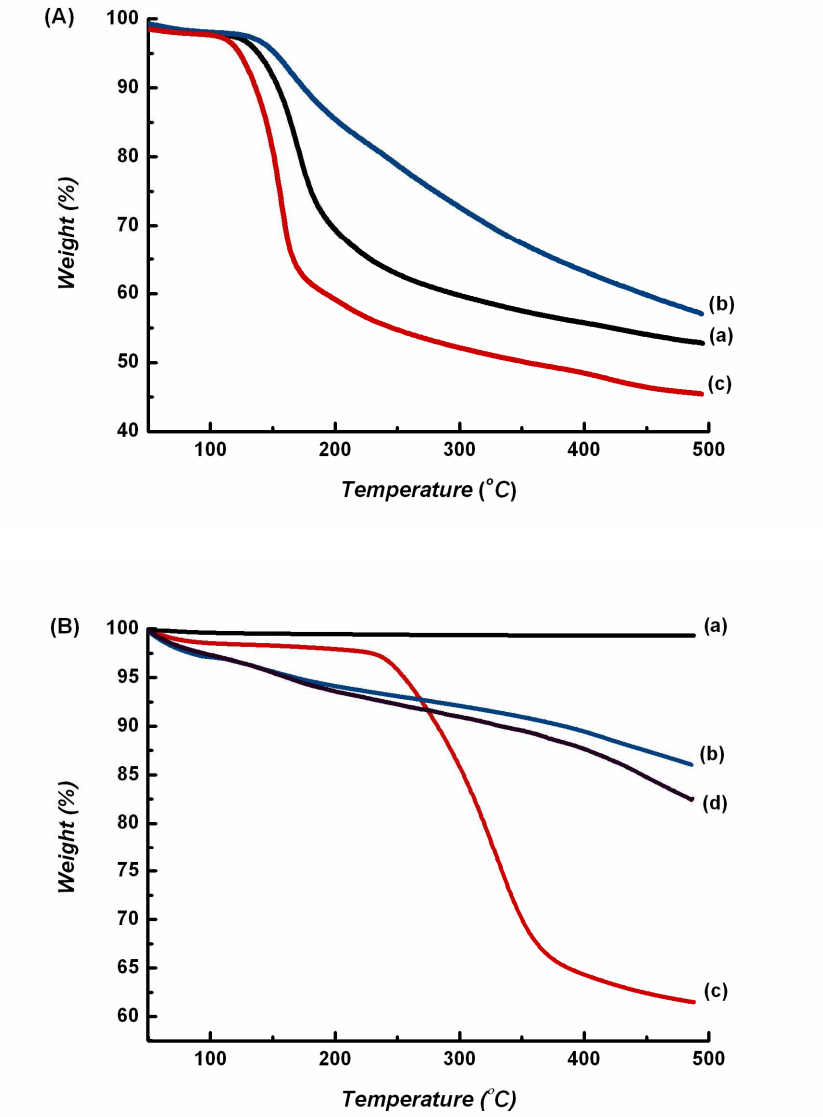

Fig. 2.6. Thermogram in the temperature range of 50-500 °C under He atmosphere: (A) Plots of weight and temperature of the as-synthesized silica in different solutions: (a) PFS3M, (b) PFS2M, and (c) PFS1M.

(B) Plots of weight and temperature of PFS1M after calcination by (a) thermal calcination and SPP for 15 min in (b) pH 3, (c) pH 7, and (d) pH 11 solutions.

Furthermore, the mean pore diameters of mesoporous silica after SPP in solution of pH 3 were rather high compared with the mean pore diameters of mesoporous silica

after SPP in pH 7 and pH 11 solutions. These results are in good agreement with the XRD results mentioned above. Concerning the mesopore structure, the BET surface area of PFS1M, which has a 2D hexagonal arrangement, was much higher than those of the disordered wormlike mesostructures PFS3M and PFS2M, supporting the results in ref. 14.

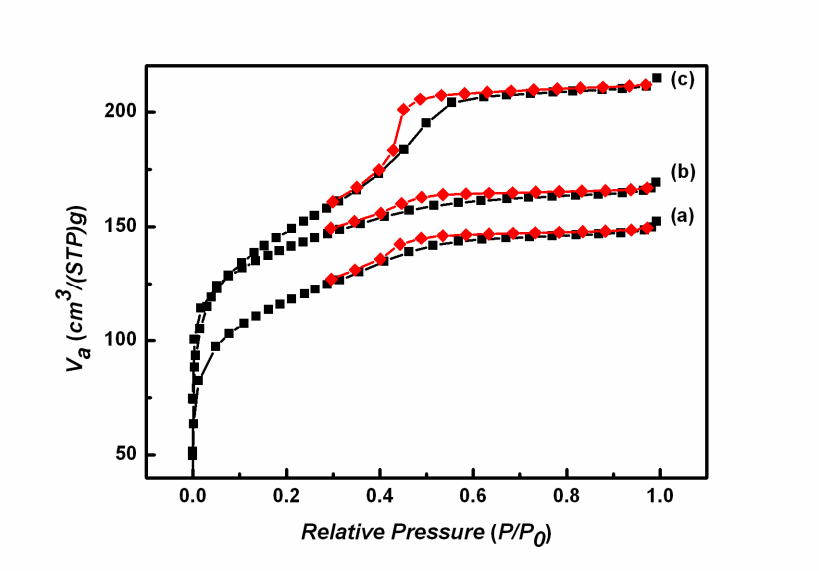

Fig. 2.7. N_2 adsorption-desorption isotherms of mesoporous silica after SPP for 15 min in pH 3 solutions: (a) PFS3M, (b) PFS2M, and (c) PFS1M.

To assess the ability of SPP for removing the organic template, the BET surface area results of the template removal using SPP in solutions of various pHs were compared with the results of calcination. The results of the comparison are shown in Table 2.1. To evaluate the ability of SPP in such application, the BET surface areas of all the particles removed using SPP in acid and base solutions of pHs 3 and 11, were higher than that of the particles removed by calcination, although the BET surface area of the particles removed by SPP in neutral solution was significantly lower than that of the particles removed by calcination. Not only the effects of applied voltage,

solution conductivity, or the duration of discharge process, each of which dependent on the number of generated active species, i.e., H, O and OH radicals, but also the acidity of the discharge solution was strongly affected the number of active species generated during discharge. It is a key point of this present study to investigate the ability of active species, especially hydroxyl and oxygen radicals, that are extensively generated during the discharge process in solutions of different pHs to decompose the organic template inside mesoporous silica. Moreover, UV radiation is also crucial for SPP and serves to accelerate organic decomposition. From our results, we can note that the numbers of generated active species in acid and base solutions are relatively higher than that of active species generated in neutral solution, as determined from the optical emission spectra in Fig. 2.8. Additionally, the use of these radicals and UV radiation generated under SPP seems to be superior to thermal calcination for this application. One of the reasons for this is the use of different media during the decomposition process. The medium used in SPP is an aqueous solution that has a high density and a high capacity for occupying the template for removal owing to the high penetration of the active species inside the mesopore of mesoporous silica. Such a medium acts as an eluant for transporting the products of the decomposition process, such as the oxidized compounds, out of the mesopores of mesoporous silica. Therefore, owing to its features, SPP is highly efficient for template removal with its short consumption time.

Table 2.1. BET surface areas, total pore volumes, and mean pore diameters of mesoporous silica in PFS3M, PFS2M, and PFS1M of pHs 3, 7, and 11 after SPP and thermal calcination.

	PFS3M				PFS2M				PFS1M			
	pH 3	pH 7	pH 11	Calcination	pH 3	pH 7	pH 11	Calcination	pH 3	pH 7	pH 11	Calcination
BET surface area $a_{s,BET}$ (m^2/g)	760	330	710	534	684	341	548	622	882	718	760	654
Total pore volume (cm^3/g)	0.27	0.13	0.20	0.18	0.24	0.21	0.22	0.21	0.33	0.24	0.27	0.25
Mean pore diameter (nm)	3.2	2.8	2.9	2.7	2.9	2.8	2.8	2.7	3.3	2.8	2.9	2.6

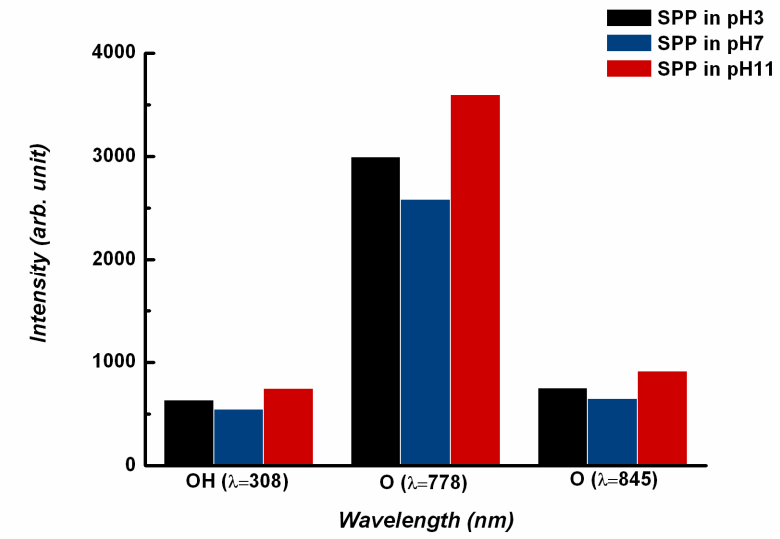

Fig. 2.8. Hydroxyl and oxygen emission spectra detected using optical emission spectroscopy at λ = 308 nm for OH band emission and λ = 778 and 845 nm for O atom emission during SPP in solutions of various pHs: 3, 7, and 11.

2.4. Conclusion

Spherical mesoporous silica materials have been successfully synthesized via the sol-gel method using a ternary surfactant system as the organic template. The pH of media used during the synthesis was varied from 3 to 11 under ambient temperature. The different pHs of the synthesized solutions significantly influenced the mesopore structure of mesoporous silica, as determined from the XRD and TEM results, which show the transformation of the structure from a disordered wormlike structure to an ordered 2D hexagonal structure with an increase in the acidity of the solution. Almost all the surfactant template was discarded by SPP in acid and base solutions, as confirmed by FTIR and thermal analyses. Compared with thermal calcination, the discharge in the acid solution had no effect on the mesopore size. Moreover, SPP in acid solution resulted in the highest BET surface area and mean pore diameter for mesoporous silica. Thus, SPP for 15 min in acid solution (pH 3) is highly efficient for template removal in mesoporous silica.

References

[1] A. M. Anpilov, E. M. Barkhudarov, Y. B. Bark, Y. V. Zadiraka, M. Christofi, Y. N. Kozlov, I. A. Kossyi, V. A. Kopev, V. P. Silakov, M. I. Taktakishvili, and S. M. Temchin, *J. Phys. D*, 2001, **34**, 993.

[2] F. D. Baerdemaeker, M. Simek, J. Schmidt, and C. Leys, *Plasma Sources Sci. Technol.*, 2007, **16**, 341.

[3] D. Staack, A. Fridman, A. Gutsol, Y. Gogotsi, and G. Friedman, *Angew. Chem., Int. Ed.*, 2008, **47**, 8020.

[4] J. Prochazkova, Z. Stara, and F. Krcma, *Czech. J. Phys.*, 2006, **56**, 1314.

[5] J.-S. Chang, S. Ono, H. Ukai, Y. C. Huang, W. Y. Chang, P. Shou, M. Sato, S. Teii, C. Liu, and K. Ting, *Int. J. Plasma Environ. Sci. Technol.*, 2007, **1**, 130.

[6] J. Hieda, N. Saito, and O. Takai, *Mater. Res. Soc. Symp. Proc.*, 2008, **1056**, HH 03-39.

[7] J. Prochazkova, Z. Stara, and F. Krcma, WDS'05 Proc. Contributed Papers, Part II, 2005, p. 414.

[8] T. Fudamoto, T. Namihira, S. Katsuki, H. Akiyama, T. Imakubo, and T. Majika, *Electr. Eng. Jpn.*, 2008, **164**, 669.

[9] D. Li, H. Zhou, and I. Honma, *Nat. Mater.*, 2004, **3,** 65.

[10] H. Yamashita, Y. Horiuchi, S. Imaoka, S. Nishio, N. Nishiyama, and K. Mori, *Catal. Today*, 2008, **132**, 146.

[11] E. Serra, A. Mayoral, Y. Sakamoto, R. M. Blanco, and I. Díaz, *Micropor. Mesopor. Mater.*, 2008, **114**, 201.

[12] P. Yang, Z. Quan, L. Lu, S. Huang, and J. Lin, *Biomaterials*, 2008, **29**, 692.

[13] A. Shimojima and K. Kuroda, *Angew. Chem.*, 2003, **115**, 4191.

[14] C. W. Wu, T. Ohsuna, T. Edura, and K. Kuroda, *Angew. Chem.*, 2007, **119**, 5460.

[15] H. M. Kao, T. Y. Shen, J. D. Wu, and L. P. Lee, *Micropor. Mesopor. Mater.*, 2008, **110**, 461.

[16] M. Mesa, L. Sierra, and J. L. Guth, *Micropor. Mesopor. Mater.*, 2008, **112**, 338.

[17] Z. Jin, X. Wang, and X. Cui, *J. Non-Cryst. Solids.*, 2007, **353**, 2507.

[18] X. Meng, D. Lu, and T. Tatsumi, *Micropor. Mesopor. Mater.*, 2007, **105**,15.

[19] Y. Wang, S. Zhu, Y. Mai, Y. Zhou, X. Zhu, and D. Yan, *Micropor. Mesopor. Mater.*, 2008, **114**, 222.

[20] S. Che, A. E. Garcia-Bennett, T. Yokoi, K. Sakamoto, H. Kunieda, O. Terasaki, and T. Tatsumi, *Nat. Mater.*, 2003, **2**, 801.

[21] Z. Jin, X. Wang, and X. Cui, *Colloids Surf. A*, 2008, **316**, 27.

[22] J. Schuster, R. Köhn, A. Keilbach, M. Döblinger, H. Amenitsch, and T. Bein, *Chem. Mater.*, 2009, **21**, 5754.

[23] J. Jiu, K. Kurumada, F. Wang, and L. Pei, *Mater. Chem. Phys.*, 2004, **86**, 435.

[24] G. D. Chukin and V. I. Malevich, *Zh. Prikl. Spektrosk.*, 1977, **26**, 294.

[25] T. Seo, T. Yoshino, Y. Cho, N. Hata, and T. Kikkawa, *Jpn. J. Appl. Phys.*, 2007, **46**, 5742.

[26] T. Morioka, S. Kimura, N. Tsuda, C. Kaito, Y. Saito, and C. Koike, *Mon. Not. R. Astron. Soc.*, 1998, **299**, 78.

[27] J. Mihály, S. Sterkel, H. M. Ortner, L. Kocsis, L. Hajba, E. Furdyga, and J. Mink, *Croat. Chem. Acta*, 2006, **79**, 497.

[28] Y. Zhou, M. L. Bruening, Y. Liu, R. M. Crooks, and D. E. Bergbreiter, *Langmuir*, 1996, **12**, 5519.

[29] P. K. Jal, M. Sudarshan, A. Saha, S. Patel, and B. K. Mishra, *Colloids Surf. A*, 2004, **240**, 173.

[30] Z. S. Zhou, C. S. Li, J. Z. Jin, and X. H. He, *J. Non-Cryst. Solids*, 2007, **353**, 2774.

Chapter 3. Solution Plasma for Template Removal in Mesoporous Silica: pH and Discharge Time Varying Characteristics

The evaluation of the ability of solution plasma process, SPP, depending on pH of discharge solution and discharge time for template removal in mesoporous silica was described. In the synthesis of mesoporous silica, ternary surfactant system containing tri-block copolymer $EO_{20}PO_{69}EO_{20}$ (P123), sodium dodecylbenzene sulfonate (SDBS), and 1,1,2,2,3,3,4,4,4-nonafluoro-1-butyl sulfonate (NFBS) was chemically used for synthesis under acid condition via sol-gel method then SPP was employed for template removal. The ordered 2D hexagonal arrangment was observed by the evidence of high resolution TEM and the diffraction mode of X-ray. The efficiency of SPP depending on pH of discharge solution and discharge time were scientifically demonstrated as a function of BET surface area. In the case of pH dependence, it was achieved that the ability of template removal in acid and base solutions were clearly higher than those of such results in neutral solution. In the term of discharge time, moreover, the percentage of template removal comparing in the result of BET surface area increased as the increase in discharge time.

3.1. Introduction

Plasma technology is widely applied as a versatile process to be used in many fields of materials science and technology. The plasmas in gas and solid phases have been developed since a long time ago and used for many industrial benefits for

instance coating processes, surface treatment processes, electronic device manufacturing processes, and nanomaterials synthesis [1-5]. Alternatively, the plasma in aqueous solution, namely solution plasma is also high potential plasma which can be applied in many fields. Although solution plasma is not extensively well-known, it has been studied for developing as a multipurpose process. Various kinds of active species can be physically generated during discharge in aqueous solution for instance the high active radicals (H·, O·, OH·, HO_2·, etc.), high energy electrons as well as UV radiation [6-10]. The different active species are specifically used as the source of many kinds of reaction. For the example, H· is subjected to be an initiator for the reduction process demonstrated in the nanoparticles synthesis [11,12]. O· and OH· are the dominated radicals for oxidation process in the decomposition of organic compounds [13,14]. However, solution plasma has some drawback because it requires a high voltage to generate the continuous plasma discharge resulting to the low energy efficiency. Then such plasma system has been considered to improve the process efficiency by several considerations especially the typical parameters including the solution conductivity, the type of electrodes, and the distance of electrode [15,16].

In mesoporous silica synthesis, the Si precursor (e.g. tetraethyl orthosilicate, TEOS) and the surfactant micelles as template are generally used to synthesize mesoporous silica with different mesopore properties. The type of surfactant, surfactant combination, and surfactant concentration are severely influenced on the mesopore arrangement, morphology, and diameter [17-20]. The porosity in mesoporous silica is obtained by the template removal which is stepwise processed in the final step. The thermal calcination and the chemical leaching are conventionally used to remove such template. Both of these processes are occupied a long time to complete the template removal. Moreover, the pore size contraction owing to the

shrinkage of the lattice structure is always observed in the high temperature of thermal method and the high contamination in the chemical use for leaching is strictly aware [21-23].

In this study, we applied the solution plasma process (SPP) for removing the organic template inside mesoporous silica which was synthesized via sol-gel method by using the ternary surfactant system, P123 block copolymer, SDBS, and NFBS as a template in acid solution. Two controlled parameters, pH of discharge solution (pH 3, pH 7, and pH 11) and discharge time (1-15 min) which strongly affected the capability of template removal in mesoporous silica were evaluated. The influences of pH solution and discharge time on mesopore structure of mesoporous silica were confirmed by X-ray diffraction (XRD) patterns and transmission electron microscope (TEM) images. The BET surface area values were used to explain the SPP efficiency depending on pH and discharge time. The evidence of optical emission spectra (OES) measured during discharge could be confirmed.

3.2. Experimental Procedures

Mesoporous silica was synthesized using the ternary surfactant system containing 0.5 g of P123 block copolymer, 0.1 g of NFBS, and 0.084 g of SDBS in 1 M HCl. This mixture was continuously stirred for 1 h to form a homogeneous solution. 2.15 g of TEOS was added into such solution. Consequently, the mixture was further kept under static condition at room temperature for 24 h to generate the white precipitate and then it was filtered out, thoroughly washed with ultrapure water and dried by air drying. In order to demonstrate the effects of pH and discharge time for removing the template, SPP was carried out by the bipolar pulsed power supply with the needle-to-

needle electrode geometry in the aqueous solution by adjusting pH of media solutions, pH 3, pH 7, and pH 11 against discharge time from 1 to 15 min. The pH adjustments were done by using 0.1 M hydrochloric acid solution (HCl) and 0.1 M sodium hydroxide solution (NaOH). The obtained materials after discharge can be denoted as P*a*-*b*, when P is mesoporous silica prepared by this surfactant system, *a* means for pH, and *b* stands for discharge time. The solution plasma parameters including typically voltage, pulse frequency, pulse width, and electrode distance were 2.4 kV, 15 kHz, 2 μs, and 0.3 mm, respectively. The SPP setup scheme image is displayed in Fig. 3.1.

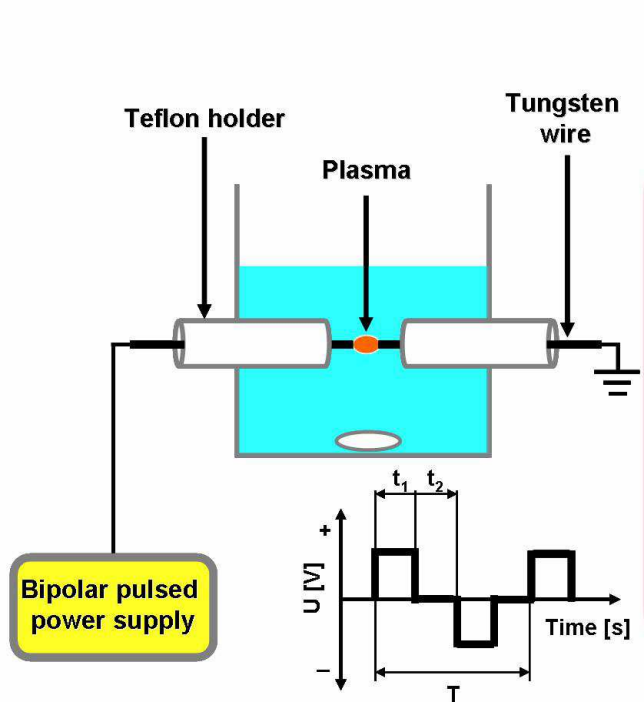

Fig. 3.1. Scheme image of the solution plasma experimental setup.

For characterizations, the electrical conductivity of various solutions before and after discharge was measured by Hanna Instrument HI 991300 EC meter. X-ray diffraction (XRD) patterns were carried out on XRD Rigaku Smartlab with Cu Kα radiation (λ = 0.154 nm). The diffraction patterns were collected in the range of 2θ =

0.1-5.0° by using a scanning rate of 0.2°/min. Transmission electron microscope (TEM) observations were performed on JEM-2500SE with an acceleration voltage of 200 kV. The surface area of the mesoporous silica particles were calculated from N_2 adsorption-desorption isotherms using the Brunauer-Emmett-Teller method which carried out on Belsorp-mini II. All samples were degassed at 150 °C for 24 h prior to the measurement. The optical emission spectra (OES) were collected by an AvaSpec-3648 Fiber optic spectrometer with 300 lines/mm of grating and 50 μm of slit size. The emission spectra were detected with an optical fiber through the quartz window at the perpendicular direction to the axis of two electrodes.

3.3. Results and Discussion

Herein, the different pHs of discharge solution and the duration of discharge time are proposed to be the major parameters for organic template removal by SPP. The electrical conductivity and temperature profile changes after discharge can be observed in our system comparing with the initial state. Various pHs leaded to the change of solution conductivity depend on the feasibility of SPP for template removal. The initial conductivity values before discharge were measured to be 235, 15, and 178 $\mu S \cdot cm^{-1}$ in pH 3, pH 7, and pH 11, respectively. The conductivity tended to be increased as the increase in discharge time resulting from the molecule dissociation and ionization. These values were respectively detected to be 703, 251, and 675 $\mu S \cdot cm^{-1}$ for 15 min of discharge in pH 3, pH 7, and pH 11. It is well-known that the conductivity is proportional to the electric current density, then discharge in pH 3 and pH 11 solutions can generate higher current density and number of the active species [15,16,24]. The increase in temperature of discharge solution after discharge from the

collision of the high energy molecules in plasma was also detected as the direct proportion since our system did not controlled the change of temperature [16]. At the initial temperature about 23 °C, the increasing temperature after discharge for 15 min was recorded at approximately 40 °C with the difference of the rising temperature about 17 °C. Both of these factors play the important role to the ability of template removal inside mesoporous silica.

The mesopore structure of the calcined mesoporous silica by SPP depending on the variety of pHs and discharge times can be confirmed by the evidence of the diffraction mode of X-ray. Fig. 3.2 shows the X-ray diffraction pattern of mesoporous silica after discharge in pH 3, pH 7, and pH 11 for 15 min (P3-15, P7-15, and P11-15) and the mesoporous silica after discharge in pH 3 for 1, 5, and 15 min (P3-1, P3-5, and P3-15), comparing with as-synthesized silica. Two peaks were observed in all cases. The first peak positions were detected around $2\theta = 0.7°$ and the small intensity of second peaks were further detected in the range of 1-1.1°. These diffraction peaks were indexed as the 2D hexagonal arrangement with the reflection of (100) and (110) [25,26]. The structural parameter (d-spacing) calculated by the diffraction angles is displayed in Table 3.1. The d-spacing values of as-synthesized silica and mesoporous silica after discharge in pH 7 and pH 11 had no significant, then it can be noted that SPP in various pHs and discharge times had no influence on the natural structure of the obtained mesoporous silica synthesized under the mentioned condition. Nevertheless, we found that the d-spacing value of mesoporous silica after discharge in pH 3 for 15 min (P3-15) was slightly shifted into the lower diffraction peak position (Fig. 3.2A(b)) providing a larger pore size than those of other cases. This effect might be explained that during discharge in acid solution, the mesopore size

was expanded owing to the repulsion between the positive charges by the hydrogen ions protonation at the silanol groups of silica backbone.

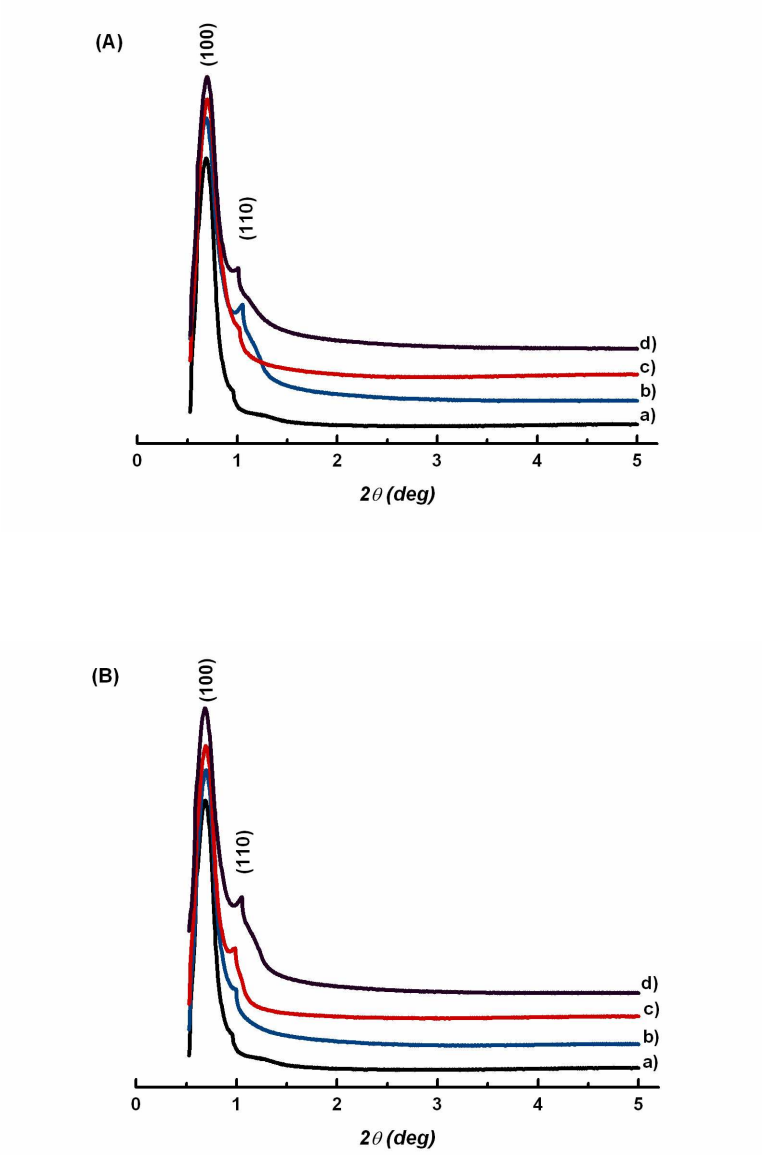

Fig. 3.2. XRD patterns of mesoporous silica with various conditions; (A) mesoporous silica discharged in different pHs at fixed 15 min of discharge time, a) as-synthesized silica, b) pH 3, c) pH 7, and d) pH 11. (B) mesoporous silica discharged at different discharge times in pH 3, a) as-synthesized silica, b) 1 min, c) 5 min, and d) 15 min.

Table 3.1. d-spacing values of (100) and (110) positions.

Sample	(100) position		(110) position	
	2θ (deg)	d-spacing (nm)	2θ (deg)	d-spacing (nm)
As-synthesized silica	0.688	12.82	0.963	9.16
P3-1	0.698	12.64	0.999	8.83
P3-5	0.693	12.73	1.010	8.74
P3-15	0.675	13.07	1.052	8.39
P7-15	0.698	12.64	0.999	8.83
P11-15	0.698	12.64	1.001	8.81

As pH varying characteristic (Fig. 3.2A), we considered the diffraction intensity which related to the number of mesopores and it found that there is no significant in term of the intensity of the first peak whereas the intensity of the second peak was clearly detected in the different quantities. At the second peak position (2θ = 1-1.1°), the intensities of as-synthesized silica and P7-15 were relatively low. On contrary, the high intensities were founded in the cases of P3-15 and P11-15. These results can be explained by the effect of the pH difference in various discharge solutions resulting to the difference of conductivity. In the cases of pH 3 and pH 11, the higher conductivity values were measured and the conductivity is severely influenced to current density leading to the possibility of the active species generation. Hence, the capability of the template removal process in acid and base solution showed to be high.

To explain the influence of the discharge time on the capability of organic template decomposition, the comparable results of various discharge times from initial step (as-synthesized silica), 1 min (P3-1), 5 min (P3-5), and 15 min (P3-15) can be used to clarify as shown in Fig. 3.2B. The obtained results clearly showed different intensities

of the second peak in XRD patterns depending on the discharge time in the direct tendency. At 1 min, the second peak intensity was not changed comparing with that peak intensity of as-synthesized silica. Consequently, the discharge time was stepwise increased until 15 min and the intensities were observed to be much higher than lower discharge time. This occurrence notes that the organic decomposition became greater as the increase in discharge time and affected by the number of active species which were high occasion to increasingly generate upon the increasing temperature and energy of the system [16].

In a good agreement of the XRD results, the high resolution transmission electron microscope images of mesoporous silica P3-15, P7-15, and P11-15 are depicted in Fig. 3.3. These images reveal the parallel channels with uniaxial cylindrical mesopore arrangement. The adjustments of pH and discharge time did not change the structural morphology of the mesopore structure.

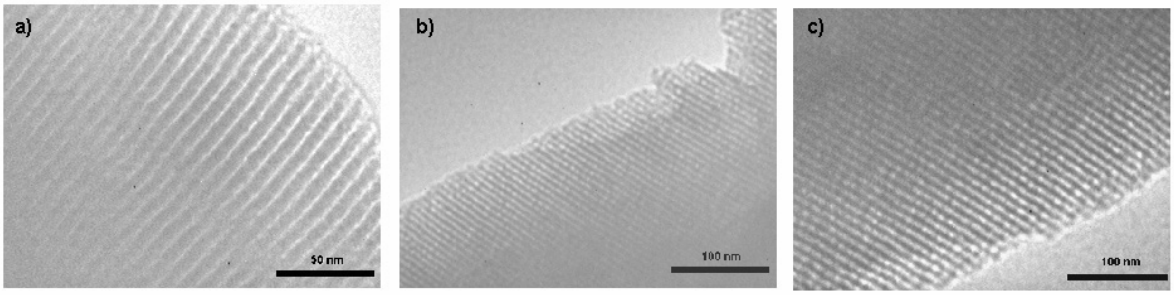

Fig. 3.3. TEM images of mesoporous silica discharged in different pHs at fixed 15 min of discharge time, a) pH 3, b) pH 7, and c) pH 11.

During discharge, various kinds of the active species for instance H·, OH·, O·, and Cl· with different concentrations were physically generated. The OES result of the generated active species discharged in pH 3 for 15 min is displayed in Fig. 3.4A. The molecular band of OH can be detected at 309.34 nm of wavelength. The atom line of

H_α was appeared at 656.16 nm. Furthermore, the atomic lines of each Cl and O were observed with two peaks at 545.31, 611.09 and 777.3, 844.85 nm, respectively [10,14,27,28]. The emission spectra of H_α·, OH·, O·, and Cl· as a function of discharge time were plotted in Fig. 3.4(B-G). The intensity of the atomic line of H_α tended to increase significantly as the increase in discharge time as shown in Fig. 3.4B. Fig. 3.4(C, D) exhibit the atomic lines of Cl in both of emission wavelengths which were shown to be high intensity in the observation during discharge in pH 3 dependent on discharge time. On contrary, the significant lower intensities in the cases of pH 7 and pH 11 were detected. This state suggests that different amount of Cl ions in discharge solution had a strong effect to the Cl line emission intensity. The intensity increment of both of O· and OH· were concentrated to evaluate since they have been proved to be the important species for oxidation in organic decomposition [13,14]. The spectra intensities of both molecular band of OH and atomic lines of O were variable by the control of different pHs and discharge times as shown in Fig. 3.4(E-G). With the difference of pHs, the OH and O intensities were detected to be the highest value in the case of the discharge in pH 11. Consequently, their intensities tended to slightly decrease as founded in pH 3 and the lowest intensities were observed in the case of pH 7.

Considering to the previous study in our group, by using the same power supply for plasma generation, the detectable active species were identified to be high density which continuously formed between the pulses. The temporal evolution of active species was independent on discharge time in the circulation system which for controlling the solution temperature. On contrary, the increase in the number of active species by the effect of conductivity increment depending on time was detected in the

non-circulation system. Therefore, this result can be supported in this present study [16].

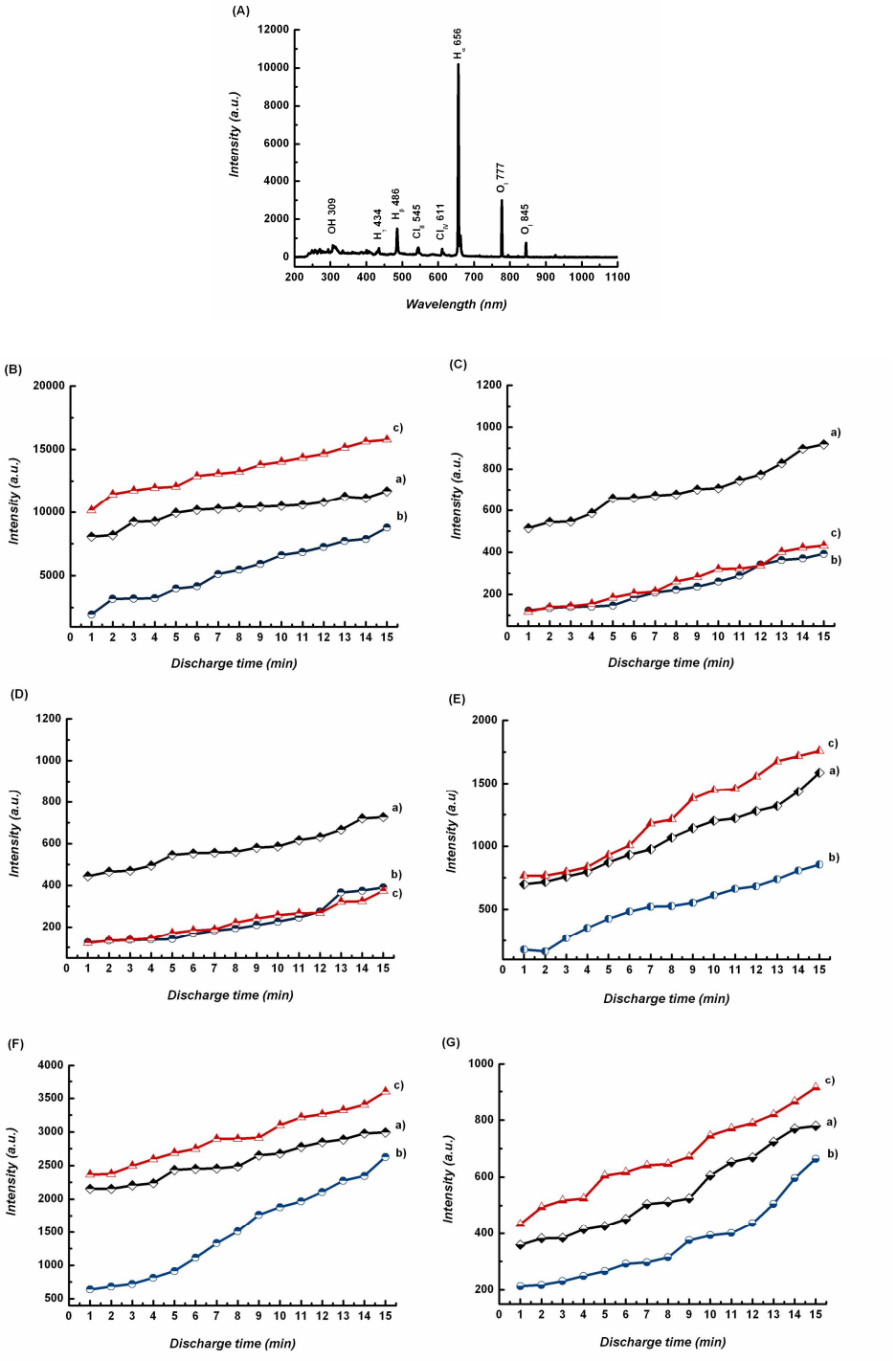

Fig. 3.4. Optical emission spectra during discharge; (A) emitted spectra in the range of λ = 200-1100 nm of discharge in pH 3 for 15 min (B) the atomic line of H_α at λ = 656.16, (C, D) the atomic lines of Cl at λ = 545.31 and 611.09 nm, (E) the

molecular band of OH at λ = 309.34 nm and (F, G) the atomic lines of O at λ = 777.3 and 844.85 nm, depending on pHs, a) pH 3, b) pH 7, and c) pH 11.

Herein, we reported the surface area of samples in the term of BET surface area analyzed by the adsorption-desorption patterns of nitrogen gas at different relative pressures and they could be realized the ability of SPP in our viewpoint. BET surface area values of samples were compared with different discharge conditions in various pHs and discharge times. The summary of BET surface area was plotted as shown in Fig. 3.5. BET surface area of as-synthesized silica was reported to be 155 m^2/g. At the first minute of discharge time, BET surface areas of P3-1, P7-1, and P11-1 were respectively increased to be 276, 171, and 264 m^2/g and reached to be 882, 484, and 760 m^2/g at 15 min of discharge time. The increase in BET surface area was regarding to the increases in the conductivity, temperature, and numbers of OH· and O· with discharge time. These occurrences resulted to the decomposition of the organic matters. In comparison of BET surface area after discharge in pH 3, pH 7, and pH 11, BET surface area of mesoporous silica after discharge in pH 7 was lower than those of surface areas in the cases of pH 3 and pH 11 in all ranges of discharge time. These results go along with the results of OES in a good agreement and they can be also confirmed the XRD results in the term of intensity.

Nevertheless, in the cases of pH 3 and pH 11, the higher OH and O intensities were emitted from discharge in pH 11 whereas the lower BET surface area was obtained. These results can be explained by the supporting studies which discussed that the pulsed discharge in water was reported to be less effective for organic decomposition at the higher pH values caused by the reaction between OH· and a product of organic decomposition, namely carbonate ions. Therefore, the great efficiency of such

application was obtained after reducing pH [13,29]. Additionally, the oxidation by OH· was occurred with a high effectiveness in the acid condition, especially in the range of pH 3-5 [30].

The contrary discussions were also reported that the oxidation activities by OH· to decompose phenol and acetic acid were more effective in the solution at pH over 12 and the inhibition of the decomposition ability by high amount of Cl ions was observed at pH about 1 [31]. Moreover, the greater efficiency of discharge for phenol degradation was done with the feed of oxygen gas during discharge in high pH condition caused by the high possibility of the hydrogen peroxide formation and dissociation to OH· [32]. However, those of two factors might not influence in this study since the range of pH was varied from 3 to 11 and the oxygen gas did not applied in our system.

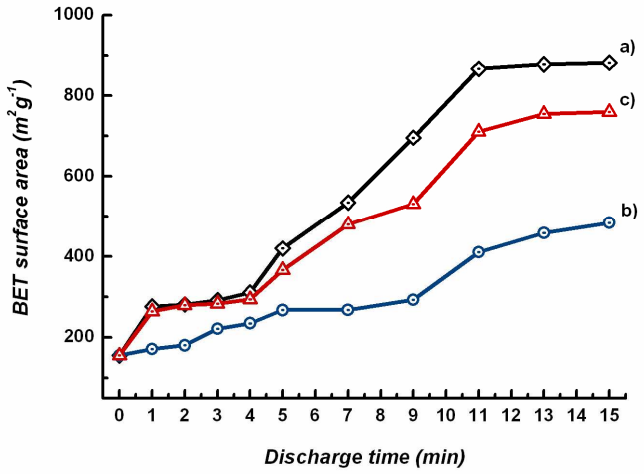

Fig. 3.5. BET surface area values of mesoporous silica discharged in different pHs of discharge solution as a function of discharge time a) pH 3, b) pH 7, and c) pH 11.

3.4 Conclusion

The varying characteristics of pH and discharge time during discharge for template removal in mesoporous silica were investigated in this study. Both of these effects play the important role as the main factor for discharge process in aqueous solution. However, they had no influence on the mesopore feature of mesoporous silica by the confirmations of XRD patterns and TEM images. The numbers of active species, especially OH· and O· which were the sources of oxidation were depended on pH and discharge time, yielding to the changes of electrical conductivity and temperature. The intensities of active species measured during discharge in pH 3 and pH 11 were observed to be higher than that of the result in pH 7 and they tended to increase as the increase in discharge time. BET surface area after discharge in pH 3 for 15 min was reported to be the highest value supporting by the OES results. Therefore, not only the instrument parameters such as the applied voltage and the distance between electrodes have strong effects in SPP but also pH and discharge time which were realized in this study.

References

[1] M. Kuzuya, T. Sawa, M. Mouri, S. Kondo, and O. Takai, *Surf. Coat. Technol.*, 2003, **169/170**, 587.

[2] J. Píchal, J. Koller, L. Aubrecht, T. Vatůna, P. Špatenka, and J. Wiener, *Czech. J. Phys.*, 2004, **54**, 828.

[3] C. Liu, Y. Masuda, Y. Wu, and O. Takai, *Thin Solid Films*, 2006, **503**, 110.

[4] Q. Cao, C. Kocabas, M. A. Meitl, S. J. Kang, J. U. Park, J. A. Rogers, in: A. Javey, J. Kong (Eds.), Carbon Nanotube Electronics, Springer, US, 2009, p.211.

[5] O. Takai, *Pure Appl. Chem.*, 2008, **80**, 2003.

[6] Y. Wu, M. Kuroda, H. Sugimura, Y. Inoue, and O. Takai, *Surf. Coat. Technol.*, 2003, **174/175**, 867.

[7] A. M. Anpilov, E. M. Barkhudarov, Y. B. Bark, Y. V. Zadiraka, M. Christofi, Y. N. Kozlov, I. A. Kossyi, V. A. Kopev, V. P. Silakov, M. I. Taktakishvili, and S. M. Temchin, *J. Phys. D: Appl. Phys.*, 2001, **34**, 993.

[8] F. D. Baerdemaeker, M. Simek, J. Schmidt, and C. Leys, *Plasma Sources Sci. Technol.*, 2007, **16**, 341.

[9] D. Staack, A. Fridman, A. Gutsol, Y. Gogotsi, and G. Friedman, *Angew. Chem. Int. Ed.*, 2008, **47**, 8020.

[10] J. Prochazkova, Z. Stara, and F. Krcma, *Czech. J. Phys.*, 2006, **56**, 1314.

[11] J. Hieda, N. Saito, and O. Takai, *Mater. Res. Soc. Symp. Proc.*, 2008, **1056**, HH 03-39.

[12] J. Hieda, N. Saito, and O. Takai, *J. Vac. Sci. Technol. A*, 2008, **26**, 854.

[13] A. T. Sugiarto, T. Ohshima, and M. Sato, *Thin Solid Films*, 2002, **407**, 174.

[14] H. Wang, J. Lei, X. Quan, and Y. Wu, *Appl. Catal. B: Environ.*, 2008, **83**, 72.

[15] S. Potocky, N. Saito, and O. Takai, *Thin Solid Films*, 2009, **518**, 918.

[16] C. Miron, M. A. Bratescu, N. Saito, and O. Takai, *Plasma Chem. Plasma Process.*, 2010, **30**, 619.

[17] X. Meng, D. Lu, and T. Tatsumi, *Micropor. Mesopor. Mater.*, 2007, **105**, 15.

[18] A. G. S. Prado and C. Airoldi, *J. Mater. Chem.*, 2002, **12**, 3823.

[19] C.-Y. Chen, H.-X. Li, and M. E. Davis, *Micropor. Mater.*, 1993, **2**, 17.

[20] F. Bérubé and S. Kaliaguine, *Micropor. Mesopor. Mater.*, 2008, **115**, 469.

[21] R. van Grieken, G. Calleja, G. D. Stucky, J. A. Melero, R. A. García, and J. Iglesias, *Langmuir*, 2003, **19**, 3966.

[22] C.-M. Yang, B. Zibrowius, W. Schmidt, and F. Schuth, *Chem. Mater.*, 2004, **16**, 2918.

[23] F. Kleitz, W. Schmidt, and F. Schüth, *Micropor. Mesopor. Mater.*, 2003, **65**, 1.

[24] P. Lukes, M. Clupek, V. Babicky, and P. Sunka, *Plasma Sources Sci. Technol.*, 2008, **17**, 024012.

[25] Z. Jin, X. Wang, and X. Cui, *Colloids and Surfaces A: Physicochem. Eng. Aspects.*, 2008, **316**, 27.

[26] D. Li, H. Zhou, and I. Honma, *Nat. Mater.*, 2004, **3**, 65.

[27] H. S. Uhm, J. H. Kim, and Y. C. Hong, *Phys. Plasma*, 2007, **14**, 073502.

[28] M. Sun, Y. Wu, J. Li, N. H. Wang, J. Wu, K. F. Shang, and J. L. Zhang, *Plasma Chem. Plasma Process.*, 2005, **25**, 31.

[29] A. T. Sugiarto, S. Ito, T. Ohshima, M. Sato, and J. D. Skalny, *J. Electrost.*, 2003, **58**, 135.

[30] S. F. Kang, C. H. Liao, and S. T. Po, *Chemosphere*, 2000, **41**, 1287.

[31] N. Sano, T. Fujimoto, T. Kawashima, D. Yamamoto, T. Kanki, and A. Toyoda, *Sep. Purif. Technol.*, 2004, **37**, 169.

[32] P. Lukes and B. R. Locke, *J. Phys. D: Appl. Phys.*, 2005, **38**, 4074.

Chapter 4. Single-step and Room-temperature Synthesis of Ag Nanoparticles in Mesoporous Silica by Solution Plasma

The synthesis methodologies and the promising benefits of Ag nanoparticles and their composites have been extensively studied in the fields of materials science and engineering owing to the great properties of Ag nanoparticles. In particular, the chemical path, the laser ablation, and the chemical deposition are easily employed to generate various types and morphologies of Ag nanoparticles. The novel strategy, namely solution plasma process (SPP) has been reported and described what happen during discharge process to produce many kinds of metallic nanoparticles by our group research. SPP provides a great performance not only for Ag nanoparticles preparation but also for organic template removal process inside mesoporous silica which was used as the supporting material. During SPP, the high active species, especially H, O, and OH radicals are generated and they play the important role in term of the sources of the reduction and oxidation reactions. Ag nanoparticles on mesoporous silica were obtained after discharge for only 10 min due to the high effectiveness of such species for both Ag nanoparticles synthesis and organic template removal inside mesoporous silica simultaneously. This report also discusses with many scientific techniques and highlights several promising capabilities of SPP for the expected applications as the short consumption time and low contaminations processes.

4.1. Introduction

Nanoparticles are extensively investigated considering their significant physicochemical characteristics. Owing to the great properties for instance optical, electronic, and catalytic activities, they have been promising to widely apply for various applications such as the optical and electronic devices, the signal-selected sensors, and the variety of catalysts [1-5]. Ag nanoparticles supported on oxides have a potential of novel catalyst. For an example, Ag nanoparticles on and/or in the SBA-15 type mesoporous silica shows the catalysis for the CO conversion reaction. The conversion efficiency was ca. 100% at more than the reaction temperature of 270 °C [5]. In the case of catalyst composed of nanoparticles, the structure, shape, size, and the interfacial state among the catalytic carrier are extremely crucial to control and promote the catalyst. In particular, the relation between nanoparticles and supported materials has been known to be crucial to the catalytic property even in the case of single-nano particles.

Ag nanoparticles have been synthesized using reducing agents such as sodium borohydride ($NaBH_4$). It demonstrates that the obtained nanoparticles can easily be regulated in the diameter and shape [6]. The thermal decomposition technique using high-power ion beam was successfully used to form the Ag nanoparticles film on substrate [7]. The laser ablation containing silver nanowire fraction and sodium citrate reducing agent was the recent method to prepare Ag nanoparticles with a wide size distribution and various particle morphologies [8]. However, it is difficult to synthesize Ag nanoparticles at the inner space of mesoporous silica with even the chemical reduction method because the concentration profile of ions in the inner space.

We had successfully developed solution plasma (SP), which is one of non-thermal plasma in aqueous solution. This plasma is defined by a glow discharge in aqueous solution, and it stabilized by the exchanges of ions and electrons between gas and liquid phases. This plasma provides hydrogen radicals to aqueous solution, on the other hand, aqueous solution provides raw materials as ions and organic compounds. These substances react on the interface of gas and liquid phases.

Using the solution plasma process (SPP), we had demonstrated a high efficient process for nanoparticles synthesis without the addition of any reducing agent [9,10]. Characteristically, the lifetime of hydrogen radical was comparatively long since the concentration of hydrogen radical is higher than that of conventional chemical reaction fields, i.e. radical chain length become long. This indicates that the hydrogen radical has a potential to work as reactive agent in the inner space. Moreover, SP can also remove the organic template from the inorganic and organic compounds for the synthesis of mesoporous silica [11].

In this research, we aimed to synthesis the Ag nanoparticles in mesoporous silica on the single step. Namely the effects of both reduction and oxidation prepare Ag nanoparticles impregnated on mesoporous silica at the same time as template removal inside mesoporous silica, which was used for the supporting material. Mesoporous silica was easily prepared via sol-gel method in acid solution then SPP was employed for such Ag nanoparticles impregnation and the organic template removal simultaneously. The samples were characterized by X-ray diffraction (XRD), transmission electron microscopy (TEM), scanning electron microscopy (SEM), UV-VIS spectroscopy, energy-dispersive X-ray spectroscopy (EDX), and N_2 adsorption-desorption isotherm method.

4.2. Experimental Procedures

4.2.1. Chemicals

Tetraethyl orthosilicate (TEOS), 1,1,2,2,3,3,4,4,4-nonafluoro-1-butane sulfonate (NFBS), hydrochloric acid (HCl), sodium hydroxide (NaOH), and silver nitrate ($AgNO_3$) were purchased from Wako Pure Chemical Industries, Ltd, Japan. Triblock copolymer P123 ($EO_{20}PO_{69}EO_{20}$) and sodium dodecylbenzene sulfonate (SDBS) were purchased from Sigma-Aldrich, INC, USA. All chemicals were further used without any purification.

4.2.2. Synthesis of Mesoporous Silica and Ag Nanoparticles Incorporated Mesoporous Silica.

In a synthesis, the mesoporous silica was synthesized following the previous work [11]. In brief; the surfactant system was firstly prepared by dissolving triblock copolymer P123, fluorinated surfactant NFBS, and SDBS in 3 M HCl solution. This mixture was continuously stirred until forming a homogeneous solution. Consequently, TEOS was added into the solution, and then the mixture was further kept under static condition at room temperature for 24 h to generate a white precipitate. The precipitate was collected by filtration, thoroughly washed with distilled water and leaved it to dry by air drying. To obtain Ag nanoparticles on mesoporous silica, a drop of silver nitrate ($AgNO_3$) solution and 0.15 g of triblock copolymer P123 were mixed in 150 ml of pure water to prepare the total concentration of 1 mM $AgNO_3$. After the homogeneous solution was obtained, 1 g of the as-synthesized silica was added into such solution then the discharge was further processed. SPP was carried out with bipolar pulsed power supply in the prepared solution by controlling the discharge parameters. The schematic illustration of SPP

setup is displayed in Fig. 4.1. The typically applied parameters: voltage, pulse frequency, pulse width, and electrode distance, were 1.6 kV, 15 kHz, 2 μs, and 0.3 mm, respectively. However, the discharge time for SPP was the key point of the formation of Ag nanoparticles on mesoporous silica. In this study, the discharge time was varied from 10 to 20 min with 5 min of time interval.

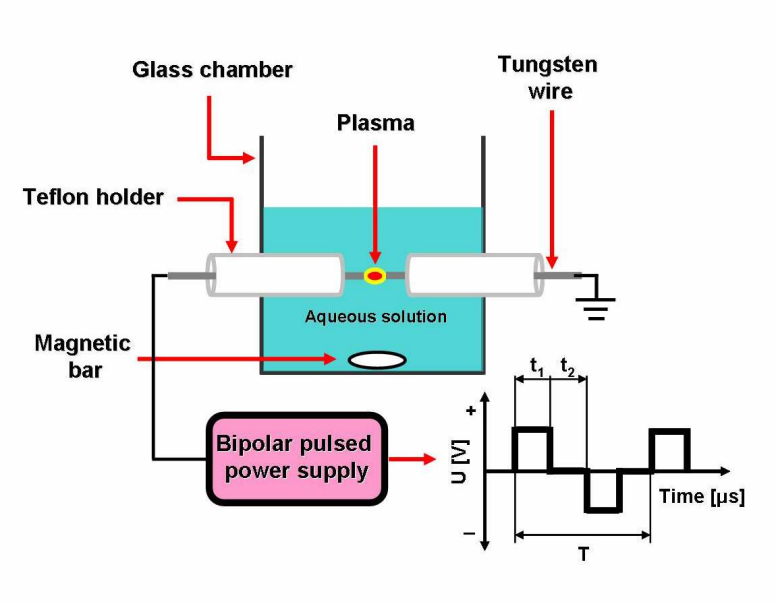

Fig. 4.1. Schematic illustration of SPP setup.

4.2.3. Characterization

X-ray diffraction (XRD) patterns were measured using XRD Rigaku Smartlab with Cu Kα radiation (λ = 0.154 nm). The diffraction patterns were collected in the range of 2θ = 0.1-90° using a scanning rate of 1°/min. Transmission electron microscopy (TEM) observations were performed on JEM-2500SE at an acceleration voltage of 200 kV. Scanning electron microscopy (SEM) images were achieved on JSM-6330 F (JEOL) at an acceleration voltage of 15 kV and the magnification in the range of 1500-18000. UV-VIS optical spectra were recorded using a Shimadzu UV-3600 UV-VIS-NIR spectrophotometer by scanning wavelength from 200-700 nm. The sample

solutions were poured into a quartz cell with 1 cm absorption length. Energy dispersive X-ray (EDX) spectra were detected using Hitachi Miniscope TM-1000. Surface area of the mesoporous silica particles was calculated using the Brunauer-Emmett-Teller method from N_2 adsorption-desorption isotherm which carried out on Belsorp-mini II. All samples were degassed at 150 °C for 24 h prior to the measurement.

4.3. Results and Discussion

SPP was proposed to be used for both Ag nanoparticles formation on mesoporous silica and surfactant template decomposition in one batch of discharge. Both SPP abilities: the reduction from Ag^+ to Ag^0 nanoparticles and the decomposition by oxidation of the organic template were realized by evidence of XRD patterns. Fig. 4.2 shows the diffraction patterns of Ag nanoparticles on mesoporous silica at various discharge times for 10, 15, and 20 min. Since the investigated samples are composed by two types of materials, XRD patterns were analyzed corresponding to two regions at $2\theta < 5°$ and $2\theta > 38°$. In the first region as shown in Fig. 4.2A, the broad peaks were obtained and assigned to mesoporous silica at a characteristic diffraction angle (2θ) at approximately 0.7°. From this diffraction peak position, we evaluated the obtained pore size to be 12.46 nm. Other diffraction peaks could not be observed. From these results, we note that a disordered arrangement of mesopores was obtained. Consequently, the second region in the range of $2\theta = 38\text{-}65°$ as displayed in Fig. 4.2B representing the diffraction patterns characteristic of Ag nanoparticles. The three main peaks of Ag nanoparticles were measured at 38, 44.3, and 64.4° which correspond to the reflections of (111), (200), and (220), respectively. These reflections can be

attributed to lattice planes of face-centered-cubic structure (fcc) of Ag nanoparticles. As compared with the diffraction patterns of silver bulk, the observed Ag nanoparticles peaks was a broad line width and it was influenced by nanocrystalline structure of Ag nanoparticles [12,13]. Following Debye-Scherrer equation, the average crystalline size of Ag nanoparticles in Ag nanoparticles on mesoporous silica system could be calculated to be 17.24, 22.72, and 22.89 nm after SPP discharge time for 10, 15, and 20 min, respectively [14-16]. As increasing the SPP discharge time, the diffraction peak intensity significantly increased, yielding the increase in amount of Ag nanoparticles [5]. This can be explained that the Ag nanoparticles formation was initially started and the crystalline growth was stepwise occurred during discharge via reduction and both of them were proportional to the increase in discharge time.

TEM images can obviously provide evidence of the Ag nanoparticles on mesoporous silica. Fig. 4.3 shows TEM image in the bright field mode and high-resolution TEM (HRTEM) image as well as the element mapping mode determined by TEM image and they are observed the dispersed Ag nanoparticles on mesoporous silica. Various Ag nanoparticles sizes are detected in TEM image with the larger size at approximately 20 nm and the good dispersive smaller size at approximately 5 nm (Fig. 4.3a). The element mapping mode in Fig. 4.3b is used to confirm the good dispersion of Ag nanoparticles on mesoporous silica. It notes by the fact that Ag nanoparticles were observed not only the coating on outside of mesoporous silica surface but also the impregnation inside mesopores. The larger particles size was detected as the increase in discharge time which is in good agreement with the mentioned XRD results, see Table 4.1. In this study, we intended to use SPP in the shortest time as possible for template removal inside mesoporous silica and for Ag

nanoparticles impregnation. However, the observed average Ag nanoparticles size was founded to be 15.95 nm for only 10 min of discharge time. Subsequently, as the increasing discharge time from 15 to 20 min, the average sizes of Ag nanoparticles were 23.62 and 25 nm, respectively. The average sizes of Ag nanoparticles calculated from the results of TEM and XRD has no significant, the difference was recorded only 6.89%.

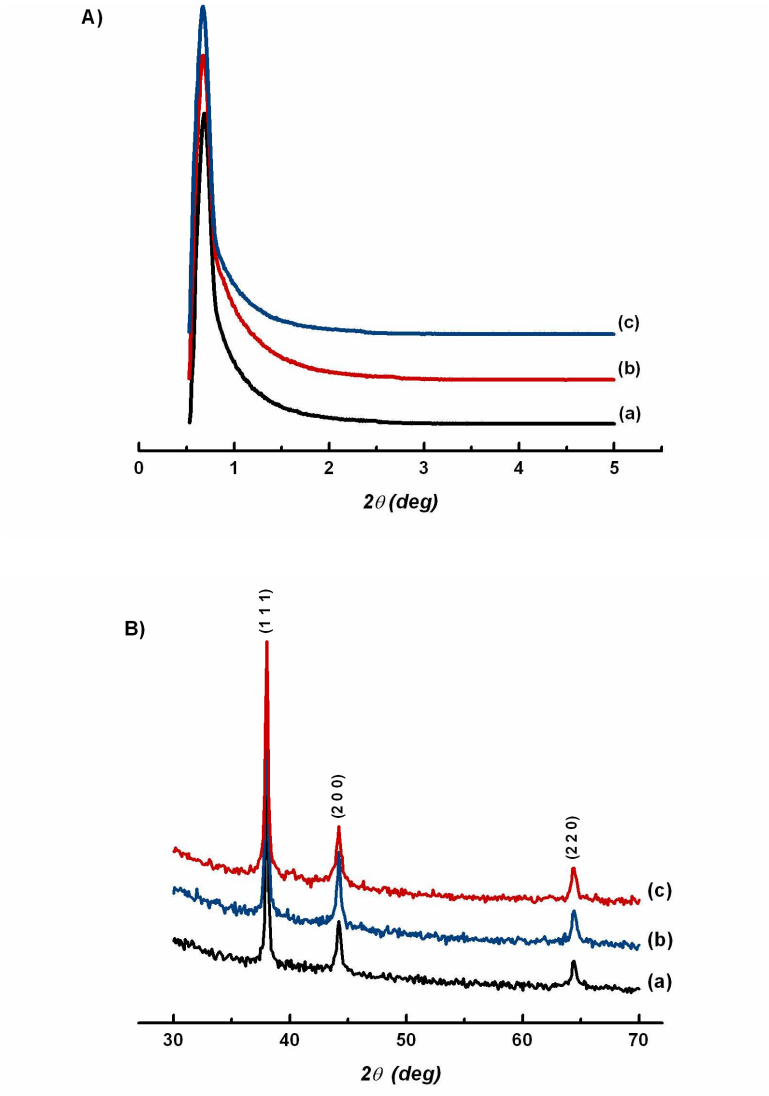

Fig. 4.2. XRD patterns of Ag nanoparticles on mesoporous silica, A) mesoporous silica region and B) Ag nanoparticles region, at various discharge times, (a) = 10 min, (b) = 15 min, and (c) = 20 min.

Table 4.1. Average size of Ag nanoparticles estimated by XRD and TEM.

Discharge time (min)	Average size of Ag nanoparticles (nm)	
	XRD	TEM
10	17.24	15.95±3.84
15	22.72	23.62±9.91
20	22.89	25±6.35

The size distribution of Ag nanoparticles prepared using SPP was rather high owing to the non-homogeneous condition which is difficult to be controlled and it has been reported as a drawback of such process. In comparing with the chemical path, the size distribution of Ag nanoparticles coating on mesoporous silica by chemical synthesis are relatively smaller than those of silver nanoparticles prepared using SPP in this study [5,12]. This suggests that the uniform morphology and narrow size distribution of Ag nanoparticles are easily controlled by chemical reaction. However, SPP is developed to be a one step process to remove the template in mesoporous silica and to incorporate Ag nanoparticles on mesoporous silica for exceptionally promising short consumption time process.

Although various geometries of Ag nanoparticles have been reported for instance spherical [12,17], and triangular shapes [18], as well as rod-like structure [19]. The spherical shape, which is the thermodynamical crystalline structure, is normally presented in the different systems owing to the lowest surface energy of this nanoparticles type. Also in this study, the spherical Ag nanoparticles with an almost perfect fcc orientation were presented by high-resolution TEM (HRTEM) image as displayed in the inset of Fig. 4.3a which is in a good agreement of XRD results. The

diffraction mode was shown in the upper right corner of such image. The spots corresponding to the orientation of [111] direction of fcc arrangement were observed with the plane reflections of (220) [18].

Scanning electron microscope was carried out to observe the morphology of mesoporous silica particles and Ag nanoparticles on mesoporous silica after SPP as shown in Fig. 4.4. The highly dispersed spherical shape mesoporous silica was obtained with an average particle size at approximately 3 μm. In the case of high magnification, we could observe the dispersed Ag nanoparticles on the surface of the mesoporous silica with various particles sizes depending on discharge time. This result indicates that the discharge time was long enough for Ag nanoparticles growth and accumulation to increase the particle size.

The optical absorption spectroscopy is one of reliable techniques for monitoring the formation of Ag nanoparticles by the surface-plasmon resonance (SPR) characteristic. SPR absorption spectra of Ag nanoparticles in UV-VIS range depend on the size, shape, and the surrounding media based on the collective oscillation of electrons. In the case of Ag nanoparticles, the absorption maximum of SPR peak normally observes around 400 nm. In this study, SPR absorption maxima of Ag nanoparticles were recorded in the range from 418 to 441 nm depending on the increasing discharge time as shown in Fig. 4.5. The red shift of the maximum absorption peak is influenced by larger Ag nanoparticles size. The broader SPR peak with a shoulder describes the effect of high Ag nanoparticles size distribution [6,20,21]. This finding is supported by TEM images which revealed evidence of a wide range of Ag nanoparticles size.

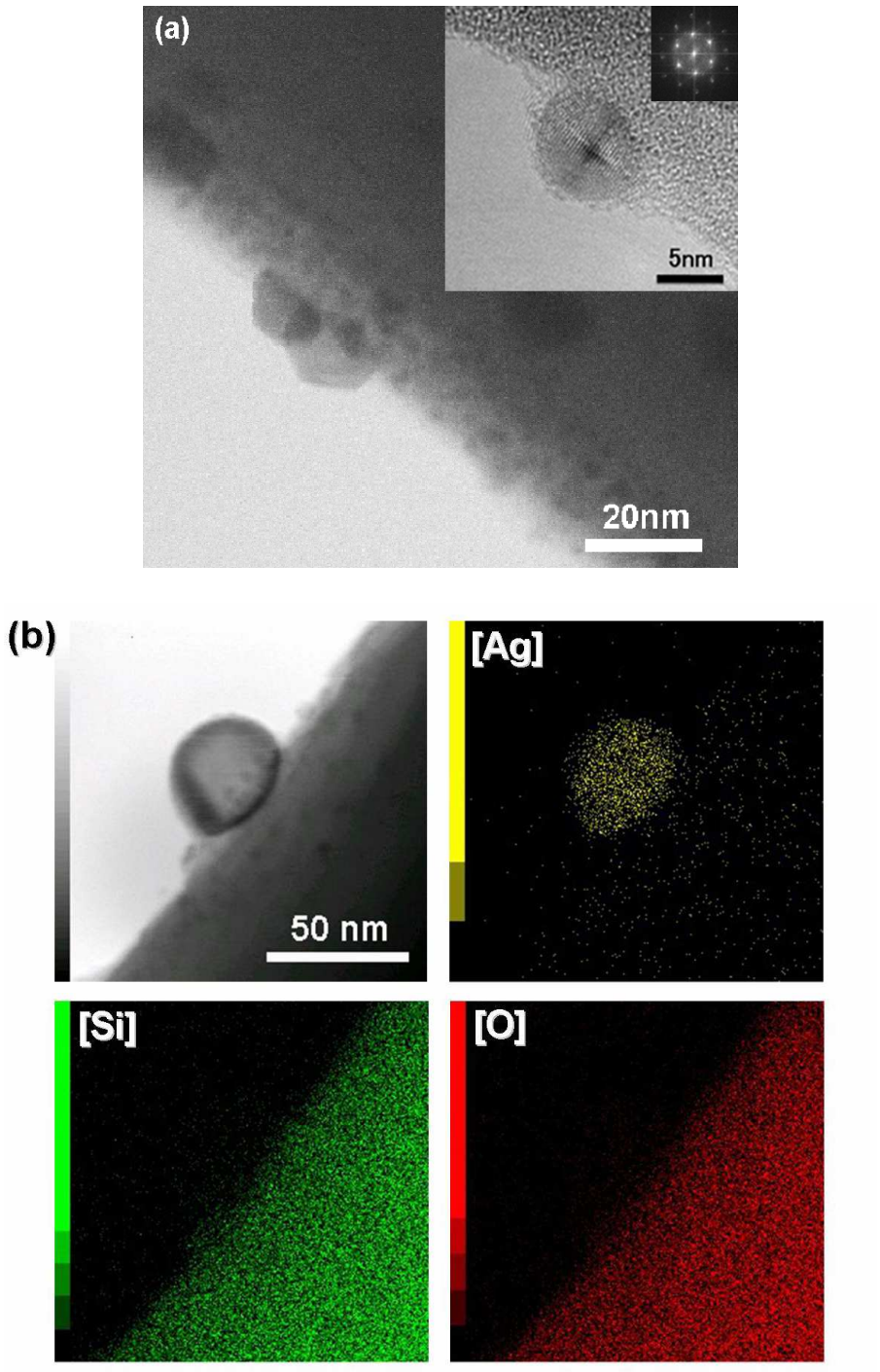

Fig. 4.3. Transmission electron microscope (TEM) images in (a) bright-field mode and high-resolution TEM and (b) element mapping mode determined by TEM image of Ag nanoparticles on mesoporous silica after SPP for 10 min containing Ag element, Si element, and O element.

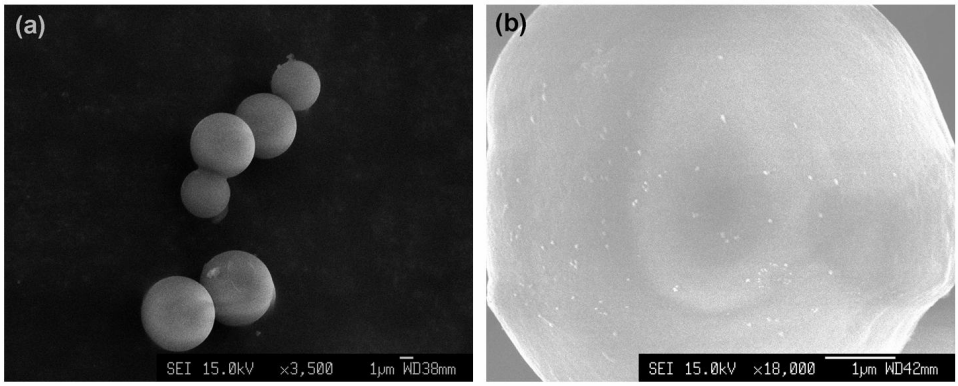

Fig. 4.4. Selected SEM images of Ag nanoparticles on mesoporous silica after SPP for 10 min, (a) low magnification and (b) high magnification.

The SPR absorption peak intensity also plays an important role for a quantitative evaluation of the amount of the synthesized Ag nanoparticles. There is a significant difference of Ag nanoparticles amount when we compared the intensity of the SPR absorption at various discharge times. It notes that the highest amount of Ag nanoparticles was found when the discharge time was 20 min.

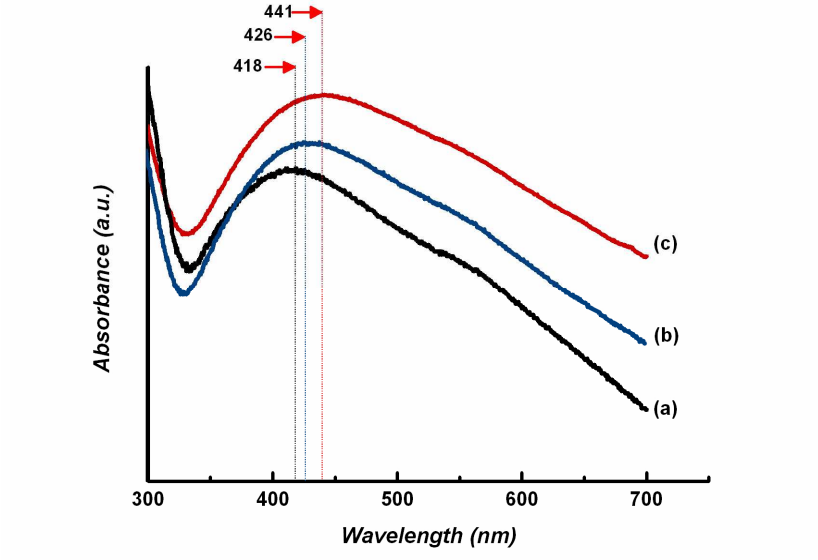

Fig. 4.5. UV-VIS absorption spectra of Ag nanoparticles on mesoporous silica at various discharge times, (a) = 10 min, (b) = 15 min, and (c) = 20 min.

The formation of Ag nanoparticles is also confirmed by EDX spectra which are the relation of the percentage of Si and Ag from EDX spectra in a function of discharge time as displayed in Fig. 4.6. The evaluated amount of Ag nanoparticles in the case of SPP for 10 min was at approximately 12.7% from the total amount of all elements. After the discharge time increased from 15 to 20 min, the percentages of Ag nanoparticles were evaluated to be 13.57 and 14.45%, respectively. The increased percentages of Ag nanoparticles amount for 5 min increment of discharge time were respectively calculated to be 6.85% (from 10 to 15 min discharge time) and 6.48% (from 15 to 20 min discharge time). It is clear that Ag nanoparticles amount was proportional to the discharge time confirming by the results of XRD and UV-VIS spectra. Moreover, from EDX spectra, this process was proved to be a clean process. Only Si and Ag elements were detected without any contamination.

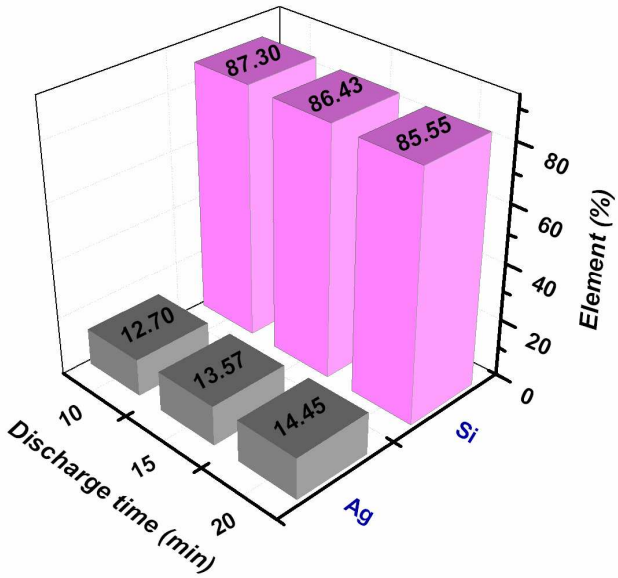

Fig. 4.6. Summary of the element percentage calculated from EDX spectra.

Beside the nanoparticles synthesis using SPP, the feasibility of SPP for organic decomposition also has been investigated. During SPP, organic compounds and dyes are easily decomposed via oxidation by hydroxyl radicals generated during discharge and the by-products for instance the oxidized compounds and the water soluble compounds might be produced after the discharge process [11,22-25]. Moreover, the hydroxyl and oxygen radicals were recently proved to be the oxidation source for the template decomposition inside the mesoporous silica, as reported in the previous study [11]. The occurrence of the expected reactions during SPP can be proposed by the scheme image as shown in Fig. 4.7. In plasma, the cleavage of water molecule was presented and the species were energetically excited by the plasma. Consequently, the generated active species was extensively transferred in to the liquid phase and the propagation to produce the numerous active species was continuously occurred. During SPP, the generated active species could be detected in the optical emission spectra in the different emission wavelength for instance OH = 308 nm, H_γ = 434 nm, H_β = 486 nm, H_α = 656 nm, O = 778, and 845 nm (Fig. 4.8) [26,27]. Among various active species, there is the high possibility to stepwise react with the reactants which are containing in such solution. Herein, the reduction of Ag ions to Ag nanoparticles and the oxidation to decompose the organic template inside mesopores were scientifically taken place via the dominated hydrogen and hydroxyl radicals, respectively.

In this study, the ability of oxidation during discharge in template removal process was estimated by the term of surface area calculating from N_2 adsorption-desorption isotherms which was determined by the function of the amount of the absorbed gas (N_2) on the surface of samples.

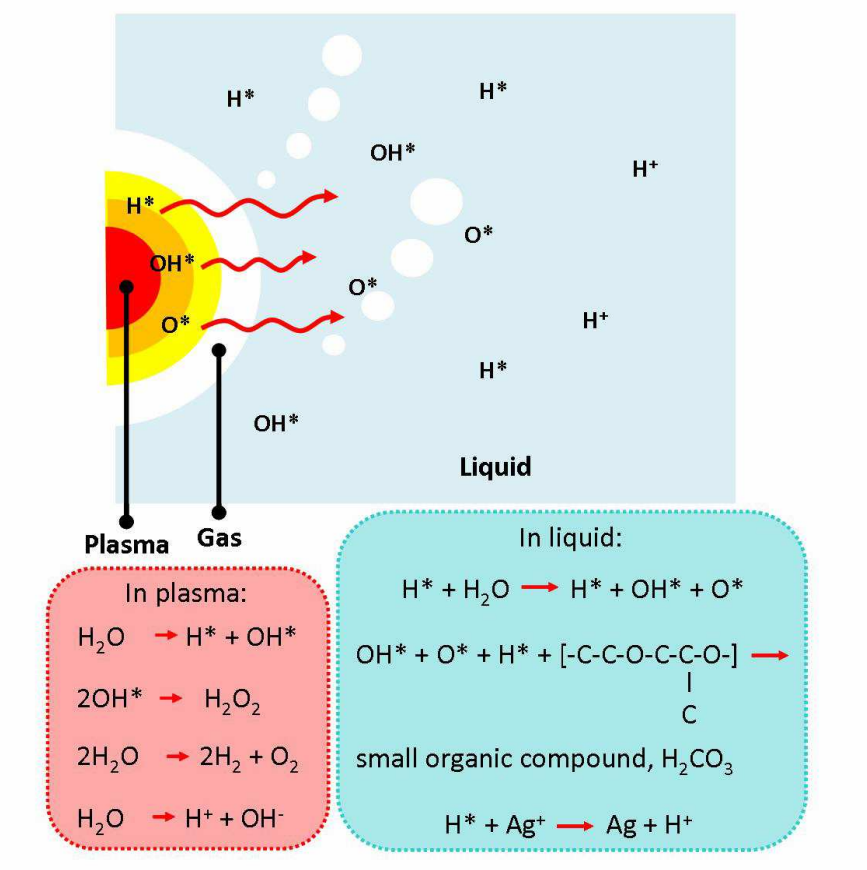

Fig. 4.7. Schematic illustration of the generated reactions during SPP both in plasma and liquid phases.

Fig. 4.9 shows N_2 adsorption-desorption isotherms of Ag nanoparticles on mesoporous silica at different discharge times, 10, 15, and 20 min which belong to type IV isotherm corresponding to a characteristic cylindrical-like pore structure. These isotherms exhibit hysteresis loops with sloping curves in the range of the relative pressure (p/p_0) from 0.4 to 0.6. The summary of the structural parameters of mesoporous silica including the BET surface area, total pore volume, and mean pore diameter calculated using N_2 adsorption-desorption isotherms are displayed in Table 4.2.

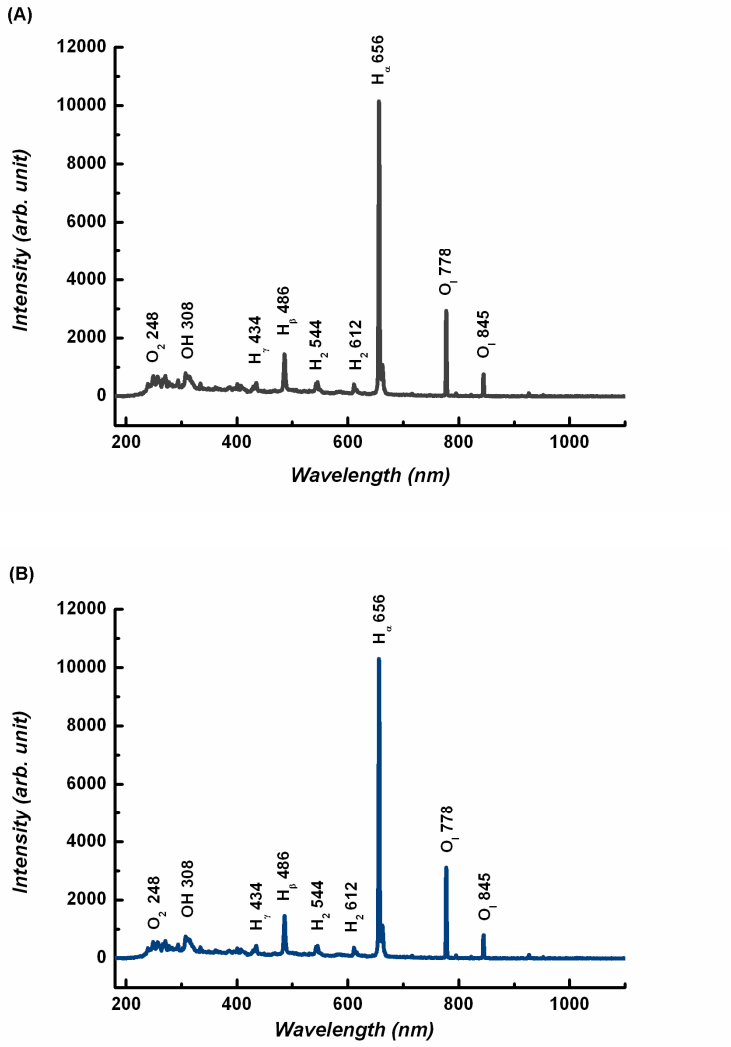

Fig. 4.8. Optical emission spectra of various active species during SPP for (A) 10 min and (B) 20 min.

The BET surface area and total pore volume of as-synthesized silica before discharge were calculated to be 215 m^2g^{-1} and 0.15 cm^3g^{-1}, respectively. After discharge process under various discharge times from 10, 15, and 20 min, both of BET surface area and total pore volume were changed with an increasing tendency to be 515, 639, and 650 m^2g^{-1} and 0.18, 0.21, and 0.21 cm^3g^{-1}, respectively. The tendency of the increase in the BET surface and total pore volume was

straightforwardly dependent on the discharge time which influenced the duration of the oxidation. Compared with the result of the thermal calcination, which is well known that the contraction of mesopores generally occur after such process, the BET surface area was found to be 534 m^2g^{-1} whereas the value of total pore volume showed the magnitude of 0.18 cm^3g^{-1}. As the results of Ag nanoparticles on mesoporous silica samples, higher BET surface area and total pore volume were found after discharge for 15 and 20 min. Although Ag nanoparticles were formed and incorporated in mesoporous silica, most of template was decomposed and mesopores were stabilized without mesopores contraction. From these results, we suggest that SPP in this system provide high efficient for template remove which has no effect to reduce pore size. Nevertheless, in the case of discharge time for 10 min, BET surface area was obtained to be lower than that of calcination result, this case explains that this process had no enough time for completely removal the surfactant template inside mesopores. Some parts of surfactant template still remained effecting to obstruct the adsorption of the adsorbed gas on the surface of materials. This feature is in good agreement with our previous work which realized that surfactant template was totally removed using SPP for 15 min.

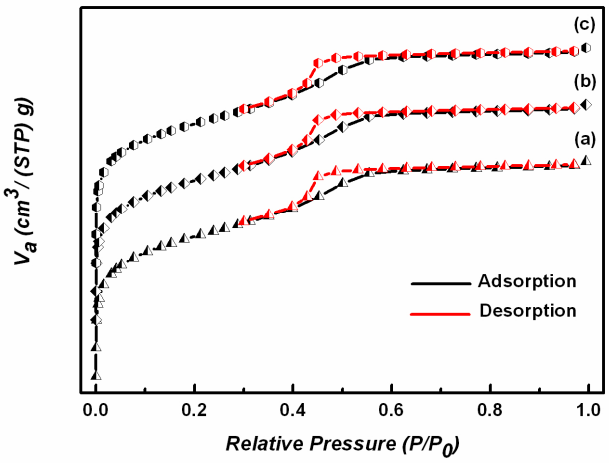

Fig. 4.9. N_2 adsorption-desorption isotherm of Ag nanoparticles on mesoporous silica at different discharge times, (a) 10 min, (b) 15 min, and (c) 20 min.

Table 4.2. Structural parameters of Ag nanoparticles on mesoporous silica samples.

Discharge time (min)	BET surface area, a_{BET} (m^2g^{-1})	Total pore volume (cm^3g^{-1})
0*	215	0.15
10	515	0.18
15	639	0.21
20	650	0.21
Thermal calcination**	534	0.18

*As-synthesized silica without Ag nanoparticles

**Mesoporous silica after thermal calcination for 6 h in air atmosphere

4.4. Conclusion

Solution plasma process was successfully applied to synthesize Ag nanoparticles on mesoporous silica using only Ag precursor without any reducing agent and also to discard the organic template in mesoporous silica simultaneously. The large Ag nanoparticles with the average size at approximately 20 nm were observed after SPP for 10-20 min meanwhile the small size about 5 nm was dispersed well in mesoporous silica. The completed template removal was found after SPP for 15 min. The expected mechanism could be explained as following: a) the generated hydrogen radicals in the discharge play the role of the reduction agent to reduce Ag^{+} to Ag^{0} and then Ag nanoparticles were coalesced into silver clusters which were freely dispersed in the solution and incorporated on the supporting material, b) the oxidation also extensively occurred by the generated hydroxyl radicals which decomposed the organic compound inside the mesopores of mesoporous silica particles. The obtained Ag nanoparticles on mesoporous silica were relatively larger size comparing to the Ag nanoparticles synthesized via commercial chemical reaction as a result of increased discharge time. The amount of Ag nanoparticles and the ability of template removal were dependent on the discharge time proportionally. Finally, SPP was proved to be a short consumption time process for simultaneous Ag nanoparticles formation on mesoporous silica and template removal with no influence on mesopores size.

References

[1] N. A. M. Barakat, K.-D Woo, M. A. Kanjwal, K. E. Choi, M. S. Khil, and H. Y. Kim, *Langmuir*, 2008, **24**, 11982.

[2] J. N. Anker, W. P. Hall, O. Lyandres, N. C. Shah, J. Zhao, R. P. Van Duyne, *Nat. Mater.*, 2008, **7**, 442.

[3] J.-H. Kim, W. W. Bryan, and T. R. Lee, *Langmuir*, 2008, **24**, 11147.

[4] M. Aminuzzaman, A. Watanabe, and T. J. Miyashita, *Nanopart. Res.*, 2009, **12**, 931.

[5] D. Tian, G. Yong, Y. Dai, X. Yan, and S. Liu, *Catal. Lett.*, 2009, **130**, 211.

[6] M. Yamamoto, Y. Kashiwagi, and M. Nakamoto, *Langmuir*, 2006, **22**, 8581.

[7] V. S. Kovivchak, V. I. Dubovik, and R. B. Burlakov, *Journal of Surface Investigation. X-rays, Synchrotron and Neutron Techniques*, 2009, **3**, 268.

[8] P. Smejkal, J. Peleger, K. Siskova, B. Vlckova, O. Dammer, and M. Slouf, *Appl. Phys. A*, 2004, **79**, 1307.

[9] J. Hieda, N. Saito, and O. Takai, *J. Vac. Sci. Technol. A*, 2008, **26**, 854.

[10] J. Hieda, N. Saito, and O. Takai, *Mater. Res. Soc. Symp. Proc.*, 2008, **1056**, HH 03-39.

[11] P. Pootawang, N. Saito, and O. Takai, *Jpn. J. Appl. Phys.*, 2010, **49**, 126202-1.

[12] Y. H. Kim, D. K. Lee, and Y. S. Kang, *Colloids Surf. A: Physicochem. Eng. Aspects*, 2005, **257-258**, 273.

[13] M. S. Leite, V. Rodrigues, and D. Zanchet, *Progr. Colloid Polym. Sci.*, 2004, **128**, 131.

[14] J. I. Langford and A. J. C. Wilson, *J. Appl. Cryst.*, 1978, **11**, 102.

[15] R. Das, S. S. Nath, D. Chakdar, G. Gope, and R. Bhattacharjee, *J. Nanotechnol. Online*, 2009, **5**, 1.

[16] X. H. Xiao, L. P. Guo, F. Ren, J. B. Wang, D. J. Fu, D. L. Chen, Z. Y. Wu, Q. J. Jia, C. Liu, and C. Z. Jiang, *Appl. Phys. A*, 2007, **89**, 681.

[17] K. Belser, T. V. Slenters, C. Pfumbidzai, G. Upert, L. Mirolo, K. M. Fromm, and H. Wennemers, *Angew. Chem.*, 2009, **121**, 3715.

[18] A. Courty, A. I. Henry, N. Goubet, and M. P. Pileni, *Nat. Mater.*, 2007, **6**, 900.

[19] C. Ni, P. A. Hassan, and E. W. Kaler, *Langmuir*, 2005, **21**, 3334.

[20] Y. Sun, Y. Liu, Z. Guizhe, and Q. Zhang, *J. Polym. Res.*, 2008, **15**, 269.

[21] F. Douglas, R. Yanez, J. Ros, S. Marin, A. de la Escosura-Muniz, S. Alegret, and A. Merkoci, *J. Nanopart. Res.*, 2008, **10**, 97.

[22] B. Yang, M. Zhou, and L. Lei, *Chemosphere*, 2005, **60**, 405.

[23] P. Baroch, V. Anita, N. Saito, and O. Takai, *J. Electrostat.*, 2008, **66**, 294.

[24] A. T. Sugiarto, T. Ohshima, and M. Sato, *Thin Solid Films*, 2002, **407**, 174.

[25] H. Wang, J. Lei, X. Quan, and Y. Wu, *Appl. Catal. B: Environ.*, 2008, **83**, 72.

[26] F. D. Baerdemaeker, M. Simek, J. Schmidt, and C. Leys, *Plasma Sources Sci. Technol.*, 2007, **16**, 341.

[27] J. Prochazkova, Z. Stara, and F. Krcma, *Czech. J. Phys.*, 2006, **56**, 1314.

Chapter 5. Solution Plasma for Ag Nanoparticles Incorporation in Mesoporous Silica and Its Preliminary Catalytic Test for Oleic Acid Hydrogenation

The incorporation of Ag nanoparticles on mesoporous silica and its hydrogenation ability were described in this study. Mesoporous silica was synthesized via sol-gel method in acid solution and used as the supporting material. The template removal process and Ag nanoparticles incorporation were concurrently taken place in the novel glow discharge system in aqueous solution, namely solution plasma process under the controlled discharge conditions. Only 15 min of the discharge time, the template inside mesoporous silica was mostly removed resulting in FTIR spectra and Ag nanoparticles were formed confirming by the evidences of XRD patterns and TEM images. The preliminary test of catalytic ability for hydrogenation for converting the unsaturated oleic acid to the saturated stearic acid was monitored using UV-vis spectroscopy after the oxidizing reaction with permanganate ions (MnO_4^-). It found that the conversion was observed to be 12.83% in butanol system and reached to 90.56% in ethanol system.

5.1. Introduction

Solution plasma process (SPP) has been demonstrated as a versatile process with high performance for many applications including nanoparticles synthesis, water purification, organic compound decomposition as well as sterilization. Despite SPP

has been recently developed and has a short history, this method offers many benefits by the numerous active species and radiation present in this type of plasma. The active species including hydrogen radical ($H^{\cdot}$), oxygen radical ($O^{\cdot}$), hydroxyl radical ($OH^{\cdot}$), hydroperoxyl radical ($HO_2^{\cdot}$), high energy electrons, and UV radiation are produced during the discharge process resulting in high reaction rates and different effective chemical reaction paths [1-3]. The dominated active species such as hydroxyl radicals which are generated in high amount during SPP have a high potential to decompose the organic compounds in water pollution treatment and template removal inside mesoporous silica owing to its oxidation activity [4-6]. The generated hydrogen radicals play an important role as reducing agent in nanoparticles synthesis via reduction reaction, as gold nanoparticles with various crystalline geometries which have been reported in our group [7].

In nanoparticles field, Ag nanoparticles are extensively investigated considering their significant physicochemical characteristics. There are many published articles have been reported that Ag nanoparticles are widely applied in various advantages for instance the microbial inhibition, sensors, optical devices, and electronic devices owing to its unique properties [8-13]. Typically Ag nanoparticles can be easily synthesized by a reaction containing silver ion solution (i.e. $AgNO_3$) and stepwise reduction reaction using the common reducing agents for instance $NaBH_4$. The thermal decomposition technique using high-power ion beam was successfully used to form the Ag nanoparticles film on substrate [14]. The laser ablation containing silver nanowire fraction and sodium citrate reducing agent was the recent method to prepare Ag nanoparticles with a wide size distribution and various particle morphologies [8]. Moreover, the clean synthesis of Ag nanoparticles using γ-irradiation in the ethanol system containing $AgNO_3$, sodium citrate was proposed and the particle size could be

controlled by irradiation dose [15]. In term of application, Ag nanoparticles incorporated in various types of supporting materials have been reported in many fields. In the catalyst, the highly dispersed Ag nanoparticles on Aerosil-200 silica provided the ethylene hydrogenation activity over 550 K [16]. The high activity and selectivity of chloronitrobenzenes conversion to chloroanilines by the hydrogenation in the Ag nanoparticles and the silica support system was also reported [17].

Herein, mesoporous silica used as supporting material was prepared via sol-gel method in acid solution. To incorporate AgNPs and remove template inside mesopores without addition of reducing and oxidizing agents, SPP was employed at only 15 min of processing time. The obtained materials were characterized by X-ray diffraction (XRD), transmission electron microscope (TEM), and fourier transform infrared spectroscopy (FTIR). The hydrogenation using Ag nanoparticles incorporated mesoporous silica as catalyst was also evaluated using the unsaturated oleic acid as the reactant. The product after hydrogenation was determined in the term of oxidizing activity using permanganate ion and UV-VIS spectroscopy was employed to monitor the absorbance of the product after oxidation.

5.2. Experimental Procedures

5.2.1. Materials

Tetraethyl orthosilicate (TEOS), 1,1,2,2,3,3,4,4,4-nonafluoro-1-butane sulfonate (NFBS), hydrochloric acid (HCl), sodium hydroxide (NaOH), silver nitrate ($AgNO_3$), and potassium permanganate ($KMnO_4$) were purchased from Wako Pure Chemical Industries, Ltd, Japan. P123 copolymer ($EO_{20}PO_{69}EO_{20}$) and sodium dodecylbenzene

sulfonate (SDBS) were purchased from Sigma-Aldrich, INC, USA. All chemicals were further used without any purification.

5.2.2. Ag nanoparticles incorporated mesoporous silica synthesis and its hydrogenation test

In a synthesis, the surfactant system containing 0.5 g triblock copolymer P123, 0.1 g NFBS, and 0.084 g SDBS was dissolved in 3 M HCl and continuously stirred until homogeneous solution. Consequently, a weight of 2.15 g silica precursor (TEOS) was added into the solution, and then the mixture was further kept under static condition at ambient temperature for 24 h to form the white precipitate. To impregnate Ag nanoparticles on mesoporous silica, a solution of 150 ml containing 0.5, 1, and 5 mM $AgNO_3$ and 0.15 g of triblock copolymer P123 were prepared. After that 1 g of the as-synthesized silica was added into such solution and the discharge was further processed for 15 min using bipolar pulsed power supply in the prepared solution by controlling the discharge parameters. The typically used parameters: voltage, pulse frequency, pulse width, and electrode distance, were 1.6 kV, 15 kHz, 2 μs, and 0.3 mm, respectively.

The preliminary test for hydrogenation was evaluated by the following steps. The mixture of 1.5 g oleic acid, 40 ml ethanol (butanol), and 0.02 g catalyst, Ag nanoparticles incorporated mesoporous silica was prepared in the round-bottom flask and such mixture was purged by H_2 gas for 15 min. Then it was heated in the temperature-controlled water bath at 50 °C for 1 h. The collected solution was kept in the test tube and a drop of 0.5 M $KMnO_4$ was added. The oxidized solution was determined the remaining permanganate species by using UV-VIS spectrophotometer.

The as-synthesized Ag nanoparticles incorporated mesoporous silica were studied by X-ray diffraction measurement which were carried out on XRD Rigaku Smartlab

with Cu Kα radiation (λ = 0.154 nm). The diffraction patterns were collected in the range of 2θ = 0.1-90° by using a scanning rate of 1°/min. TEM observations were performed on JEM-2500SE with an acceleration voltage of 200 kV. Fourier transform infrared (FTIR) spectra were measured on a Digilab FTS-7000 series. All the samples were mixed with dehydrated potassium bromide (KBr) and then made into pellets using a hydraulic press. The collected spectra were measured with 256 scans in the range of 4000-400 cm^{-1}. The resolution of collection was 2 cm^{-1}. Surface area and pore diameter were calculated using Brunauer-Emmett-Teller (BET) and Barrett-Joyner-Halenda (BJH) methods from N_2 adsorption-desorption isotherm measured on Belsorp-mini II. In the catalytic test, UV-VIS optical spectra were recorded with a Shimadzu UV-3600 UV-VIS-NIR spectrophotometer by scanning wavelength from 200-700 nm. The sample solutions were poured into a quartz cell with 1 cm absorption length.

5.3. Results and Discussion

The formation of Ag nanoparticles on mesoporous silica after SPP for 15 min in various $AgNO_3$ concentrations are found in XRD patterns as shown in Fig. 5.1. XRD patterns were divided into two regions. Firstly around 0.8°, the broad diffraction peaks were detected without any higher diffraction peak (Fig. 5.1A). This feature was regarding to the worm-like mesopores characteristic. In the second region (Fig. 5.1B), we observed three peaks at 38, 44, and 64° corresponding to (111), (200), and (220) plane reflections of faced-center cubic (fcc) structure of AgNPs [18]. The difference of the peak intensity was also found to be the highest value in the case of the synthesis using 5 mM $AgNO_3$ and the intensity referred to the amount of Ag nanoparticles in

each system. Hence, the amount of Ag nanoparticles was proportional to the $AgNO_3$ concentration.

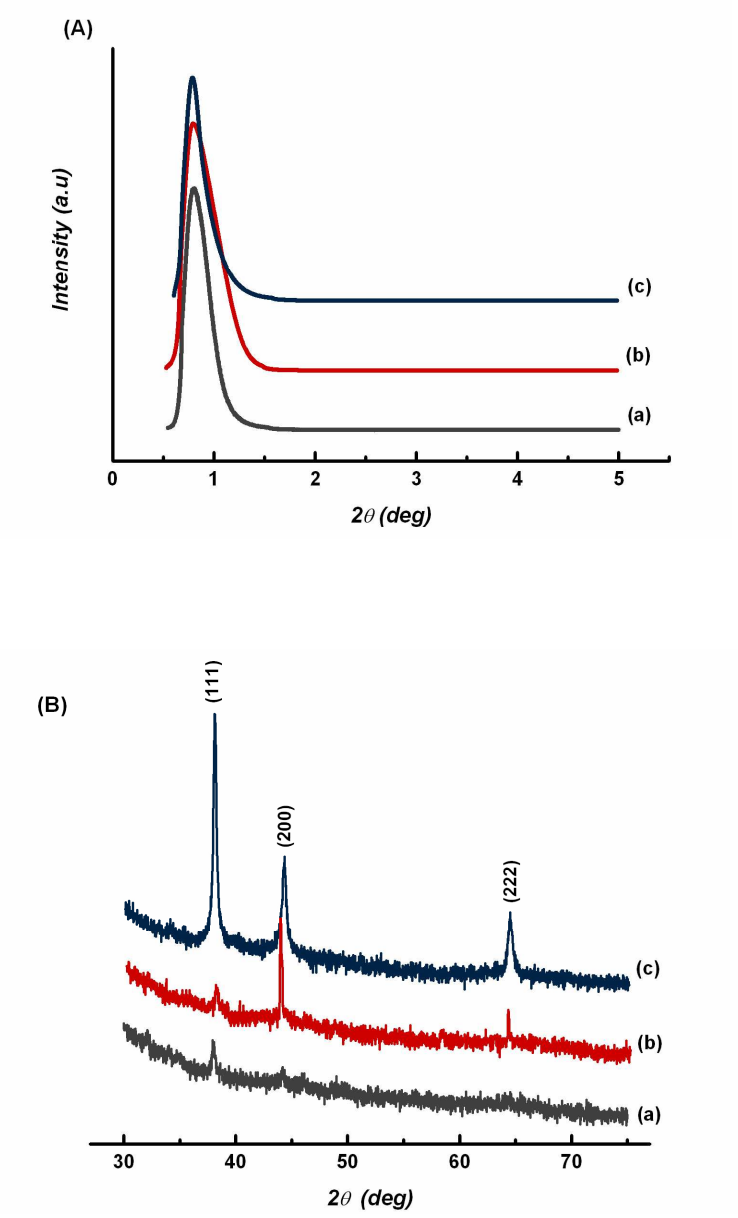

Fig. 5.1. XRD patterns of Ag nanoparticles incorporated mesoporous silica synthesized by SPP for 15 min in (a) 0.5 mM $AgNO_3$, (b) 1 mM, and (c) 5 mM: (A) XRD plots of Si region and (B) Ag nanoparticles region.

Fig. 5.2(a,b,c) show TEM images of the dispersed AgNPs on mesoporous silica with the average sizes about 5.76, 15.66, and 32.31 nm after discharge in the uses of 0.5, 1, and 5 mM $AgNO_3$, respectively. The AgNPs contents calculated by a wide-area scanning of EDX were 9.89, 13.57, and 25.78%, respectively. The high-resolution TEM image (Fig. 5.2d) reveals fcc structure of AgNPs attached on worm-like silica matrix. This evidence could not observe the ordered arrangement and it was hardly confirmed the interplane diffraction of silica in XRD, even if well-ordered mesopores were constructed [19].

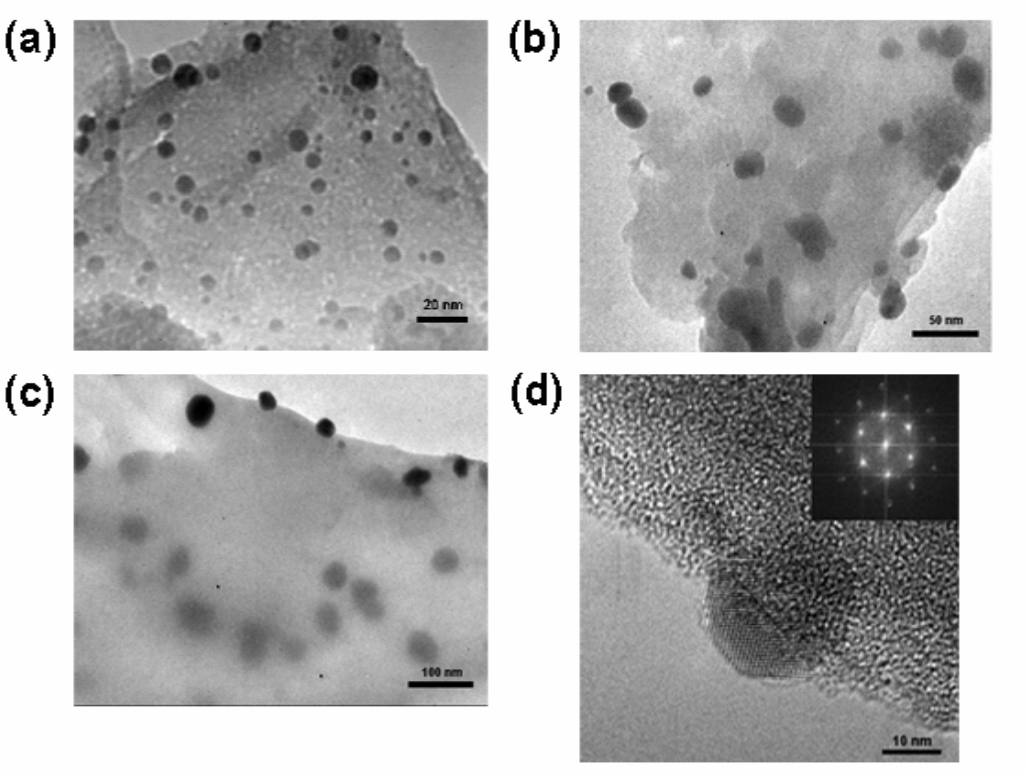

Fig. 5.2. TEM images of Ag nanoparticles incorporated mesoporous silica at various $AgNO_3$ concentrations, (a) 0.5 mM, (b) 1 mM, and (c) 5 mM, and (d) high-resolution TEM image of fcc Ag nanoparticles attached on mesoporous silica surface.

FTIR spectra pay regard to the feasibility of SPP for organic template decomposition as displayed in Fig. 5.3. In as-synthesized silica (Fig. 5.3a), the vibrational peaks were observed at approximately 3100-3700 cm^{-1} (O-H stretching), 2800-3000 cm^{-1} (C-H stretching), 1480 cm^{-1} (C=C stretching), 1730 cm^{-1} (O-H bending), 1380 cm^{-1} (SO_3 stretching), and 1150-1250 (unclear band of C-F stretching) corresponded to the main functional groups of the surfactant system [20,21]. The silica backbone was confirmed by the peaks which were observed in the range of 1000-1250 and 800 cm^{-1} [22].

After SPP for 15 min (Fig. 5.3b), only the remaining peaks of O-H stretching, O-H bending, and Si-O stretching, corresponding to the silica framework and the absorbed moisture inside mesopores were respectively observed at 3100-3700, 1730 and 1650, and 1000-1250 and 800 cm^{-1}. The results of such materials after SPP can be noted that the organic template was discarded during SPP. Moreover, the results are comparable to that of the thermal-calcined mesoporous silica which was reported in Ref. 23.

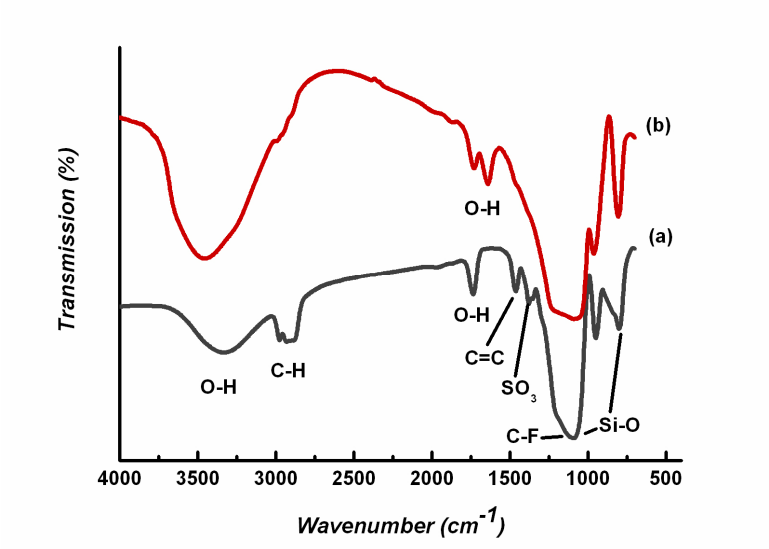

Fig. 5.3. FTIR spectra and the functional bands of (a) the as-synthesized silica and (b) Ag nanoparticles incorporated mesoporous silica synthesized by SPP for 15 min using 1 mM $AgNO_3$.

BET surface area and pore diameter pay attention to the use of mesoporous silica as catalyst and they were calculated from N_2 adsorption-desorption isotherms. BET surface area and pore diameter were reported to be 675, 639, and 581 m^2g^{-1} and 3.3, 3.2, and 2.9 nm for 0.5, 1, and 5 mM $AgNO_3$, respectively (shown in Fig. 5.4). The increase in $AgNO_3$ concentration resulted to the increases in nucleation and particle growth to obstruct the gas adsorption.

The occurrence of the Ag nanoparticles formation and the decomposition of organic template can be explained owing to the reduction by hydrogen radicals and the oxidation by hydroxyl radicals generated during SPP and the overall reactions are written below.

$$H_2O \rightarrow H^{\cdot} + OH^{\cdot} \quad (5.1)$$

$$H^{\cdot} + H_2O \rightarrow H^{\cdot} + OH^{\cdot} \quad (5.2)$$

$$H^{\cdot} + Ag^{+} \rightarrow Ag^{0} + H^{+} \quad (5.3)$$

$$OH^{\cdot} + \text{organic compound} \rightarrow \text{small organic compounds}, H_2CO_3 \quad (5.4)$$

The water molecule cleavage was occurred and the active radicals were excited by the plasma energy during discharge (5.1), then such radicals were transferred into a liquid phase. The propagation of the excitation to produce the high number of radicals in a liquid solution was consequently occurred (5.2). The dominated hydrogen radicals acted as the initiator for Ag ion reduction to Ag nanoparticles (5.3). Moreover, the hydroxyl ions have been reported to be the important species for oxidation [5,6]. In this case, the organic surfactant containing P123 block copolymer, SDBD, and NFBS was decomposed to the small and water-soluble organic compounds by the hydroxyl radicals (5.4) and such products were removed outside the mesopores.

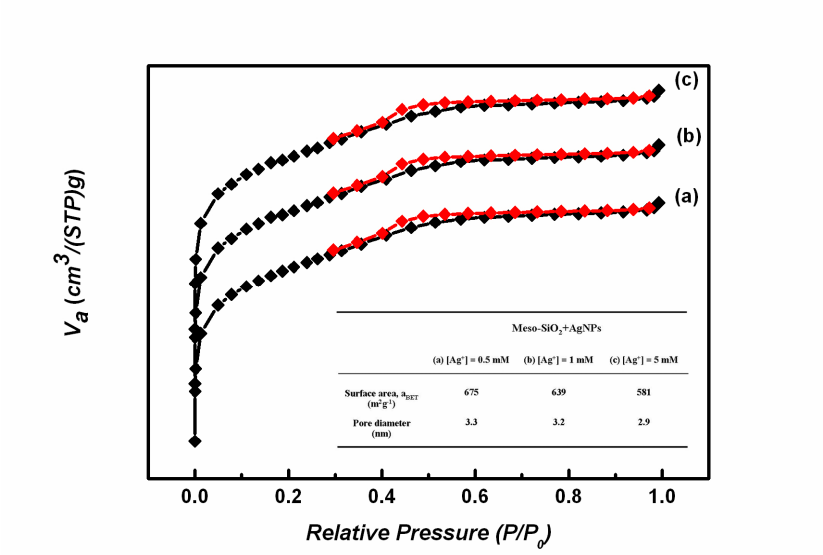

Fig. 5.4. N_2 adsorption-desorption isoterms and the structural parameters, BET surface area and pore diameter calculated by N_2 adsorption-desorption isoterms of samples prepared using different $AgNO_3$ concentrations, (a) 0.5 mM, (b) 1 mM, and (c) 5 mM.

To investigate the preliminary catalytic test for oleic acid hydrogenation, the sample prepared using 1 mM $AgNO_3$ was employed as catalyst, owing to the balance of AgNPs content and high enough of surface area. The percent conversion of the unsaturated oleic acid to the saturated product was calculated using UV-VIS absorbance of the remained permanganate species which referred to amount of outcome after hydrogenation (Fig. 5.5). The involved reactions in this system are illustrated in Fig. 5.6. The percent conversion was reported to be 90.56% in ethanol and only 12.83% in butanol. The catalytic activity in ethanol system was comparable to the oleic acid hydrogenation using ruthenium-tin on SiO_2 in tetradecane system (42.2% of conversion) [24]. In this case, the solubility of mixture plays an important role in catalytic activity. Before hydrogenation, oleic acid in ethanol was high

solubility resulting to the high catalytic activity as the homogeneous catalysis type. Moreover, the outcome after hydrogenation could be easily separated from ethanol since the phase separation was formed and the removal of ethanol was simple [25].

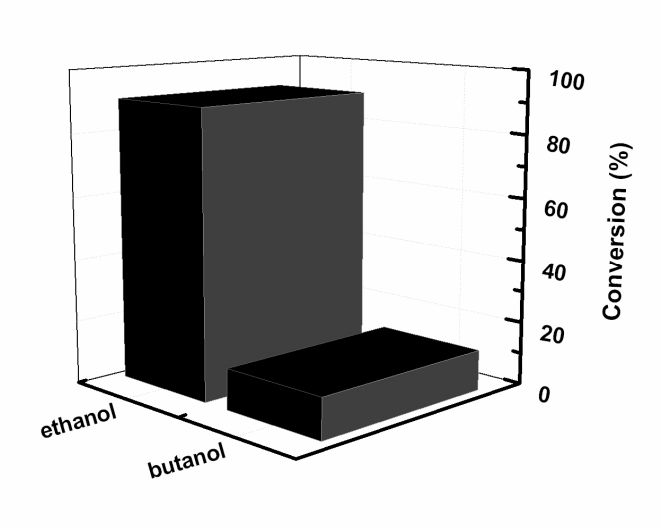

Fig. 5.5. Percent conversion of the saturated stearic acid after hydrogenation using Ag nanoparticles incorporated mesoporous silica as catalyst in ethanol and butanol systems.

To confirm the catalyst stability, the percent weight loss of AgNPs after 3 cycles was observed only 5.21%, confirming by a wide-area scanning of EDX as plotted in Fig. 5.7. Therefore, AgNPs-incorporated mesoporous silica prepared by SPP was high catalytic efficiency and stability for many catalysis cycles.

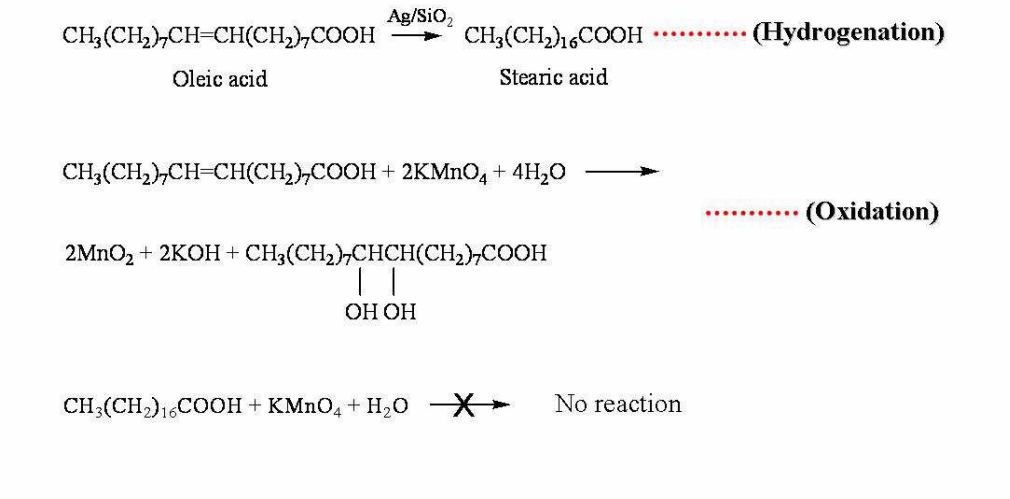

Fig. 5.6. Overall reactions of hydrogenation and oxidation of oleic acid.

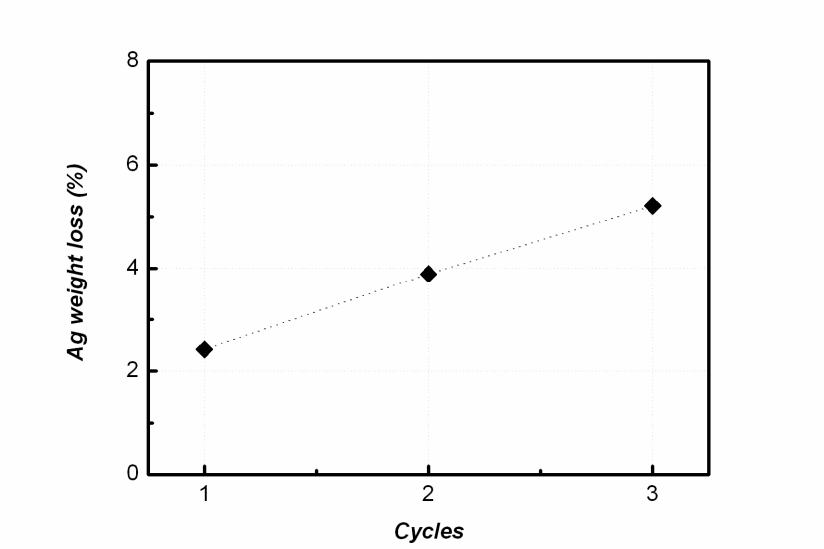

Fig. 5.7. Percent weigth loss of Ag after repeating of hydrogenation.

5.4. Conclusion

AgNPs incorporation and template removal of mesoporous silica were prepared in one-step process by SPP. AgNPs formation was confirmed by XRD and TEM results with various particle sizes dependent on $AgNO_3$ concentration. The decreases in BET surface area and pore diameter were observed as increasing $AgNO_3$ concentration. FTIR spectra were confirmed the high efficient SPP for template decomposition. For the catalytic test, the unsaturated oleic acid was mostly hydrogenated to the saturated stearic acid in ethanol by the homogeneous catalytic effect and the obtained materials had high stability after repeating in several cycles of hydrogenation.

References

[1] O. Takai, *Pure Appl. Chem.*, 2008, **80**, 2003.

[2] B. Yang, M. Zhou, and L. Lei, *Chemosphere*, 2005, **60**, 405.

[3] P. Baroch, V. Anita, N. Saito, and O. Takai, *J. Electrostat.*, 2008, **66**, 294.

[4] S. Potocky, N. Saito, and O. Takai, *Thin Solid Films*, 2009, **518**, 918.

[5] A. T. Sugiarto, T. Ohshima, and M. Sato, *Thin Solid Films*, 2002, **407**, 174.

[6] H. Wang, J. Lei, X. Quan, and Y. Wu, *Appl. Catal. B-Environ.*, 2008, **83**, 72.

[7] J. Hieda, N. Saito, and O. Takai, *J. Vac. Sci. Technol. A*, 2008, **26**, 854.

[8] A. Kumar, P. K. Vemula, P. M. Ajayan, and G. John, *Nat. Mater.*, 2008, **7**, 236.

[9] K. Belser, T. V. Slenters, C. Pfumbidzai, G. Upert, L. Mirolo, K. M. Fromm, and H. Wennemers, *Angew. Chem.*, 2009, **121**, 3715.

[10] B. Chudasama, A. K. Vala, N. Andhariya, R. V. Upadhyay, and R. V. Mehta, *Nano. Res.*, 2009, **2**, 955.

[11] J. N. Anker, W. P. Hall, O. Lyandres, N. C. Shah, J. Zhao, and R. P. Van Duyne, *Nat. Mater.*, 2008, **7**, 442.

[12] Y. Tang and M. Ouyang, *Nat. Mater.*, 2007, **6**, 754.

[13] Y. Ohko, T. Tatsuma, T. Fujii, K. Naoi, C. Niwa, Y. Kubota, and A. Fujishima, *Nat. Mater.*, 2003, **2**, 29.

[14] V. S. Kovivchak, V. I. Dubovik, and R. B. Burlakov, *Journal of Surface Investigation. X-rays, Synchrotron and Neutron Techniques*, 2009, **3**, 268.

[15] F. K. Liu, Y. C. Hsu, M. H. Tsai, and T. C. Chu, *Mater. Lett.*, 2007, **61**, 2402.

[16] H. Ehwald, *Catal. Lett.*, 1994, **25**, 149.

[17] Y. Chen, C. Wang, H. Liu, J. Qiu, and X. Bao, *Chem. Commun.*, 2005, **42**, 5298.

[18] A. Courty, A. I. Henry, N. Goubet, and M. P. Pileni, *Nat. Mater.*, 2007, **6**, 900.

[19] G. Larsen, E. Lotero, and M. Marquez, *J. Phys. Chem. B.*, 2000, **104**, 4840.

[20] G. D. Chukin and A. I. Malevich, *J. Appl. Spectrosc.*, 1989, **50**, 418.

[21] Y. Zhou, M. L. Bruening, Y. Liu, R. M. Crooks, and D. E. Bergbreiter, *Langmuir*, 1996, **12**, 5519.

[22] Y. Wang, S. Zhu, Y. Mai, Y. Zhou, X. Zhu, and D. Yan, *Micropor. Mesopor. Mater.*, 2008, **114**, 222.

[23] P. Pootawang, N. Saito, and O. Takai, *Jpn. J. Appl. Phys.*, 2010, **49**, 126202-1.

[24] M. J. Mendes, O. A. A. Santos, E. Jordao, and A. M. Silva, *Appl. Catal. A Gen.*, 2001, **217**, 253.

[25] J. D. Richter and P. J. Van Den Berg, *J. Am. Oil Chem. Soc.*, 1969, **46**, 163.

Chapter 6. Summary

This thesis was described the investigation of SPP effecting on various potential applications. Solution plasma has a high feasibility to decompose organic template and eliminate from mesoporous silica. This process also provides high efficiency to incorporate Ag nanoparticles in mesoporous silica without any addition of reducing agent. Comparing to the conventional processes for template removal and nanoparticles synthesis, solution plasma shows the better properties in the term of low consumption time, ease of handling, and low contamination.

In this thesis, the content is divided into six chapters:

Chapter 1 is written on the introductions of SPP, mesoporous silica, and Ag nanoparticles which explain in the detail to make much more understanding in the overall research.

Chapter 2 describes the investigation of the solution plasma feasibility for organic template removal. The mesoporous silica particles in form of spherical shape have been successfully synthesized via the sol-gel method by a ternary surfactant system as the template. The different concentration of the synthesized solutions significantly influenced the mesopore structure of mesoporous silica. From the XRD and TEM investigations, the transformation of the structure from a disordered wormlike structure to an ordered 2D hexagonal structure with an increase in the acidity of the solution is observed. The surfactant template was mostly discarded by SPP in acid and base solutions confirmed by FTIR and thermal analyses. To overcome the drawback of thermal calcination which influences to the mesopore reduction, SPP is expected to

be employed as a novel process to remove organic template without the effect on the mesopore size and morphology. Moreover, SPP is purposed to be a short consumption time process for such application comparing with the conventional processes as thermal calcination and chemical leaching. Finally, SPP for 15 min in acid solution (pH 3) is thus concluded to be a best condition for template removal in mesoporous silica.

Chapter 3 discusses on the characteristics of pH discharge solution and discharge time involved the ability of organic removal in mesoporous silica. Both of these effects play the crucial role as the main factor to the solution plasma capability. The difference of pHs discharge solution had no influence on the mesopore feature inside mesoporous silica after discharge confirming by the XRD and TEM results. The intensities of OES spectra of OH molecular band and O atomic lines as the sources of oxidation were measured during discharge in pH 3 and pH 11 and observed to be higher than that of the result in pH 7. The tendency of such intensities was increased as the increase in discharge time. The effectiveness and performance of solution plasma can be controlled not only the instrument parameters such as the applied voltage, the electrode distance but also other parameters such as pH solution and discharge time which were realized to be the important effect in this study.

Chapter 4 studies and discusses on the feasibility of solution plasma for Ag nanoparticles incorporation on mesoporous silica and template decomposition simultaneously. SPP was applicable to synthesize Ag nanoparticles on mesoporous silica using only Ag precursor without any reducing agent. Two particle sizes were observed in TEM results, the large Ag nanoparticles with the average size at approximately 20 nm were observed after SPP for 10-20 min meanwhile the small size about 5 nm was highly dispersed in mesoporous silica matrix. The template

removal was found after SPP for 15 min. Although, the obtained Ag nanoparticles were relatively larger size than Ag nanoparticles synthesized via commercial chemical reaction, SPP was proved to be a short consumption time process for simultaneous Ag nanoparticles formation on mesoporous silica and template removal with no influence on mesopores size.

Chapter 5 discusses on the potential application of the Ag nanoparticles-incorporated mesoporous silica for hydrogenation of the unsaturated oleic acid. The Ag nanoparticles incorporation and the template removal of mesoporous silica were prepared in one-step process by SPP for 15 min at different of $AgNO_3$ concentration, 0.5-5 mM. The investigations of XRD and TEM gave the results of Ag nanoparticle-incorporated mesoporous silica with various particle sizes dependent on the $AgNO_3$ concentration whereas the FTIR spectra were confirmed the SPP ability for template decomposition. For the catalytic test of hydrogenation, the obtained material using 1 mM $AgNO_3$ concentration was applied as catalyst for oleic acid hydrogenation. It found that in the ethanol system, the hydrogenation over 90% was observed whereas the hydrogenation was partially occurred in the butanol system.

Owing to the solution plasma properties, SPP has a high efficient process to promisingly apply in other fields not only in the discussion in this thesis. This thesis presents the breakthrough of this plasma types to widely use in the mentioned benefits. Moreover, solution plasma will be further developed and accomplished as a versatile process in other prospective advantages in near future.

Acheivements

I. Scientific journals

1. Solution Plasma Process for Template Removal in Mesoporous Silica Synthesis, **P. Pootawang,** N. Saito, and O. Takai, *Jpn. J. Appl. Phys.*, **49** (2010) 126202-1-7.

2. Solution Plasma for Template Removal in Mesoporous Silica: pH and Discharge Time Varying Characteristics, **P. Pootawang**, N. Saito, and O. Takai, *Thin Solid Film*s, accepted.

3. Single-step and Room-temperature Synthesis of Ag Nanoparticles in Mesoporous Silica by Solution Plasma, **P. Pootawang**, S.-P. Cho, N. Saito, and O. Takai, *J. Colloid Interf. Sci.*, submitted.

4. Ag Nanoparticles Incorporation in Mesoporous Silica Synthesized by Solution Plasma and their Catalysis for Oleic Acid Hydrogenation, **P. Pootawang**, N. Saito, and O. Takai, *Mater. Lett.*, accepted.

II. Publications in proceeding of conferences

1. Single Crystal Mesoporous Silica Preparation Assisted by Solution Plasma Process for Organic Template Removal, **P. Pootawang**, N. Saito, and O. Takai, 2008 International Symposium on Micro-Nanomechatronics and Human Science (From Micro & Nano Scale Systems to Robotics & Mechatronics Systems), Nagoya University, Nagoya, Japan, 6-9 November 2008.

2. A Novel Method for Organic Template Removal Using by Solution Plasma Process for Single Crystal Mesoporous Silica Synthesis, **P. Pootawang**, N. Saito, and O. Takai, The 1st Korea-Japan Joint Forum on Sol-gel Science and Technology, Korea

Advanced Institute of Science and Technology (KAIST), Daejeon, Korea, 4-6 December 2008.

3. Single Crystal Mesoporous Silica Preparation Assisted by Solution Plasma Process for Organic Template Removal, **P. Pootawang**, N. Saito, and O. Takai, 3rd Nagoya Univ.-UCLA International Symposium, Nagoya University, Nagoya, Japan, 8-9 December 2008.

4. Novel Method for Organic Template Removal Assisted by Solution Plasma Process in Single Crystal Mesoporous Silica Synthesis, **P. Pootawang**, N. Saito, and O. Takai, The IUMRS International Conference in Asia 2008 (IUMRS-ICA 2008), Nagoya Congress Center, Nagoya, Japan, 9-13 December 2008.

5. Single Crystal Mesoporous Silica using Solution Plasma Process for Template Removal, **P. Pootawang**, N. Saito, and O. Takai, Ninth International Symposium on Biomimetic Materials Processing (BMMP-9), Nagoya University, Nagoya, Japan, 20-23 January 2009.

6. ソリューションプラズマ・カルシネーションによるメソポーラスシリカの合成, **P. Pootawang**, N. Saito, and O. Takai, JIM Annual Spring Meeting 2009, Tokyo Institute of Technology, Tokyo, Japan, 28-30 March 2009.

7. Time and pH Dependence in Template Removal from Single Crystal Mesoporous Silica using Solution Plasma Process, **P. Pootawang**, N. Saito, and O. Takai, ISPC Pre-Symposium in Japan, Kyoto University, Kyoto, Japan, 30 May 2009.

8. Time-varying Characteristic in Template Removal from Single Crystal Mesoporous Silica by Solution Plasma, **P. Pootawang**, N. Saito, and O. Takai, International Conference on Materials for Advanced Technologies 2009 (ICMAT2009) and International Union of Materials Research Societies- International Conference in Asia

2009 (IUMRS – ICA 2009), Suntec Singapore International Convention & Exhibition Centre, Singapore, 28 June – 3 July 2009.

9. Solution Plasma Process for Template Removal in Single Crystal Mesoporous Silica Synthesis, **P. Pootawang**, N. Saito, and O. Takai, International Symposium on Plasma Chemistry 19 (ISPC19), Ruhr-University Bochum, Germany, 27-31 July 2009.

10. Simultaneous Ag Nanoparticles Impregnation and Template Removal of Mesoporous Silica Using Solution Plasma, **P. Pootawang**, N. Saito, and O. Takai, 2009 International Symposium on Micro-NanoMechatronics and Human Science (From Micro & Nano Scale Systems to Robotics & Mechatronics Systems), Nagoya University, Nagoya, Japan, 8-11 November 2009.

11. Processing of Mesoporous Silica by Solution Plasma and Polyacrylic Acid Functionalization, **P. Pootawang**, N. Saito, and O. Takai, 2009 MRS Fall Meeting, Hynes Convention Center, Boston, Massachusetts, USA, 30 November-4 December 2009.

12. One Batch Process for Ag Nanoparticles Impregnation and Template Removal on Mesoporous Silica, **P. Pootawang**, N. Saito, and O. Takai, 2nd Japan-Korea Joint Forum on Sol-Gel Science and Technology, Osaka Prefecture University, Osaka, Japan, 26-28 June 2010.

13. Solution Plasma for Template Removal in Mesoporous Silica: pH and Discharge Time-Varying Characteristics, **P. Pootawang**, N. Saito, and O. Takai, 10th Asia-Pacific Conference on Plasma Science and Technology (APCPST) and 23rd Symposium on Plasma Science for Materials (SPSM), Lotte Hotel Jeju, Jeju, Korea, 4-8 July 2010.

14. Simultaneous Ag Nanoparticles Impregnation on Mesoporous Silica and Organic Template Removal using Solution Plasma, **P. Pootawang**, N. Saito, and O. Takai, 3rd

International Conference on Advanced Nano Materials (ANM2010), Palais des Rose Hotel, Agadir, Morocco, 12-15 September 2010.

15. Amino Functionalization on SBA-15 Mesoporous Silica using Solution Plasma and its Ability for Gold Nanoparticles Growth, **P. Pootawang**, N. Saito, and O. Takai, 2010 International Symposium on Micro-NanoMechatronics and Human Science (From Micro & Nano Scale Systems to Robotics & Mechatronics Systems), Nagoya University, Nagoya, Japan, 7-10 November 2010.

16. Amino Functionalization on SBA-15 Mesoporous Silica by Solution Plasma as the Active Site for Au Nanoparticles Growth, **P. Pootawang**, N. Saito, and O. Takai, The 12^{th} International Symposium on Eco-materials Processing and Design (ISEPD2011), The Empress Hotel, Chiang Mai, Thailand, 8-11 January 2011.

Acknowledgments

This thesis arose in part out of years of research that has been done since I came to Takai laboratory, Department of Materials, Physics and Energy Engineering, Graduate School of Engineering, Nagoya University. By that time, I have worked and participated in many activities with a great number of people whose contribution in the assortment of ways to my research and the thesis building deserved special mention. It is a warm pleasure to express my appreciation to them all in my humble acknowledgment.

In the first place I would like to record my gratitude to my supervisor, Prof. Osamu Takai and co-supervisor, Prof. Nagahiro Saito for providing me a gold opportunity to study in the excellent environment and high attractive place and for giving me his kind supervision, suggestion, and guidance from the very beginning stage of this research as well as giving me extraordinary experiences through out my work. Above mentioned and the most needed, they provided unflinching encouragement and invaluable support me a lot. Their truthfully scientist intuitions has bring me as a wonderful ideas and passions in scientific field, which exceptionally inspire and develop my growth as a student and a scientist that I want to be.

I would like to deeply thankful to Prof. Yasushi Inoue, Prof. Tatsuru Shirafuji, and Assoc. Prof. Maria Bratescu, whose encouragement, guidance, and support from the initial to the final level enabled me to develop an understanding of my research.

I would like to gratefully acknowledge to Assoc. Prof. Sang-Pyo Cho and Assist. Prof. Osamu Terakado, whose help and support me in experiment.

I would also express my appreciation and thank to Ms. Eriko Kondo and Mrs. Keiko Ito to kindly provide me lot of assistance before and after I came to Japan. I am very thankful to all Takai's group members including students and researchers.

Lastly, I would like to heartily express my deepest thanks to my parent and my family to educate me being as a strong person and give me the high moral support with their inestimable love.